DISSERTATIONES
CHIMICAE
UNIVERSITATIS
TARTUENSIS
240

INDREK SAAR

Development of novel on-site chemical analysis tests – from alternative materials and technologies to functional prototypes

DISSERTATIONES CHIMICAE UNIVERSITATIS TARTUENSIS
240

DISSERTATIONES CHIMICAE UNIVERSITATIS TARTUENSIS
240

INDREK SAAR

Development of novel on-site chemical analysis tests – from alternative materials and technologies to functional prototypes

UNIVERSITY OF TARTU
Press
1632

Institute of Chemistry, Faculty of Science and Technology, University of Tartu, Estonia.

The dissertation is accepted for the commencement of the degree of Doctor of Philosophy in Chemistry on June 10th, 2025, by the Council of Institute of Chemistry, University of Tartu.

Supervisors:	Research Fellow Hanno Evard, PhD. University of Tartu, Estonia
	Professor Ivo Leito, PhD. University of Tartu, Estonia
Opponent:	Professor Nicole Pamme, PhD. Stockholm University, Sweden
Commencement:	27th August 2025, at 14:15. Auditorium 1020, Ravila 14a, Tartu.

This work has been partially supported by ASTRA project PER ASPERA Graduate School of Functional Materials and Technologies receiving funding from the European Regional Development Fund under project in University of Tartu, Estonia.

ISSN 1406-0299 (print)
ISBN 978-9916-27-925-0 (print)
ISSN 2806-2159 (pdf)
ISBN 978-9916-27-926-7 (pdf)

Copyright: Indrek Saar, 2025

University of Tartu Press
www.tyk.ee

TABLE OF CONTENTS

LIST OF ORIGINAL PUBLICATIONS

I. Evard, H.; Priks, H.; **Saar, I**.; Aavola, H.; Tamm, T.; Leito, I. A New Direction in Microfluidics: Printed Porous Materials. Micromachines 2021, 12 (6), 671.

II. **Saar, I**.; Evard, H. Screen Printed Particle-Based Microfluidics: Optimization and Exemplary Application for Heavy Metals Analysis. Micromachines 2023, 14 (7), 1369.

III. Laaneväli, A.; **Saar, I**.; Nasirova, N.; Evard, H. Multi-Step Particle-Based Microfluidic Test for Biotin Measurement. Microfluid Nanofluid 2024, 28 (10), 71.

IV. **Saar, I**.; Evard, H. Real-World Implementation of Particle-Based Microfluidics: On-Spot Test for Iron and Copper Ions in Water. ACS Omega 2025, 10 (1), 1800–1808.

PATENT APPLICATIONS:

V. Evard, H.; **Saar, I**.; Laaneväli, A. Method of producing an analysis device, analysis device, analysis arrangement and analysis method. WO2024126727A1, 2024

VI. **Saar, I**.; Evard. H.; Zapata, E. Analytic device, liquid handling system and chemical analysis method. PCT/IB2025/052999, Priority date: 21.03.2024 (The patent application has been refiled with modifications, but it has not been reviewed or published at the time of submission of this thesis, therefore the full text has not been made available in the Publications section.)

Author's contribution:

Publication I: The author performed part of the experiments related to photolithography and screen printing. Participated in data interpretation and writing the manuscript.

Publication II: The author was responsible for planning and performing the experiments and data interpretation. Lead author in preparing the manuscript.

Publication III: The author participated in the planning and data interpretation. Performed the screen printing, 3D design and printing, final device development and most of the experiments with the final

analysis test. Lead author in writing about the aforementioned parts in the manuscript.

Publication IV: The author was responsible for planning and performing the experiments and data interpretation. Lead author in preparing the manuscript.

Publication V: The author's share of the patent is 33.3%.

Publication VI: The author's share of the patent is 51%.

ABBREVIATIONS

BC	bathocuproine
biotin-F	biotin-5-fluorescein
BP	bathophenanthroline
DMG	dimethylglyoxime
DTZ	dithizone
DWP	direct write printing
FeCu (test)	iron and copper (test)
HM (chip)	heavy metal (chip)
LFA	lateral flow assay
LOC	lab-on-a-chip
LOD	limit of detection
PAD	paper-based analytical device
PAN	1-(2-pyridylazo)-2-naphthol
PBM	particle-based material
PCA	3-carboxypropyl group
p-DACA	p-dimethylaminocinnamaldehyde
PDMS	poly(dimethylsiloxane)
PL	photolithography
PLA	poly(lactic acid)
POC	point-of-care
PSA	3-sulfopropyl group
Re	Reynolds number
RH	relative humidity
RSD	relative standard deviation
SEM	scanning electron microscopy
SP	screen printing
SPE	solid phase extraction
TLC	thin layer chromatography
WHO	World Health Organization
XG	xanthan gum

1. INTRODUCTION

Analytical chemistry is vital to almost every aspect of our lives. It is used to ensure the safety of the food and water we consume, perform medical diagnostics and environmental monitoring, optimise processes in industry and agriculture, and check for product quality, among other applications. The general challenge of determining the chemical composition of a diverse range of objects has been largely solved by powerful laboratory instruments. However, this lab-based analysis comes with considerable drawbacks. Most of the instruments are expensive, require laboratory infrastructure, and highly qualified specialists to operate them. Moreover, sample transportation and limited access to suitable facilities can result in delays of several days or even weeks. This is often too long, and the results are needed faster to make time-critical decisions. Therefore, the ability to perform analysis on-site, to receive time-critical results immediately with relatively low cost and easy-to-use equipment, would have a significant impact on the lives of billions of people.

Microfluidics is a promising platform to address this challenge. By miniaturising the chemical analysis laboratory into a portable format – an analysis chip – testing could be carried out in remote locations, anywhere in the world. Considerable progress has been made towards that goal in the last few decades and performing complex multi-step analysis has been successfully demonstrated. However, the currently developed devices are still expensive and often require bulky auxiliary instrumentation and trained specialists to operate them.

An alternative direction with paper-based devices has also been under active development over the last decade, and it can lower the material and production costs significantly. Moreover, the focus with these devices has been greatly on ease of use, limiting the required user skill and risk of errors. However, what paper-based devices gain in simplicity and cost, they lose in the analytical performance, i.e. in the necessary selectivity and sensitivity to measure analytes in real-world samples. To solve this, better control over test fabrication and integration of additional components is needed. This could be achieved by fine-tuning the material characteristics and functionalising different chip regions without excessively increasing the overall device complexity and cost.

In this work, alternative materials and methods to produce microfluidic chips that function similarly to paper-based microfluidic devices were investigated. Screen printing of microparticles on a glass substrate was discovered as an especially promising approach to produce chips with well-tuned properties. This method is inexpensive, offers high flexibility and accuracy, and it is suitable for rapid prototyping and mass production. Following an initial investigation, screen printing was studied in depth to create novel microfluidic chips with adjustable properties and combine multiple materials and analysis steps into a single device. The overall goal was to demonstrate the fundamentals of the new technology and develop a fully functional prototype that could be used for on-site chemical analysis, without highly specific instrumentation or skills required from users.

2. LITERATURE OVERVIEW

2.1 Microfluidics and on-site chemical analysis

Microfluidics, according to most definitions, deals with small amounts of fluids (10^{-6} to 10^{-18} litres), using systems that have at least one dimension in the range of several hundred micrometres or less.[1,2] This often involves complex channel networks in which those liquids and their components can be precisely manipulated. The miniature scale offers multiple advantages such as low amounts of consumed reagents and samples, small device dimensions, faster analysis and reaction times, and makes use of phenomena that only occur in small scale, allowing the manipulation of even single cells and molecules.[3,4] This makes microfluidics a valuable technique that finds applications in a wide range of fields such as chemical analysis, synthesis, cell culture, drug transport and medical diagnostics.[5–7]

Miniaturising and streamlining chemical analysis could be considered the most prominent goals of microfluidics.[1,8] In an ideal setting, the entire analysis could be carried out on site with a single standalone miniature device, which is often referred to either as a micro total analysis system or a lab-on-a-chip (LOC) device.[9,10] Unlike commercial simple testing kits, these devices are intended to perform multiple analysis steps automatically, without the need for the user to directly interact with the test, thereby limiting user-related errors. The user would also not need to handle any hazardous chemicals. At the same time, LOC devices should maintain necessary analytical performance and provide reliable and repeatable results similar to laboratory analysis. Although the miniaturisation of chemical analysis with LOC devices has been demonstrated, part of the goal usually remains incomplete and instead of being lab-on-a-chip devices, they often remain chip-in-a-lab devices.[11,12] This means that some expensive and bulky auxiliary instrumentation (e.g. pumps, detection devices) and skilled personnel to perform the analysis are still required. To avoid these limitations, this work focuses from the outset on developing on-site analysis devices.

Different guidelines and objectives have been set to describe an ideal analysis device or test for on-site analysis, especially for applications related to medical diagnostics. The terms analysis “device” and “test” are regarded as synonyms throughout this work and refer to a standalone device to which the sample can be added, and which can later be used to interpret the analysis results. One of the most prominent sets of criteria for such analysis tests was introduced by the World Health Organization (WHO) in 2003 under the acronym of ASSURED.[13] These criteria state that the devices should be Affordable, Sensitive, Specific, User friendly, Rapid and robust, Equipment-free, and Deliverable to end-users. Improvements have been proposed to this classification (e.g. REASSURED) that include Real-time connectivity, Ease of specimen collection and replace the criterion of Equipment-free with Environmentally friendly.[14] In terms of developing LOC devices for real-world applications, several external factors

must also be considered, which include the sample and analyte type and the field of application itself.[10,15]

The most important areas where on-site tests are needed include medical diagnostics, environmental analysis, national security and forensics, and different industrial applications (e.g. food industry, agriculture).[3,16,17] In all these fields, widespread screening for harmful substances (e.g. contaminants, toxins, drugs) or monitoring of some common analyte levels is required. The specific application can greatly dictate the precision of the results and whether they must be quantitative in nature, as well as how fast and simple the devices must be to use. For instance, with point-of-care (POC) tests in medical diagnostics, the analysis must be carried out immediately near the patient, which puts higher importance on analysis time, while the tests are still performed in a stable indoor environment by experienced individuals.[18] At the same time, some applications, e.g. environmental monitoring, might require conducting the analysis in remote outdoor locations under variable ambient conditions and limited access to power. Finally, commercial POC tests for regular home-users should be considered separately as they must be very simple to use while the requirement for highly accurate analytical results can be lower.[19]

LOC devices can be applied for the measurement of various sample types that include solids, liquids and gases.[16,20,21] In relation to this work the focus is only on analysis of water-based samples. This sample type was chosen because: (1) water is one of the most important matrices in real-world applications (e.g. environmental or drinking water, blood and urine, etc.), and (2) liquid samples demand less pretreatment before analysis and are therefore more suitable for demonstration of novel technologies, which is the main goal of this work. Nevertheless, water-based samples are still extremely diverse and can demand very different sample preparation methods, depending on the specific sample and the analyte being measured. Moreover, matrix effects can be especially important in the case of LOC devices, since the influence of additional components impacts liquid flow and therefore the entire sample analysis.[3,15]

All types of analytes, including ions, small molecules, proteins, antibodies, enzymes as well as bacteria and cells have been shown to be detectable with LOC devices.[9,15] In this work, the focus is on chemical analysis and therefore examples for ions and small molecules are mostly considered. For instance, monitoring metal cations in water is required, because many of them (e.g. lead, cadmium, mercury) are toxic even in small quantities.[22] At the same time, iron, copper, manganese and zinc are essential micronutrients, which makes it necessary to analyse their content in agriculture and food industry.[23] Furthermore, LOC devices for these metals are important in medical diagnostics to measure their deficiencies or excess in the body, which can lead to different serious medical conditions.[24,25] Similarly, common anions such as nitrate, phosphate and sulphate must be monitored in those same fields.[26] In addition to ions, many small molecules such as glucose, cholesterol and vitamins are crucial analytes to be monitored in POC diagnostics.[18,27,28]

2.2 Passively driven microfluidics

Microfluidic devices are divided into active and passive, based on their operating principles.[2] Active devices rely on external pumps and power sources for operation, which help to achieve high analytical performance and precision. In the case of passively driven microfluidics, however, no external auxiliary sources are used to generate the liquid flow. This leads to easier manufacturing, more compact and portable devices and a lower need for qualified specialists to perform the analysis, which all contribute to lowering overall costs throughout the entire process. All this also makes passively driven microfluidics more suitable for on-site analysis and it is therefore chosen as the main direction in this work as well. The main techniques to achieve liquid flow in passive devices are pressure-driven, capillary, hydrostatic, surface-tension and vacuum-based or any of their combinations.[2] While all those approaches have their advantages and disadvantages, the flow induced by capillary action, can be considered the most prominent for producing simple, robust and inexpensive analysis tests.[29,30]

2.2.1 Theoretical background of passively driven microfluidics

To better understand the underlying phenomena and to help design and fabricate the devices accordingly, some theoretical background into capillary flow mechanics is needed. Capillary action is defined as the spontaneous wicking of liquid in narrow spaces without the assistance or even in opposition to external forces.[31] Capillary flow can occur both in tubes with a small diameter as well as in media that contain an open network of pores with suitable size range. In general, capillary flow depends on two types of intermolecular forces: (1) the interaction between the solid material surface and the molecules of the liquid and (2) the cohesive forces between the liquid molecules.[32] These forces often form complex equilibria that are also influenced by the surrounding liquid-air and solid-air surface energies. Different variables that describe these forces and their combinations include fluid density and viscosity, surface tension and contact angle. These characteristics can be used to calculate the Reynolds number (Re), which is a quantity for describing whether fluid flow in a specific situation is laminar or turbulent:

$$Re = \frac{\rho u L}{\mu} \qquad (1),$$

where ρ is the fluid density, u is the fluid velocity, L is characteristic length of the system (e.g. the capillary or pore diameter in porous materials), and μ is the fluid dynamic viscosity. In capillary flow, the Re values are less than 1, indicating laminar flow. This also means that viscous forces are dominant, and the flow velocity is mostly determined by the equilibrium between the surface tension and viscous resistance.[33]

Another equation to approximate the laminar capillary flow of liquids (assuming $Re < 1$ and only one-dimensional flow through constant cross-section occurs) is the Lucas-Washburn equation:[34]

$$L_f^2(t) = \frac{\gamma r t \cos(\theta)}{2\mu} \qquad (2),$$

where L_f is the liquid front travel distance in time t; γ is the surface tension or liquid-air surface energy, $\cos(\theta)$ is the contact angle, r is the pore diameter. A crucial conclusion from this equation is that the liquid flow rate depends on the square root of time. Therefore, in terms of practical applications it means that from a certain point, increase in the sample volume (e.g. to improve the sensitivity) will result in a significant increase in the required analysis time.

Finally, Darcy's law is used to describe the spontaneous imbibition of liquids in porous permeable media with constant cross-section (assuming $Re < 1$ and that the system is level with the ground, i.e. gravitation does not play a role):

$$Q = -\frac{\kappa A}{\mu L}\Delta P \qquad (3),$$

where Q is the volumetric flow rate, κ is the intrinsic permeability of material (describing porosity and its distribution), A is the cross-sectional area perpendicular to flow, and ΔP is the pressure drop occurring over a length L in the channel along the flow direction.[32,35]

The impact of liquid viscosity is apparent from all these equations, which highlights the influence of sample type and matrix components (e.g. salinity) on the functioning of passively driven devices. In addition to the properties of the liquid, all these equations include the porosity of the solid material. However, usually only parallel capillaries with constant circular cross-sections are considered in these equations as a simplification. The actual effective pore diameter, pores' distribution and homogeneity in materials is considerably more complex and it makes accurate modelling of the flow dynamics difficult.[36] Moreover, in the case of paper, swelling of fibres occurs during wetting which leads to changes in the material's porosity.[17,32] Nevertheless, it is apparent that precise control over the material's porosity (both pore size and distribution) allows manipulation of the intrinsic capillary flow mechanics in the material and consecutively can have a great impact in the development of passively driven microfluidic devices. In this work, emphasis is placed on developing fabrication techniques that allow controlling the porosity of the material, however the focus will be on the experimental investigation rather than theoretical modelling of the effects.

2.2.2 Examples of passively driven microfluidics

Passively driven flow has been demonstrated with various LOC systems.[2,37] Conventionally, this involves etching channel networks into glass or silicon substrates in a cleanroom environment. Similarly, polymers such as poly(dimethylsiloxane)

(PDMS) or poly(methylmethacrylate) (PMMA) are often used, however, surface treatment is needed to make these channels hydrophilic. The capillary network formed by these approaches is usually closed, as the channels are surrounded by solid walls on all sides. Although the resulting devices enable precise liquid manipulation, the necessary production conditions and associated costs can significantly inhibit their commercialisation and mass production.[38]

An alternative approach to create passively driven devices is to use a porous network inside the materials to enable capillary flow. While the same materials can be used for this purpose (e.g. by using a sacrificial template method to create porous PDMS sponges), a more cost-effective direction is often preferred.[39] This involves choosing materials that are inherently porous, which can significantly reduce the complexity and costs for the production. Examples of these materials include cellulose paper, cotton fabric, glass fibres and nitrocellulose.[40,41]

In broad terms, all inherently porous material based and capillary-driven devices could be classified as paper-based analytical devices (or PADs) by referring to the most prominently used material (i.e. cellulose paper) among them. However, often separate classifications are used in relation to the device's complexity or operating principles. For example, testing strips and lateral flow assays (LFAs) are regarded as separate entities from the PADs (examples in **Figure 1**), despite having similar porous membrane as the primary functional component of the system.[40,41] In terms of clarity, the distinction between PADs, LFAs and testing strips is also made in this work. It could be said that none of these approaches fall under the general definition of microfluidics as the sample amounts can often reach up to several hundred microlitres or more (see **Table 4** for examples). However, when considering the production costs and operating principles, they are considerably more cost-effective, portable and robust than conventional LOC devices. This also makes them a more promising and practical direction for fulfilling the ASSURED criteria of on-site analysis devices.[15,41] Finally, another difference from the conventional LOC systems is that the capillary network in PADs and related devices is open to the surrounding environment (unless restricted afterwards, e.g. by laminating the paper), which makes them more susceptible to ambient conditions (e.g. evaporation).[15,42] Although this can raise issues with sample volume control and repeatability, it can provide beneficial attributes, e.g. for analyte concentration.

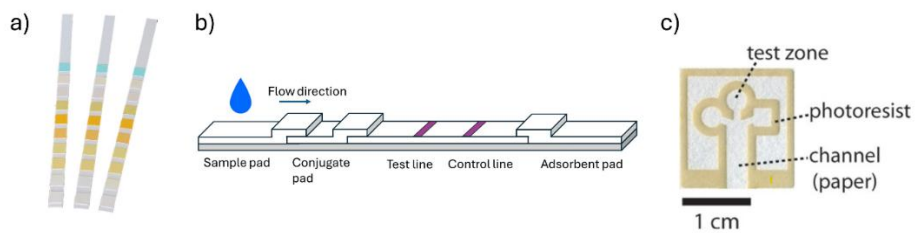

Figure 1. Different paper-based test devices. **a)** Urine testing strips (e.g. One+Step DUS 10[43]*)*; **b)** Structure of a conventional LFA; **c)** First PAD reported by the Whitesides' group. Adapted with permission from [44], copyright 2010 American Chemical Society.

Testing strips or dipsticks simply comprise pads of paper that are impregnated with detecting reagents. Upon contact with the sample liquid and if analytes are present, the reagents provide a colorimetric signal, allowing detection by visually comparing the colour change to a chart to determine the results. They are used for measuring pH and other simple chemical compounds or in medical diagnostics, to detect metabolic products from urine. The main advantages of testing strips are low cost and simplicity; however, their specificity and detection limits are typically poor and the analysis can be semi-quantitative at best.

Similar to dipsticks, LFAs rely on one-dimensional liquid flow; however, their composition is more complex, combining the advantages of different materials. The devices usually consist of several porous membranes that include a sample pad, conjugate pad, nitrocellulose membrane (with test and control lines) and an absorbent pad. Each of these membranes is slightly overlapped with the adjacent ones to provide a continuous flow of liquid through the device, and they are located on a backing pad for structural support. Most LFA applications are related to medical diagnostics (e.g. pregnancy and COVID tests) and they rely typically on antibodies, which provide high specificity. However, the detection limits of LFAs remain poor, and mostly only qualitative analysis is performed with them.

PADs (often called paper-based microfluidic devices or μPADs) are differentiated from dipsticks and LFAs, because additional fabrication steps have been applied to paper to create a network of flow channels. This allows to manipulate the flow in two or even three dimensions and gives the opportunity to perform more complex analysis, consisting of several consecutive or parallel steps. It also makes PADs similar to conventional LOC devices, as several routine laboratory analysis steps can be implemented into a single miniature device.[15,16,41]

2.3 Paper-based analysis devices

The working and detection principles of the technology developed in this work are fundamentally similar to PADs, because most of the underlying phenomena remain the same regardless of the exact porous material used to make the device. Therefore, PADs have been chosen as the main inspiration for this thesis and are discussed in more depth in this chapter. Moreover, the published research involving PADs has exponentially increased over the last 15 years, which offers a wealth of background information and numerous examples.

2.3.1 Paper as the substrate for passively driven devices

Cellulose paper has been used for chemical analysis for centuries in the form of litmus paper and urine testing strips. Confining specific areas on paper for analysis was reported already in the first half of 20th century by Yagoda with the spot tests for nickel and copper ions that used paraffin barriers.[45] This was further improved in 1949 by Müller and Clegg, who created a fluidic system on paper, consisting of confined eluent addition and waste areas that were connected by a nar-

row analysis channel for paper chromatography.[46] Although this could be considered as the start of patterned paper microfluidics, in reference to the definition of the PADs, the real lift-off as well as introduction of the term "patterned paper-based assay" came in 2007 by Whitesides' group that brought the PADs to the spotlight (**Figure 1c**).[47]

There are a variety of reasons why paper is considered as an excellent base material for passively driven chemical analysis tests. First, it consists of a cellulose fibre network that has average fibre diameters between 1–100 μm, which results in pore spaces ranging from 1–10 μm between the fibres. Combined with the hydrophilic functional groups of cellulose, it gives rise to strong capillary-driven flows. The molecular and physical structure of paper can be seen in **Figure 2**. The carbohydrate composition also offers good opportunities for surface functionalisation and its high surface-to-volume ratio provides good reagent and analyte adsorption capabilities. This can lead to enhanced sensitivity for detection. Mechanically, paper is durable and flexible, allowing repeated bending and folding, while it can be used without external support or substrates. Finally, it is inexpensive, environmentally friendly and biodegradable, and a wide variety of paper with different properties (porosity, thickness) is commercially available.[15,32]

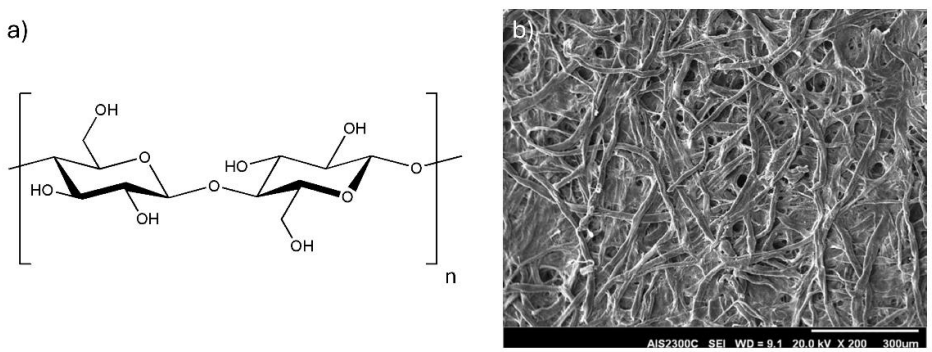

Figure 2. The structure of paper. **a)** Molecular structure of cellulose; **b)** Scanning electron microscopy (SEM) image of Whatman grade 1 paper. Reprinted with permission from [48], copyright 2019 Wiley.

Despite all these appealing characteristics of paper, there are some drawbacks that discourage its use in LOC devices. First, pore size and distribution, and the thickness of the material are critical parameters that influence the flow characteristics of the device. Therefore, it is desirable to closely control and adjust these factors accordingly during the production of PADs. In the case of paper, however, these characteristics are generally determined by the manufacturing process and are difficult to alter later. Although the wide availability of different paper materials helps to compensate for this, finding a paper with a specific combination of characteristics, especially in the testing phase, can turn out to be troublesome. Moreover, various additives can occur in paper depending on its production process, and the orientation of cellulose fibres can also affect the flow characteris-

tics.[49,50] Therefore, the batch-to-batch variability of both paper and the PAD can have a considerable influence on the final performance of the device.

2.3.2 Patterning the paper to produce PADs

To transform paper into a usable microfluidic system, flow paths (also called channels) must be created into its structure to control the liquid flow direction. In general, this is achieved in one of two ways – either by cutting a specific pattern out of the paper or making parts of the paper impassable for the liquids used. Numerous techniques have been demonstrated to realise both approaches and they can be compared based on achievable resolution and precision, the complexity and speed of the process, the required equipment and reagents, and the overall costs. The following brief overview of the techniques and their main advantages and drawbacks is based on several thorough review articles.[15,16,32,51]

In the case of cutting, different levels of complexity, cost and accuracy can be applied, starting from crude manual cutting with scissors or a knife to automatic bladed cutting machines to laser-cutting. The advantage of cutting is the simple nature of the process that does not consume any additional reagents. Also, with sophisticated methods (i.e. with a CO_2 laser), a high level of accuracy can be easily achieved, although the instrument costs increase. On the other hand, cutting diminishes the structural integrity of paper and makes it fragile, which means that a backing substrate is often required.

The techniques for blocking certain areas of the paper to make them impassable for liquids generally involve either masking, printing or stamping. Photolithography (PL) was the initial method applied by Whitesides' group in 2007, and it yields results with high resolution and precision.[47] PL (**Figure 3a**) consists of impregnating a sheet of paper with a negative photoresist, applying a photomask containing the desired patterns on top of it and then exposing the system to UV light to crosslink the exposed parts of the photoresist. Afterwards, the unexposed resist is removed with a solvent, forming the desired channel structure in the paper. The main drawbacks of the method are complex multi-step fabrication and need for expensive reagents and equipment, which also hinder mass production. Other demonstrated masking techniques such as plasma etching or chemical vapour deposition have similar issues with a complex fabrication process and high costs for mass production.

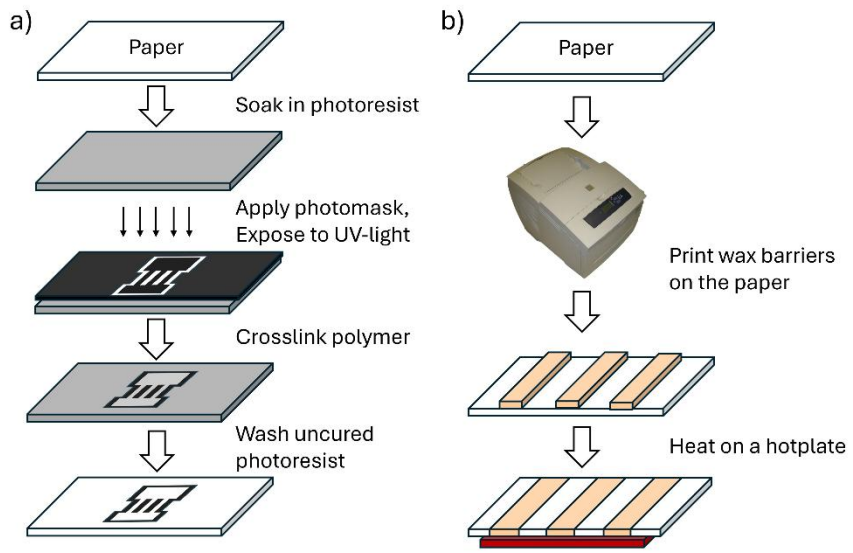

Figure 3. PAD fabrication methods for creating hydrophobic barriers. **a)** Patterning with PL; **b)** Forming hydrophobic wax barriers with a wax printer.

In terms of mass producibility, different printing techniques have been proposed as a more suitable alternative. These include wax, inkjet, laser, screen and flexographic printing. With all of them, wax or some other hydrophobic solution (e.g. polystyrene in toluene) is deposited on the paper to form the confined channel systems. Although post-treatment processes (e.g. heating the paper to allow the formation of the barrier throughout its entire thickness) are sometimes required, they are usually relatively simple and suitable for large-scale production. The main steps for wax printing can be seen in **Figure 3b**. However, compared to PL or laser cutting, the resolution achievable with printing is often lower, especially if a subsequent melting step must be performed. Moreover, there is still need for specialised equipment (e.g. a printing machine, screens with different designs) and depending on the printer, the range of usable inks and substrates may be limited. Nevertheless, since the printing equipment is often commonly used in other fields of application (especially with inkjet and laser printers), printers are inexpensive and can be relatively easily modified to produce PADs. Moreover, with some of the techniques (e.g. inkjet and screen printing), other necessary reagents and components (e.g. electrodes) can be integrated with the PAD by using the same method, which can significantly simplify the overall PAD production.

Finally, different stamping methods have also been applied to produce the PADs. These function by applying a stamp covered with hydrophobic ink, molten wax or polymer onto paper to form the hydrophobic barriers. Compared to printing, it can be even faster, and no dedicated printer is needed. However, the stamping procedure and ink must be carefully optimised, new stamps are required for every design and the overall resolution and precision of the method is often

relatively poor. One additional limitation that applies to all techniques relying on impassable barriers to contain the liquids is the compatibility of these barriers with different solvents. This brings out the advantage of cutting techniques, where these issues are essentially eliminated. In general, all the fabrication techniques have their advantages and limitations, and no universally best approach can be determined.

2.3.3 Reagent deposition and storage on PADs

In addition to patterning the paper to control the liquid flow, incorporating reagents into the test is the other required production step of PADs to provide specific functionality to them. A comprehensive overview of various methods for reagent integration and storage, both in dry and liquid form, was presented by Hitzbleck and Delamarche.[52] Whether dry or liquid reagents are needed can depend on the applied working principles of the test as well as on the reagents themselves – e.g. their stability during storage. In the case of dried reagents, solution-based deposition usually is used, where the reagent is initially dissolved in a solvent. This solution is applied to the device and the solvent is allowed to evaporate. This way, uniform reagent distribution at various concentrations can be achieved. At the same time, the production costs are kept low and the devices themselves can be simple and robust, since the reagents are later released into the system by simply dissolving or coming into contact with the sample or other solvents. In the case of paper, the hydrophilic surface and high surface-to-volume ratio also mean that many reagents can be easily immobilised on the surface and, during analysis, the reactions can occur rapidly.

The methods for dry reagent deposition can be broadly divided into contact and non-contact techniques and, similar to PAD patterning, they vary in terms of accuracy, throughput and cost. However, deposition is possible in a consistent and reproducible manner, while still keeping the related costs low. Pipetting robots, sprayers and piezoelectric inkjet printers are the prevalent examples of non-contact methods, where the reagent depositor does not come into direct contact with the substrate. This means that multiple reagents can be deposited over the same area without the risk of cross-contamination. To achieve repeatability with these methods, control over ambient conditions (humidity, temperature) is crucial. In the case of contact methods such as screen, pin or microcontact printing, the delivery structure (stencil, pin, stamp) is brought to direct contact with the substrate. The advantage of, for instance, microcontact printing is that monolayers of molecules can be transferred onto a substrate without drying artefacts (e.g. concentration gradient due to the coffee ring effect). In case of PADs, pipetting and inkjet printing (**Figure 4a** and **b**) are the most widely employed techniques.[53]

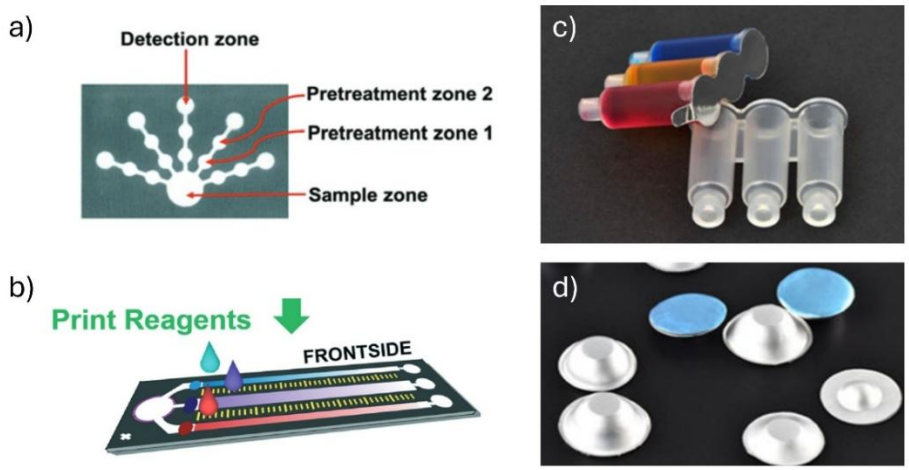

Figure 4. Examples of reagent storage on PADs. **a)** PAD with multiple pretreatment zones where reagents were pipetted and dried. Used with permission of Royal Society of Chemistry, from [54]; permission conveyed through Copyright Clearance Center, Inc. **b)** PAD where inkjet printer was used to deposit reagents. Used with permission of Royal Society of Chemistry, from [55]; permission conveyed through Copyright Clearance Center, Inc. **c)** Example of commercially available liquid storage tanks for LOC devices. Used with permission of *microfluidic ChipShop* GmbH, from [56]. **d)** Commercially available prefilled aluminium blister reservoirs. Used with permission of *microfluidic ChipShop* GmbH, from [56].

Although storing liquids on PADs is rare, it has been extensively applied to conventional LOC devices.[52,57] For instance, liquids can be stored in containers or tanks (**Figure 4c**) that are screwed or plugged into the device before or during use.[56] This can provide increased flexibility, since different cartridges can be applied to the same device to analyse different analytes or samples and the stability of reagents is not directly linked to the storage conditions of the device. One critical aspect of integrating liquid reagents with different LOC devices is the release of the reagents into the device. This can be achieved either manually or automatically. For instance, cartridges filled with liquid can contain a membrane that is punctured when it is plugged into the device to release the reagent. Similarly, blister pouches (**Figure 4d**) can be used that are compressed either manually or automatically with electronic actuators to release the reagents.[58] Since storing liquids is not required with simple PADs, only a few examples of it have been demonstrated.[59,60] However, the need for liquid storage will become crucial if multi-step analysis is desired, since additional liquids would be needed to perform washing and further elution steps.[61,62]

2.3.4 Sample volume and evaporation control

The added sample volume is a crucial parameter of PADs. For quantitative results, the sample amount must be known and applied in a reproducible manner. However, tools to deposit accurate volumes in laboratory conditions (e.g. automatic pipettes and syringes) are typically not available in resource-limited, on-site settings or for regular home users. Therefore, alternative strategies must be employed to guarantee the reliability and repeatability of the tests. Compared to conventional LOC devices, sample volumes with PADs are usually larger (often varying in the range of tens to hundreds of microlitres). In case of simple devices, this is partly because no additional liquids besides the sample are used, meaning that the sample must wick through the entire capillary system of the PAD. To some extent, this already provides significant control over the sample volume, since the excess will not be absorbed by the capillary network of the PAD.[63] However, the cellulose network can still slowly expand and absorb more liquid over time, which complicates the determination of the final sample volume. In addition, eluting excessive volumes through the reaction or detection zones of the device can cause migration of the reagents and result in incomplete reactions and distorted signals.[64,65] Alternatively, a timing-based system could be incorporated to indicate the end-point of the analysis (e.g. through colour change in a specific region) or an exact analysis time can be defined in the device's instructions.[55,66] However, this introduces an additional step that must be carefully monitored by the user, which is a potential source of error.

Another important aspect to consider is that PADs are often at least partially open to the environment and due to high surface area of paper, the impact of sample evaporation is significant. Although the open channel system can provide an advantage (e.g. to achieve analyte concentration),[67] it makes the device's performance highly dependent on ambient conditions (humidity, temperature). Moreover, due to the good adsorbent properties of paper, the risk of contamination can be significant. Therefore, enclosing methods are often applied for functional devices intended for the real-world use.[15] The most popular among them is laminating the PAD with plastic films, which also improves the mechanical strength of the device.[15,68] Alternatively, a laser-printer can be used to print a layer of toner, or the device can be covered with a layer of wax.[42] However, the influence of these methods on the device's flow characteristics and on any deposited reagents must be considered. Moreover, the device cannot be fully enclosed, since sample addition and detection areas must remain accessible to perform the analysis. Finally, this also means that a further fabrication step needs to be included into the production, and the biodegradability and ease of disposal of the PAD may decrease (e.g. in case of lamination).

2.3.5 Advanced flow control

As discussed in Sections 2.2.1 and 2.3.2, the liquid flow in PADs is mostly determined by selecting the paper with the desired porosity, pore size and thickness, and by forming a two-dimensional channel structure into it. However, techniques for improved wicking control have also been employed that allow for more complicated flow systems, precise timing and the ability to perform multiple steps sequentially or in parallel. For instance, by stacking several layers of paper with adhesive on top of each other (e.g. with double-sided tape like in **Figure 5a**), three-dimensional (3D) designs have been incorporated into PADs.[15,65,69] Their advantage is the possibility to create more complex channel systems that can lead to increased sample throughput or more multiplexed analysis without significantly increasing the device's dimensions. In addition to simply stacking, paper allows for folding, bending or twisting to realise the 3D designs.[16] This has been utilised with origami PADs that can be constructed from a single piece of paper, without additional adhesives and possibly allowing for faster and cheaper assembly.[70] However, their manual fabrication procedure and issues with reproducibility have been identified as potential drawbacks.[32]

Another approach for improved flow control in PADs involves using valves and switches to slow, redirect or turn off (or on) the liquid flow in some parts of the system.[16,71] These valves can either operate passively or require some stimuli from the user or external instrumentation for activation. For example, mechanically operated valves usually rely on connecting (or disconnecting) two hydrophilic channel parts of the system (**Figure 5b**) and this connection can be made by folding, sliding, rotating or pushing some specific parts of the device. Although they are simple to operate, an additional step is needed from the user that can require precise movement or timing. This activation can be automated by integrating simple electronic circuits with the PADs that can be connected to microcontrollers and potentially even further wirelessly to smartphones.[72] In this way, timed activation of linear actuators, electromagnetic field or local heating can take place without direct external intervention. However, this also increases the complexity and cost of the devices.

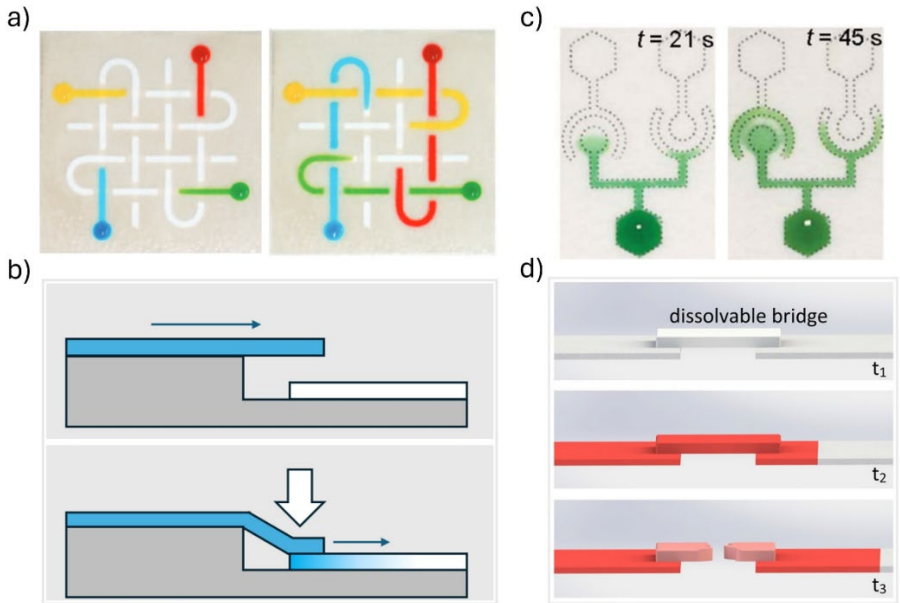

Figure 5. Examples of advanced flow control. **a)** Top view of a 3D PAD at different timepoints, liquids can pass each other at different levels of the device. Adapted with permission from [69], copyright 2008 National Academy of Sciences, U.S.A. **b)** Depiction of mechanically operated valve. When pressure is applied on the top layer, a connection is made, and liquid can pass through to the second layer. The blue arrow shows the elution direction. **c)** A demonstration of a diode valve, where liquid can only pass through the system in one direction. Used with permission of Royal Society of Chemistry from [73], permission conveyed through Copyright Clearance Center, Inc. **d)** Depiction of an erodible bridge that allows for the liquid to pass through for a limited amount of time. Reprinted with permission from [74], copyright 2013 American Chemical Society.

Alternatively, passively operated valves are often the preferred choice for PADs, since they do not need user intervention or external devices to function. The prevalent examples are dissolvable barriers, made of sugar or polymers that delay or slow down the liquid flow until the barrier is dissolved.[75] This approach can provide fine-tuning of the flow speed by simply varying the concentration of the barrier. Another example, using surfactants, demonstrated a diode valve (**Figure 5c**) that allowed only one-directional flow through the system.[73] Furthermore, erodible bridges (**Figure 5d**) work on similar principle and can be used to stop the liquid flow after a certain amount of liquid has passed through the system and dissolved the bridge.[74,76] Besides precise reagent addition, they can be beneficial for controlling the sample volume that is allowed to pass through the system for analysis. Moreover, absorption-based valves, where swelling of material causes an attached paper strip to break and automatically create flow connections in the system, can also be regarded passive, since no external intervention is needed.[71] Despite allowing completely self-contained analysis devices, one potential

drawback of some of the passive valves can be the extended activation time, especially if multiple valves are needed in the system. In addition, allowing for excessive amounts of the barrier or bridge material to pass through the system can also create inconsistencies in the liquid flow and interfere with subsequent steps on the test (e.g. create artefacts for the colorimetric detection).[16]

2.4 Improved analysis with PADs

The working principle of dipsticks and LFAs is relatively straightforward, and it consist of one directional flow of sample through the test, followed by a visual signal readout for qualitative results. However, this also limits the currently available tests, as they require relatively selective and sensitive reagents to be applicable for real-world samples, and such reagents mostly do not exist. To overcome this barrier, one or more routine laboratory analysis techniques can be combined within a single test to widen their applicability and improve the performance.[18,32] These techniques include sample preparation approaches such as preconditioning, filtration, preconcentration (and purification) and chromatographic separation. Furthermore, the combination of these techniques, as well as using semi-quantitative or quantitative signal readout, can significantly improve the analysis. In the following section, these aspects are discussed in detail.

2.4.1 Main sample preparation techniques

Sample preconditioning is necessary to compensate for variances from external factors and to provide similar conditions for different samples during the analysis. This includes adjusting sample pH, masking potentially interfering components or adjusting some other conditions (e.g. introducing an oxidising or reducing agent). For instance, with many LFAs, liquid buffer mixtures are included in the package that must be mixed with the sample before applying it to the test. Similarly, the reagents can be stored in powder form and dissolved in the sample before applying it on the test. The disadvantage of having separate conditioning reagents is that it introduces an extra step for the user, which might increase user-related errors. Alternatively, pretreatment regions can be located already in the device between the sample addition and detection areas.[54,65] The preconditioning reagents will be dissolved after the sample is applied to the test and the conditioning step can take place. This makes the tests simpler, and sequential conditioning is also possible by having multiple preconditioning zones. As a disadvantage, however, this kind of storage might be unsuitable for some reagents due to their instability. Moreover, the migration and undesired mixing of reagents can occur, or the efficiency of the conditioning step may be lowered, if extended conditioning times are required.

Filtration involves separating solid components from the liquid sample phase by using a membrane which is passable to liquids, but particles that are bigger than the open porous network of the membrane are retained. It is an important

step to guarantee the homogeneity of the sample and is needed, for instance, with various environmental samples that may contain precipitates (e.g. sand or dirt particles). In the case of conventional LOC devices, this is essential, because the channels can otherwise become clogged.[77] However, in the case of PADs, the porous network can already act as the filter itself in most cases. In addition, filtration is critical in medical diagnostics for separating blood cells from the plasma in whole blood samples. With PADs this mostly involves integrating a blood separation membrane over the sample addition zone, which allows only plasma to flow further into the device and be susceptible to analysis.[78]

Preconcentration is often needed for PADs to make them usable for real-world samples and especially for the analysis of trace compounds. Although different concentration strategies for PADs have been demonstrated such as isotachophoresis[79] and repeated sample addition[80], solid phase extraction (SPE) could be considered a more versatile and effective approach for this purpose. It involves using a membrane, column or a region in the test that has strong affinity towards the analyte, which is retained on the SPE material. At the same time, most of the sample matrix is passed through the membrane (with the exception of compounds that have similar chemical properties to the analyte), resulting in purifying and concentrating the analytes. The SPE region can be additionally washed to remove any residual parts of the sample matrix or even some of the less strongly adhered compounds. Finally, a stronger eluent is used to remove the retained components from the SPE material for further sample preparation or detection. The basic steps of SPE are depicted in **Figure 6a**. The choice and combination of the SPE material and the eluent (including its pH) are critical for achieving the necessary separation and preconcentration. In general, strong cation- or anion-exchange resins, or alternatively C8- or C18-functionalised surfaces are used for the SPE material.

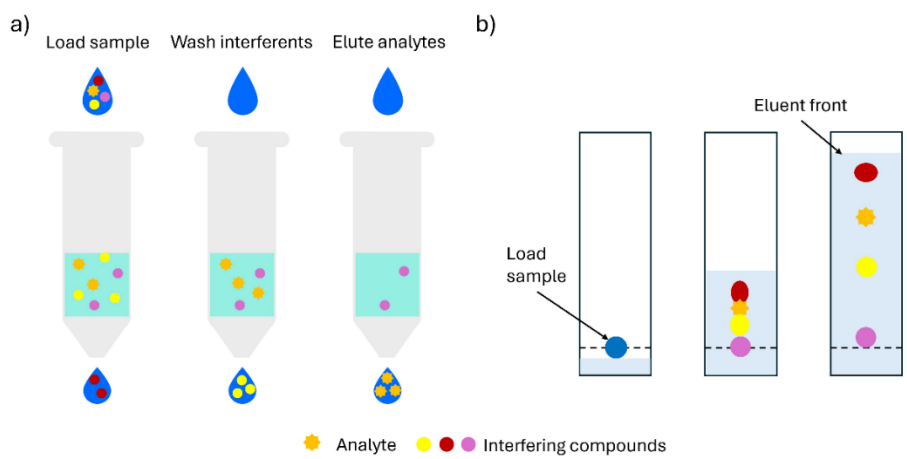

Figure 6. Illustrations of different sample preparation techniques. **a)** Main steps of SPE for analyte purification and preconcentration. **b)** Working principle of TLC for the separation of analytes from interfering compounds.

Currently in most articles where PADs are demonstrated with SPE, the SPE part has been separate from the test, i.e. as a syringe filter or a column, which allows high volumes of liquid to pass through in relatively short time. For instance, Cu^{2+} ions were retained with sulfonated poly(styrene-divinylbenzene) microspheres in a column and then selectively eluted to the PAD for detection using oxalic acid.[81] Similarly, Pb^{2+} ions were preconcentrated from 25 ml of sample using a peristaltic pump and a zirconium silicate coated filter paper disk, which was then integrated with a PAD system for analysis.[82] Despite the separate SPE part and need for more input from the user, these systems can still be regarded as low cost and portable. However, the need for multiple eluents and high sample volumes makes performing the analysis more complicated for non-experts and increases the analysis time.

Alternatively, instead of performing a full SPE procedure, systems where the analyte ions are directly captured (and detected) at the sample addition area could be considered to incorporate a simplified SPE step. This was demonstrated by Hofstetter et al., where different metals were quantified based on the diameter of the spot of the formed coloured complex.[83] This resembles simple testing strips or cards, but the analyte ions are concentrated from a larger sample volume and, if needed, a washing step could be implemented for purification. Furthermore, distance-based PADs for transition metals (discussed below in more detail) apply similar principles.[55] However they are regarded as an example of complexation chromatography in terms of this work since the sample application area is still separate from the capturing region. Finally, although these examples seem promising, highly specific and sensitive indicators that form coloured complexes with the analytes and can be uniformly immobilised on the substrate are rare.

Implementing chromatography within LOC devices has been demonstrated to separate otherwise similar and interfering ions or molecules from each other to improve the selectivity.[84,85] Although in case of conventional devices this involves usually liquid chromatography, for paper-based or other porous material based systems, paper chromatography or thin layer chromatography (TLC) can be used. The general principle is based on variable interaction strength of different ions or molecules to the stationary and mobile phases as can be seen in **Figure 6b**. In case of normal cellulose paper, the hydroxyl groups on the surface favour the adhesion of positively charged species while anionic compounds elute more easily with the mobile phase. However, with functionalisation of the surface or by choosing different substrate material, this interaction can be varied and tuned to specific needs. Similarly, the composition of the mobile phase, its pH and ionic strength can be varied for this purpose. With chromatographic separation, less specific detection reagents that have high sensitivity (e.g. dithizone (DTZ) or 1-(2-pyridylazo)-2-naphthol (PAN) for colorimetric detection of metal cations)[86] can be applied without the need to combine different masking agents. The complication of integrating chromatography with PADs is that, for colorimetric detection, the visualisation reagents are usually sprayed or pipetted directly on the spot where the analyte is on the chromatographic material. This means that additional reagents must be applied for the detection by the user and

the results can be complicated to interpret as well as provide only qualitative information. Nevertheless, several implementations of chromatography with PADs have been demonstrated that have managed to overcome this issue.

An example of paper chromatography with PADs was demonstrated essentially in the first PAD by Müller and Glegg, who separated different coloured dyes and detected the variances in transmittance over a section of the separation channel.[46] The combination of silica gel based TLC and PADs has been demonstrated for the determination of capsaicinoids in chilli samples; however, this approach involved cutting out a specific part of the TLC strip after the analyte had been separated from other components and combining it with PAD for colorimetric detection.[87] Alternatively, using amperometry has shown great promise, since electrodes can be directly integrated with the chromatographic separation channel, and the current in the channel's cross-section can be monitored for detection. These examples showed successful separation and detection of ascorbic acid and dopamine[85] and paracetamol and 4-aminophenol[88] with PADs. In addition to separating the analytes in one direction, two-dimensional chromatography can be applied for even better separation. In that case, two different mobile phases or also solid phases are used that allow to separate significantly more components (e.g. amino acids) in complex mixtures.[89,90] However, realising this step in a completely integrated PAD format which includes detection is very difficult.

Finally, instead of using the general surface chemistry and electrostatic interactions for separation, more specific types of chromatography have also been applied with PADs. These involve specific capturing of analyte species from the sample via affinity or complexation chromatography and separating compounds based on their molecular size via size exclusion chromatography. For instance, LFAs are an example of affinity chromatography where the immobilised antibodies specifically bind analytes. Another case is distance-based PADs for measuring metal cations, which can be regarded as an example of complexation chromatography.[55,91] They utilise immobilised or insoluble reagents on the paper surface that capture analyte metals from the passing sample flow, which usually results in the change of colour, allowing for the detection of the analyte species.

2.4.2 Detection strategies

With the goal of performing the analysis on the spot, no bulky, complex and expensive instrumentation should be involved. It has been previously noted that for successful real-world application of microfluidic technologies, the need for dedicated external instrumentation should be eliminated.[12,92] This means that different optical and especially colour-based methods are often preferred due to their simplicity. Interpreting colorimetric signals is also intuitive (i.e. colour means "yes" or a bigger area/higher intensity means higher concentration), making this approach well-suited for end-users. In addition, the white background of paper provides the additional benefit of good contrast for detecting reflected colorimetric signals. The principle to obtain the coloured signals on PADs mostly involves metal-ligand complexation, pH-induced colour change, aggregation of

nanoparticles and enzymatic conversion of chromogenic substrates.[16] Moreover, different types of signal readout have been demonstrated with PADs, and it can be qualitative (providing simply yes-no answer), semiquantitative (giving an estimate of the analyte concentration range), or quantitative (providing a specific numerical value).

In the case of qualitative (and semi-quantitative) results, the readout is usually achieved without any external instrumentation, making it especially promising for commercial applications. Pregnancy and COVID LFA tests are well-known examples where qualitative binary signal readout is used. In the case of chemical analysis, this would allow one to quickly determine whether an analyte (e.g. contaminant, toxic reagent) is present in the sample at a certain limit (e.g. regulatory limit) or not. Moreover, several semi-quantitative approaches have been developed that give additional information about the analyte concentration while still remaining instrument-free. Examples of this kind of systems can be counting-, distance-, radius- or timing-based.[16,66] For example, distance-based detection resembles an analogue thermometer, where the length of the formed coloured complex can be measured with a ruler or compared to an adjacent scale indicating the analyte concentration.[55,91] Despite their simplicity, these approaches still lack accuracy and can suffer from interpretation bias of the results.

For quantitative results, a calibration curve of the colorimetric signals to specific concentration values must be established. This means that digitalisation of the signal is required first, followed by image analysis with a computer-based software. Then the analyte concentration in the sample can be interpolated or extrapolated based on the calibration curve. To obtain the signals, different imaging devices shown in **Figure 7** (digital camera, scanner, smartphone) have been used with PADs.[93] Despite the need for an auxiliary device, they are relatively widespread (even in developing countries) and their use does not require much specific knowledge. This applies especially for smartphones, which in addition to taking high quality images, allow to perform the image processing and interpretation immediately by uploading the image or using a dedicated application.[94] The application could also adjust the imaging parameters (white balance, saturation, etc) to increase the repeatability of the results.

On the other hand, the widespread availability of smartphones raises some issues as well.[94] There are many different manufacturers and models, varying the camera placement and its intrinsic properties. Moreover, the relative placement with the PAD and ambient lighting conditions can have a significant effect on the results. To compensate for these shortcomings, customised devices are often employed with PADs.[95,96] However, this raises the need for auxiliary components and increases the analysis costs especially for a single analysis. As an alternative, flatbed scanners have been seen as more reliable signal readout devices. The scanners provide constant lighting conditions, and the distance between the scanner bed and detection area is always constant (although it does set a limitation to the device design).[16] The main drawback for scanners is their narrower availability and the need to connect with a computer for performing the image analysis.

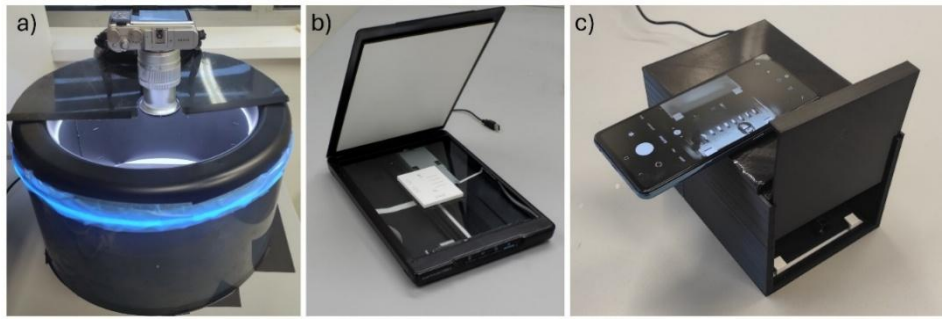

Figure 7. Different imaging devices for quantitative signal readout. **a)** Digital camera setup with controlled placement and lighting; **b)** Portable flat-bed scanner; **c)** Smartphone with a 3D-printed lightbox. All these setups were used for different application examples developed in this work.

Since the focus in this work is mostly on colorimetric detection strategies, only a brief introduction to other relevant approaches based on comprehensive review articles is provided.[16,51,93] For instance, fluorescence signal readout has been demonstrated with the benefit of higher sensitivities; however, a UV light source is required for the analysis. Moreover, the placement and consistency of the light source is even more crucial. Alternatively, another highly versatile group of methods is electrochemical detection methods. Different measurement techniques involve voltammetry, amperometry and potentiometry. In general, their advantages over colorimetric detection are faster analysis times, more reliable sample readout (i.e. not dependent on ambient light conditions and placement) and the colour of the sample does not interfere with the device. At the same time, electrodes must be often incorporated with the PAD (e.g. with screen printing a conductive ink) and external signal readout devices (e.g. potentiostats) are needed. Completely incorporated systems have also been demonstrated; however, the complexity and cost of these devices inevitably increase.[97,98]

2.4.3 Multi-functional devices

In this work, multi-functionalisation is defined as multiplexing (i.e. analysis of more than one analyte on the same test) and achieving multi-step analysis on a single test. Multiplexing is especially appealing for many screening applications where multiple compounds such as minerals, vitamins or metabolites need to be regularly monitored. Using a single device saves time, labour and money while providing more comprehensive overview of the sample. A good representation of multiplexing has been realised with commercial urine testing strips such as One+Step DUS 10 in **Figure 1a**, which allows to simultaneously monitor 10 different analytes.[43] In the case of PADs, multiplexing allows more complex analysis, since the two-dimensional structure can divide the sample from one inlet between multiple surrounding channels for various analyte detections like in

Figure 4a. This can help to limit compatibility issues between the reagents used in different channels as they do not mix this way. The multi-armed approach has been demonstrated for simultaneous detection of different metal cations, as well as other analytes (pH, glucose, proteins).[47,65] Furthermore, 3D PADs have been shown to offer even bigger potential for multiplexing, since multiple levels can be used to fit the channels around one sample inlet.[99] Finally, although PADs allow performing multiple parallel analyses with the same device, the overall complexity of the device (e.g. through the number of reagents) still increases with each analyte.

The second approach to multi-functionalisation involves performing multi-step analysis with the PADs. This is prevalent in the case of bioanalytical assays, since methods such as enzyme-linked immunosorbent assays (ELISA) or nucleic acid amplification tests (NAAT) require multiple analysis steps (e.g. sample loading, washing and sequential reagent introduction). Similarly, to fully incorporate some laboratory analysis methods (e.g. TLC or SPE) into the PADs, multiple reagents (or eluents) and their sequential delivery is also required. It must be noted that in the literature, the definition of a multi-step analysis can vary, and the examples where a blood separation membrane or pretreatment regions were incorporated to PADs are often regarded as multi-step. However, in terms of this work, they are still considered as single-step devices, since only one liquid with mostly the same composition passes through the entire test in a continuous manner. Similarly, in cases where a SPE step or a TLC separation was performed first,[81,87] the analysis did consist of multiple steps, but the PAD itself was still single-step.

The feasibility of multi-step analysis with PADs has been demonstrated on several occasions with sequential reagent delivery.[100,101] In those instances, different pure liquids or liquids with additional reagents passed sequentially through the same region of the PAD, and the sequential arrival was achieved by different channel lengths and designs. Similarly, by dividing the sample between different channels and controlling the channel geometry, an automated sandwich ELISA has been demonstrated on PADs.[102] However, these examples are mostly illustrative or applicable only for specific applications. For more robust and universal systems, using valving techniques to control the flow in the device and precise timing of different steps is needed. This has been shown with devices that implement sliding valves to perform the multi-step NAAT or ELISA assays on PADs.[103,104] However, despite the simple operation principle and compact device, most of the steps are still performed manually, which involves multiple external solution additions. Alternatively, a fully integrated multi-step PAD (with minimal steps for the user) has been developed,[62] but in this case, the test demanded significant additional components and the device increased in structural complexity.

2.4.4 Balancing device performance, complexity and cost

Although multi-functionalisation of PADs has a promising outlook and can turn these devices into useful tools for on-site analysis, it inherently increases device complexity, cost and reduces robustness. These factors, however, are all crucial for mass-producible devices intended for wide use. Moreover, even simpler PADs, currently cannot meet all the goals of ASSURED or REASSURED simultaneously. This further emphasises the need to investigate alternative directions for device production, including alternatives to paper as the base material, so that trade-offs in crucial characteristics can be avoided.

In the current work, it is envisioned that the tests must simultaneously achieve (1) sufficient analytical performance for their application, (2) portability and ease of use, and (3) low production costs. To achieve low cost, both the materials used and the production method (which must be scalable to high-volume production) must be considered. With that goal in mind, the focus in this work is put on developing novel passive flow-based microfluidic systems. Relying on passive liquid flow can help to keep the material and production costs low, since no external pumps, power sources or intricate electronic circuits are inherently needed. Similarly, this contributes to the device's portability, robustness and ease of use. Furthermore, using common materials and low reagent amounts makes the devices easily disposable and environmentally friendly. Although reaching the necessary sensitivity and selectivity can be more difficult, incorporating simplified additional analysis steps (e.g. SPE or a form of chromatography) can greatly contribute to the analytical performance while not excessively jeopardizing other device aspects.

Finally, one further drawback of relying on passive flow is increased analysis time, especially with larger sample volumes or multi-step analysis. However, even analysis times in the range of several hours for screening applications are still considerably faster than collecting and delivering the sample to a laboratory and receiving an answer. In addition, ways to automate the multi-step analysis will be investigated so that the user involvement can be still limited to adding the sample to the test and, in the end, performing the detection and interpretation of the results. This way, the hands-on time of the tests remains minimal, and the devices are also less prone to user-dependent errors.

3. RESEARCH AIM AND HYPOTHESES

The general research **aim** for this thesis was to develop alternative materials and production methods to paper-based analysis devices and demonstrate their superiority with real-world samples.

Based on this aim, the following **hypotheses** were set:

1. Methods to produce capillary-driven microfluidic chips from alternative materials to paper can be developed.
2. These methods provide the possibility to (1) combine different materials for different functionality on a single chip, (2) enable rapid prototyping, and (3) facilitate eventual mass production.
3. The chips produced with these methods can provide higher analytical performance (i.e. selectivity and sensitivity) than paper-based devices while maintaining the simplicity and low cost of analysis.

4. EXPERIMENTAL

Screen printing (SP) was the main production method throughout the entire thesis and a detailed protocol of the process, which was used in publications II-V, is provided in the following section. Furthermore, the main approaches used for characterisation of the printed material are introduced. The devices and other elements necessary to perform the analysis with the microfluidic chips are briefly described.

4.1 Screen printing

SP is used to print a paste consisting of silica gel particles and a binding agent solution, onto a smooth substrate plate (usually a glass microscope slide). As the paste dries, the binding agent (or binder) binds the particles into a mechanically stable material that adheres reliably to the substrate. The printed material on the substrate is referenced to in this work as a chip. The material wets spontaneously by capillary forces (similarly to paper), and it retains its position and shape. SP allows to print the paste in any pattern and therefore this method can be used to form microfluidic chips.

The binding agent solution was prepared by dissolving 400 mg of binder (xanthan gum (XG)) in 100 ml of deionised water. The solution was mixed with a magnetic stirrer for several hours and initially slightly heated on a hotplate, until a homogeneous mixture was achieved. Afterwards, the solution was stored in a refrigerator at 4 °C, and a new solution was prepared every two weeks. The printing paste was freshly prepared before printing by weighing the particles and adding a necessary amount of the XG solution. In case of regular silica particles (size range 15–25 μm), the printing paste was typically made by mixing 4.7 grams of silica gel particles with 10 ml of the XG solution. Due to the high viscosity, the solution amount was verified gravimetrically. The particles and binding agent solution were thoroughly mixed by hand until a homogeneous paste was obtained.

The process of preparing the stencil on the screen is depicted in **Figure 8a**. The design was created in Cricut Design Space and it was cut into removable adhesive vinyl (ORACLE 641) using Cricut Joy cutting machine. The vinyl was applied onto the screen using a weakly adhesive transfer tape that helped keep all design elements in their correct positions. Aluminium frame screens with mesh stretched at 45-degree angle from Seritek OÜ were used, and the mesh opening was mostly 142 μm in case of regular silica particles. The screen was fixed to a table with hinges, which allowed moving the screen when placing the substrate underneath it. This setup maintained the relative placement of the stencil and substrate even when placing a new glass slide under the screen. The gap distance (the distance between the mesh and substrate surface) was set to 2.2 mm by placing 3D-printed spacers under the corners of the screen.

Before printing, the substrate was secured at the edges with adhesive tape onto the table or a special 3D-printed holder. Besides fixing the lateral position of the substrate, taping prevented the substrates from sticking to the screen during

printing. The printing process is depicted in **Figure 8b** and **c**. Before printing, a portion of the paste was applied onto the screen with a spoon. The screen was then flooded – i.e. the paste was spread over the stencil openings with the squeegee. During flooding movement, only slight pressure was applied to the screen compared to the printing movement so that no paste was printed but all free mesh openings were uniformly filled. The printing step was always performed in the same direction, and flooding was usually done in the opposite direction after each printing stroke. For each chip, usually at least two layers were printed on top of each other to improve material uniformity and increase thickness. In the case of the iron and copper test (publication IV), around 40 chips were printed during one printing session (ca. 40 minutes) using 10 ml of paste. After printing, the chips were dried in an oven at 90–110 °C for two hours.

It is important to note that the applied pressure and movement speed of squeegee, as well as its angle, all affect the outcome of the SP. Therefore, in manual printing, the results are highly operator dependent.

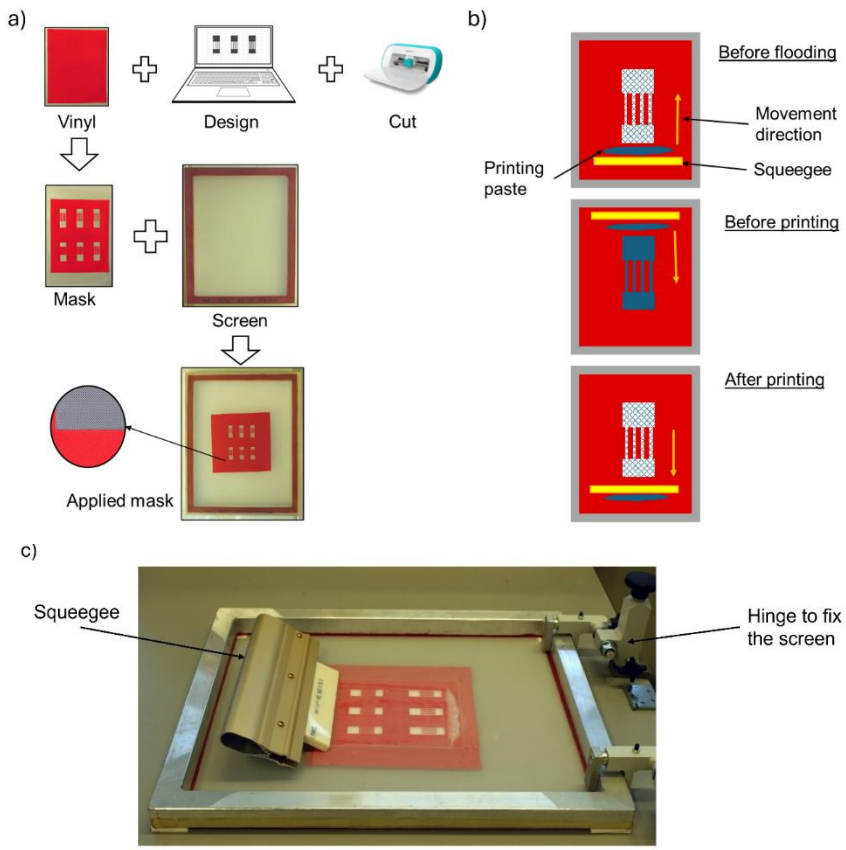

Figure 8. The setup and main steps of the SP process. **a)** Steps for preparing the screen; **b)** Steps during the printing process, based on squeegee movement. **c)** Picture of the printing setup.

4.2 Characterisation of the printed material

The main quality control of the printed chips was visual, by estimating the uniformity of the material and its accordance with the designed shape (i.e. ensuring that no defects were present). For more quantitative validation, especially for the specific applications developed in this work, the printed material thicknesses were measured after drying with a digital micrometre. This was done by covering the chip with a bare microscope slide and then measuring the total thickness of the setup as well as that of the substrate and slide individually. The thickness was measured at multiple locations over the length of the chip, since thickness gradients in the printed material, as well as in the microscope slides themselves, occasionally occurred.

During the initial development, determination of the wetting rate of the chips with different compositions was performed for comparison. This involved immersing an edge of the printed material into a coloured water solution and then determining the time it took for the liquid to wick through a fixed distance (2 cm) of the material. The more detailed protocol of the process and the results are presented in publications I and II.

4.3 Other equipment and software

Different imaging devices for colorimetric signal readout were used throughout this work, including a digital camera (Fujifilm X-A3 with XC 16–50 mm objective), a smartphone (Samsung Galaxy A52) and several flatbed office scanners (Plustek OpticSlim 550 Plus, Epson Perfection V39II and V600). Examples of these devices and their setups can be seen in **Figure 7**. For fluorescence signal detection, a custom 3D-printed reader box was built. Two UV LED lights and their electrical circuit, powered by an external AC outlet was incorporated into the reader. Signal readout was performed by placing a smartphone on top of the box and aligning the camera with an opening on top of the reader.

ImageJ image processing software was used to quantify signals from all the images. In general, this involved cropping out a region of interest that contained the detection area and splitting it into red, green and blue colour channels. Then, the channels were combined or subtracted in a way that yielded maximally sensitive and selective results for each analyte. The specific protocols are described in the Supplementary information of publications II, III and IV.

An Ender 5 Pro 3D printer with poly(lactic acid) (PLA) filaments was used to produce various elements throughout this work. In addition to the test components demonstrated in publications III and IV, other specially designed parts included holders for microscope slides and spacers in the SP setup. Furthermore, all stamps for testing alternative printing techniques and elements for the automated reservoir release and valve connections (publication VI) were 3D printed. All 3D-printed elements were designed using SolidWorks engineering software.

5. RESULTS AND DISCUSSION

5.1 Investigating different materials and fabrication methods

Capillary flow in porous materials was seen as the most promising approach for creating simple, compact and inexpensive chemical analysis tests. Although paper has numerous great characteristics as the base material, it also exhibits several drawbacks that limit the achievable analytical performance and repeatability with the devices (see Section 2.3.1). For this reason, various alternative materials and patterning approaches were investigated that could offer an alternative to PADs. The focus was on maintaining the simplicity of analysis, low cost of materials, and suitability for later mass production. At the same time, the production method should provide precise control over the material shape and thickness, and allow adjustments to the pore size. In PADs, these last two parameters can only be altered by initially selecting different paper sheets. However, since all these characteristics are essential for precise flow control in microfluidic devices, it would be beneficial to be able to control them during the device production. Therefore, instead of shaping pre-existing sheet materials, the fabrication steps should enable the formation of porous material in the desired shape from smaller base components. This approach would result in more effective use of materials as only the functional chip regions are produced, while the surrounding barriers remain void (similar to PADs made by cutting). In addition, this way the chips are compatible with wider variety of reagents, as the penetration or destruction of channel barriers by organic solvents is avoided. Although this increases the need for a substrate to support to the porous material, enclosing the porous material is typically required for functional devices.

In publication I, two types of base components were investigated to fulfil that function. One option involved using monomers that could be selectively polymerised, resulting in a porous polymer monolith with the desired shape. For this, thiol-ene click chemistry monomers in methanol were used, where methanol acted as the porogen in the mixture – i.e. it dissolved the monomers but not the formed polymer. Therefore, by varying the monomer mixture composition, the resulting material porosity could be controlled. The second approach could be classified as "particle-based," where silica microparticles were used to form a continuous material with an extensive open pore network between the particles. The material retained the desired shape due to binding agents that held the particles together and also adhered them to the substrate surface. Gypsum, similar to common TLC plates, and polyvinyl acetate were used as the binders. The porosity and surface chemistry of the formed material could be controlled by selecting particles (and binders) with different properties (size, functional groups, etc.).

To give the resulting material a desired shape, common PAD patterning techniques were implemented. In the case of monomers, a masking technique was needed to selectively cure the polymer and since this could be achieved with UV

light, PL was chosen for patterning the material. For particle-based materials (PBM), two different printing techniques, screen printing (SP) and direct write printing (DWP), were used. While the basics of SP are extensively described in Section 4.1, DWP involved using a modified extrusion-based 3D printer to deposit the particle mixture onto a substrate. The initial objective with all the fabrication techniques was to demonstrate that any geometry could be created in a single production step. A design with multiple parallel channels connecting two larger rectangular areas was chosen as the test pattern. This allowed to determine the resolution (i.e. the minimal achievable width of channels or elements) and accuracy (how closely the printed result matches the design) of each approach by varying the channel widths. It also made it possible to assess the uniformity of the material across broader flat regions. The main characteristics and results are summarised in **Table 1**.

In general, the production of porous materials with controlled shape, suitable for capillary flow-based microfluidic systems, was possible with all three approaches. The overall dimensions and porosity of the chips were also comparable to PADs, while the wetting rates were significantly improved (compared to ordinary Whatman grade 1 filter paper). However, the achievable resolution and repeatability of the chips were mostly sufficient only at the proof-of-concept stage. Furthermore, while all the materials were durable under ambient conditions and could withstand wetting with water, their structural integrity greatly relied on adhesion to the substrate. When comparing the different approaches, then PL offered potentially the most control over surface chemistry, and with selective exposure to UV light, the reactions could be precisely localised and manipulated. In the case of PBM, the surface chemistry could be mainly varied by selecting different particles, although subsequent surface modifications would remain possible. Regarding rapid prototyping and design flexibility, DWP had the distinctive advantage of allowing one to design the chip and begin production immediately, with minimal manual labour. However, in terms of production speed and potential mass production, SP was seen as the most promising option. In general, SP is already a well-established and relatively low-cost method for large-scale production in various fields. Moreover, it presented considerably fewer technical difficulties in achieving regular and repeatable results during the investigation compared to the other two methods. Therefore, SP of microparticles was chosen as the primary direction for further development.

Table 1. Comparison of the different fabricated porous materials

Example images Left image is of the produced chip; the right shows wetting experiment (with millimetre paper in the background).	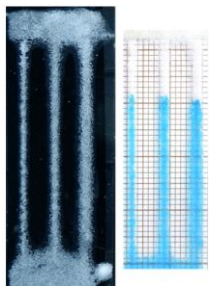	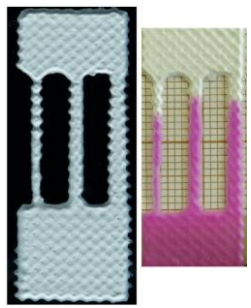	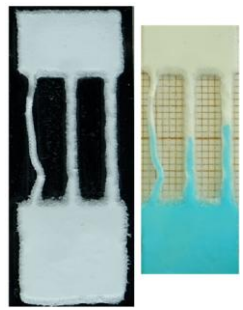	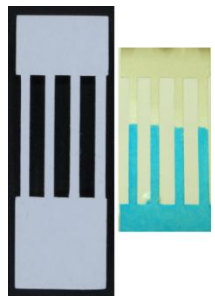
Production method	Direct write printing	Screen printing	Photolithography	Cutting machine*
Main components	Silica gel particles, polyvinyl acetate	Silica gel particles, gypsum	Thiol-ene click-chemistry monomers/ polymer	Filter paper (cellulose network)
Achieved resolution	2.3 (16% RSD) mm	2.7 (13% RSD) mm	2.1 (8% RSD) mm	ca. 0.2 mm
Wetting time	35.3s / 2cm	116s / 2cm	61.1 s/ 2cm	197 s/ 2cm
Estimated pore size (from SEM images)	34–215 µm	3–36 µm	1–9 µm	11 µm
Thickness	0.33 mm (14.8% RSD)	0.37 mm (3.8% RSD)	0.31 mm (6.8% RSD)	0.18 mm (2.0% RSD)
Main advantages	Quick prototyping	Easy to mass produce	Great control over surface chemistry and functionality	No substrate required

*PADs made from Whatman grade 1 filter paper with a cutting machine (Cricut Joy) were included in the comparison. Their resolution was based on the accuracy of the cutter determined in publication II. The porosity of the paper was stated by the manufacturer.

In addition to the three main production techniques, an alternative approach for PBM in the form of stamping was also considered. In this method, various stamps were 3D printed, and particle mixtures with different binders (gypsum, XG, etc.) were applied using them (see **Figure 9** for examples). While the approach worked for designs involving narrow channels, it proved unsuitable for covering larger areas. Moreover, the topography of the formed material was uneven, and repeatability was poor. Therefore, this approach was deemed unsuitable for the tested particle-based mixtures.

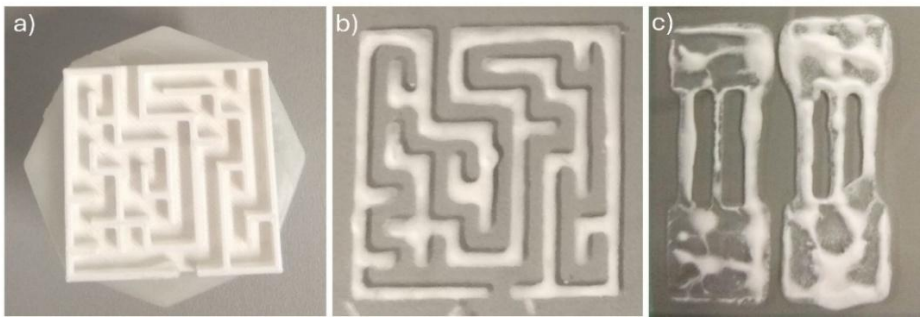

Figure 9. Examples with stamping approach. **a)** 3D-printed stamp fixed on a flask cap; **b)** Dried PBM on a glass substrate after stamping; **c)** Poor results with stamping in case of larger flat areas.

Finally, while the PBM approach for producing microfluidic devices could be considered relatively novel, a few related prior examples do exist. For instance, silica nanoparticles have been applied to form patterned nitrocellulose in relatively complex, multi-step procedure for fabricating microfluidic devices with unique optical properties.[105] Similarly, diatomite silica particles have been used to produce porous analytical devices that employ chromatographic separation for analysis.[106] However, in the latter example, the material patterning was achieved through a combination of spin-coating and tape-stripping, potentially limiting the range of possible designs and scalability for mass production. Moreover, during the writing of this thesis, at least one independent study utilising SP and microparticles was also published.[107] In that work, silica nanoparticles were combined with other materials (e.g. cellulose fibres, polyvinyl alcohol), and the benefit of directly incorporating screen-printed electrodes for detection was demonstrated.

5.2 Development of screen printing

Throughout this work several aspects of the SP process were investigated and improved. For instance, multiple key differences in the SP process can be seen when comparing the protocols used for publications I and II. This included both the printing mixture components and the printing setup. Moreover, different alternatives for the substrate material were considered.

5.2.1 Optimised printing paste

One of the main problems with SP in publication I was the rheopectic behaviour of the paste (i.e. thickening during printing). Despite the sufficiently small size of the silica particles, even with a screen that had over 30 times larger mesh openings, the paste quickly turned too viscous to pass through the mesh. This can be mainly attributed to the properties of gypsum and its crystallisation, which increase the paste's viscosity, especially when pressure is applied to it. Therefore, a different binding agent was needed – preferably one that displayed pseudoplastic (i.e. shear-thinning) properties. The particles themselves result in dilatant (i.e. shear-thickening) behaviour, and a binding agent with pseudoplastic properties could counter this. Ideally, the binding agent would serve both as a binder and a mixture thickener. The latter is needed to keep the paste homogeneous during printing (i.e. to prevent the particles from precipitating). At the same time the binding agent must hold the particles together in the dry state. Compounds that are water-soluble or dispersible and effective at low concentrations were preferred. This way, the resulting material properties would still be mostly determined by the particles, while the binder would have minimal influence on the flow processes. Water was preferred over other solvents due to its slower evaporation during the printing process, which helps limit changes in the paste viscosity. It is also safe for the equipment and operators. Finally, the water can be easily removed after printing by heating the chip over 100 °C for a short period of time.

Keeping these properties in mind, different polysaccharides (XG, guar gum, sodium alginate) were investigated as potential binding agents. Although all three provided satisfactory printing results, the material with XG (**Figure 10**) yielded the most consistent outcomes and was therefore selected as the replacement to gypsum. A detailed comparison of the tested binding agents is presented in publication II. Compared to gypsum-based mixtures, XG allowed to use screens with higher mesh densities, significantly improving printing resolution. Furthermore, the paste with XG enabled to print considerably longer designs in a single stroke, as shown in **Figure 11**, and it remained usable over extended periods. In the case of gypsum, only a few consecutive prints were possible, while no specific time limitation was observed for XG under optimal conditions, indicating its suitability for mass production. The differences were also evident in SEM images (**Figure 10**), as the XG-based material appeared more uniform and visibly consisted of only silica particles. In contrast, the gypsum-based mixture contained a significant amount of needle-like gypsum crystals. Finally, the XG-bound material was more durable when coming into contact with water and no flaking occurred even after prolonged submersion in a water bath. A comparison between SP results with the two different binders is provided in **Table 2**.

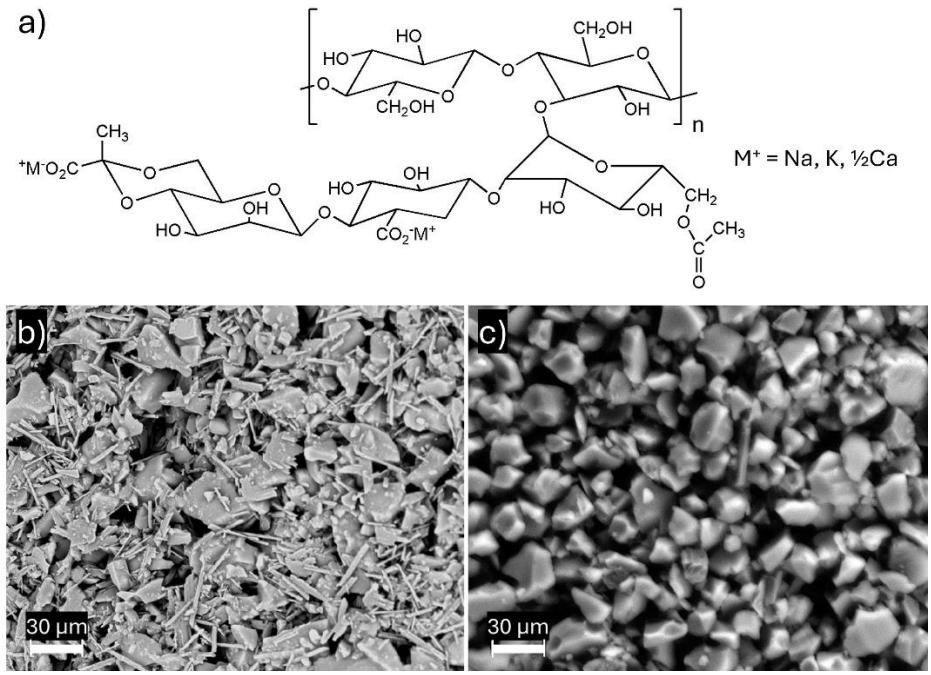

Figure 10. Replacement of the binder in the SP paste. **a)** Molecular structure of XG; **b)** SEM image of printed material using gypsum as the binder. Needle-like gypsum crystals are visible between the silica particles. **c)** SEM image of printed material using XG as the binder.

Table 2. Comparison of XG and gypsum-based printed materials.

Binder	Gypsum	XG
Particle size	3–36 µm *	15–25 µm
Screen mesh opening size	1100 µm	142 µm
Withstands long term submersion in water	No	Yes
Wetting time (/2 cm)	116.3 s	52.6s
1st layer thickness	370 µm	109 µm
Printing resolution	2.7 mm	0.5 mm
Accuracy	1.09 mm	0.2 mm

***** Estimated from the SEM image, since no specific information was provided on the package or information sheet.

One of the reasons for the good performance of the XG-based material was the strong adhesion both between the silica particles and XG, as well as between XG and the glass substrate. It has even been suggested in literature that covalent bond

formation may occur under certain conditions.[108,109] While the process was not investigated in detail, several observations supported the presence of strong adhesion. First, when the chips were submerged in water and left on an orbital shaker, the material remained firmly attached even after 24 hours. However, when the paste contained glycerol and the drying time was less than one hour, flakes of the material separated from the substrate (similar to the gypsum-based mixtures). Moreover, after washing the printed material off the substrate with a brush, a thin water layer retained the shape of the printed pattern, indicating residual surface interaction. Finally, when plastic substrates were tested, the material either detached immediately after drying or could be easily removed, whereas the printed structure itself remained intact, indicating strong cohesion between silica particles, but poor adhesion to the plastic surface.

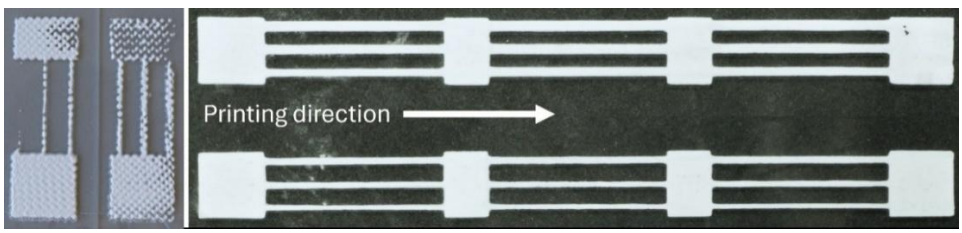

Figure 11. Change in printing paste viscosity during use. Left: gypsum-based paste; right: XG-based paste. Printing proceeded left to right. Images are at the same scale.

5.2.2 Advances in the screen printing process

Initially, in publication I, the stencil on the screen was formed using a UV-curable emulsion-based mask. However, this approach required emulsion to be washed off and reapplied even for minor design changes, making the entire process time-consuming and labour-intensive. To address this, vinyl-based adhesive masks were adopted for rapid prototyping. Once the design was ready on a computer, it could be cut with an automatic cutting machine and applied directly to the screen. This provided considerably faster and repeatable results. In general, using emulsion-based masks may offer greater accuracy and durability for mass production as they are less prone to peel off during long printing cycles. However, in terms of the current work, all the subsequent SP was carried out by using adhesive vinyl masks.

Another improvement in the SP process involved adjusting the gap distance (i.e. the space between the screen and the substrate while squeegee was not pressing on the screen). This was achieved by placing spacers with varying thicknesses under the screen corners. In publication I, a 0.25 mm gap was used, which resulted in the screen pressing into the freshly printed material (which was approximately 0.37 mm thick), imprinting the mesh pattern onto the material surface (**Table 1** SP example). In publication II, gap distances ranging from 0.3 mm to 3.2 mm were tested, and 2.2 mm was found to be optimal. This allowed

the screen to detach from the freshly printed material immediately after its formation, providing better control over the material thickness and resulting in a more uniform material surface.

Finally, the role of ambient relative humidity (RH) on both the printing process and the resulting material became apparent. Although the SP was conducted in the same laboratory at a stable temperature of around 20 °C, RH varied significantly – occasionally dropping below 20% in winter and rising up to 80% in summer. These fluctuations affected the drying rate of the paste during printing, which in turn influenced its viscosity and impacted the thickness and even the accuracy of the prints. To mitigate this, occasional spraying of deionised water onto the squeegee was used in later experiments. Although this helped to keep the paste consistency more uniform and prevent excessive drying, it introduced a subjective variable to the SP process. Alternatively, glycerol was also tested as an additive in publications II and III to slow drying, but it left residual content after drying that later eluted and interfered with the analysis. As a result, glycerol was omitted in the later stages of the work.

5.2.3 Substrate choice

Glass microscope slides (either 25 × 75 or 50 × 75 mm) were the primary substrates throughout this work. As discussed in Section 5.2.1, glass provided strong adhesion between the substrate and the printed material through XG. Moreover, glass is inexpensive, recyclable, heat-tolerant and chemically inert, making it suitable for various applications. While any glass surface could serve as a substrate, microscope slides offered additional benefits: low cost, availability, precleaned surfaces, consistent dimensions and a suitable size range. Nevertheless, for the biotin test in publication III, glass substrates had to be cut in the laboratory from larger sheets to accommodate the full design. The main drawback of glass was its brittleness, potentially limiting its use in some commercial applications. This became evident during test production for publication IV, where the sample addition zone had to be pressed firmly onto the chip, occasionally causing glass slides to break during assembly or analysis.

As alternative substrates, aluminium and various plastics were considered. In principle, any smooth surface can be used for SP. However, to withstand the drying step, the substrate must tolerate elevated temperatures (up to 100 °C). Moreover, the surface must be hydrophilic (e.g. contain hydroxyl groups) to ensure proper adhesion and retention of the printed material after drying. Among the tested plastics, polyethylene terephthalate (PET) did not withstand the drying process and began to warp, although the material remained adhered after drying. Polypropylene (PP), polycarbonate (PC) and TOPAS (cyclic olefin copolymer) tolerated the heat but showed weak adhesion of the printed material after drying. Aluminium sheets were suitable in terms of both temperature and surface properties although adhesion was weaker than with glass, especially when submerged in water. In addition, aluminium is opaque, which limits the options for colorimetric detection. Finally, the most promising alternative to glass proved to

be hydrophilised plastics. For this, commercial plasma-processed polycarbonate and TOPAS plastic slides were tested, and the results were comparable to glass slides.

5.2.4 Long term stability of the printed material

The long-term stability of the prepared tests was mainly investigated in the context of publication IV, using the iron and copper test. These tests were stored in a vacuum-sealed bags for up to one month and the results with tests after two days, two weeks and one month were compared. Over this period, no statistically significant differences in the tests' performance were observed.

One potential concern was the stability of the printed XG-containing material. A few weeks after production, the chips developed a noticeable odour, especially when water was applied to them. Since XG is a polysaccharide and silica gel readily absorbs moisture from the air, the material was assumed to be a good growth medium for yeast or bacteria. This was further supported by a resazurin test: older chips caused the applied reagent solution to turn pink immediately, while with freshly printed material the blue colour was retained. In general, storing the chips in a dry environment or under inert gas is expected to prevent the issue. This storage approach is also necessary to maintain consistent flow characteristics over time. Alternatively, additives that inhibit microbial growth could be included in the printed mixture, provided they do not interfere with the analytical performance.

5.3 Control over material properties

One important aspect and goal of combining microparticles and SP was to enable control over the resulting material properties. This applies both to the precise patterning and thickness of the material as well as to its physical and chemical characteristics. The latter can be adjusted by selecting particles with desired properties or by modifying their surface afterwards. Furthermore, unlike the commercially limited choices available for paper, SP allows multiple ways to control material thickness. This, combined with control over material shape, enables more precise manipulation of flow rates in the devices.

5.3.1 General chip design principles

As previously discussed, the more complex shapes that enable two-dimensional liquid flow control distinguish PADs from testing strips or LFAs. By controlling the shape of the porous material, multiple flow paths, timed liquid flow and reagent delivery can be achieved. In general, the same principles used in PADs were applied to the chips developed in this work. Examples of various chip designs that display some of these flow control principles are shown in **Figure 12a**.

An additional consideration in this work was the use of microscope slide substrates, which imposed certain size constraints. However, this also encouraged

the development of more compact and standardised devices, facilitating eventual mass production. In terms of porous material design, this meant incorporating turns into the channels to fit longer elements within the substrate dimensions. This was explored in publication II using an arch-shaped TLC strip (see Section 5.4.1) and in publication III with a 90-degree turn in the detection channel. While both approaches functioned as intended, care had to be taken to avoid compounds getting stuck in corners. This issue arises particularly with reagents that elute with the eluent front (e.g. biotin-5-fluorescein or biotin-F in the biotin test) – the compound can reach the corner and remain there, because the liquid in that area does not elute significantly after it wets the corner. To mitigate this, bevelled (i.e. sloped) corners and "funnels" were incorporated at transition points. The funnel shape also helped guide the entire analyte spot (which can be spread out after TLC) into a narrow channel. In addition, when liquid reservoirs were included in the test, wider rectangular areas of printed material were used to ensure full contact between the entire reservoir base and the porous material (see **Figure 18b**).

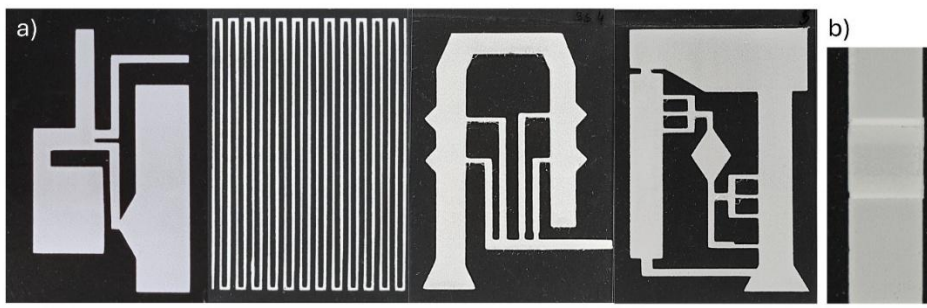

Figure 12. Chip examples with different designs. **a)** Printed chips with complex designs. All images are at the same scale with approximately 75 mm height. **b)** Chip with conjoined, separately printed regions. The middle square area (10 × 10 mm) was printed later between the surrounding regions.

The narrowest achievable channel width with the developed SP approach was 0.5 mm, and an accuracy of 0.2 mm could be achieved when adjusting the channel width. It should be noted that the accuracy mostly depended on the mask rather than the SP process itself. Nevertheless, complex miniature channel networks could be created on a single slide substrate. Moreover, it was observed throughout this work that intricate designs with multiple narrow flow channels are often not well suited to most real-world applications. To achieve sufficient sensitivity for most real samples, relatively high sample volumes are required, making the use of complex narrow channel systems often unsuitable or extremely time consuming. Similarly, accurate sample volume control in on-site applications is significantly more error-prone for small sample volumes. However, if these issues do not pose a problem, or if a preconcentration step can be performed beforehand,

the developed method can still be suitable for producing intricate miniature channel systems for analysis.

Finally, one further design aspect concerns printing different parts of the system in separate printing sessions (e.g. when printed materials with different compositions are needed on a single chip) to form a conjoined material, where elution continues smoothly from one section to the next. **Figures 12b** and **14a** show examples of such systems. Depending on the paste composition, multi-step printing can be performed either fully sequentially or with an intermediate drying step (i.e. drying the chip after printing the first part of the design). Accurate chip placement is critical for these designs to ensure proper alignment of the different parts. To achieve better connections between materials, a small overlap (e.g. 1 mm) between the regions is typically required. Alternatively, different parts can be connected manually by forcing the porous materials on separate substrates into contact with each other or with other porous materials (e.g. paper pads in publication IV). However, due to the softness of the printed material, it may detach from the substrate with this approach, especially when the material is wet.

5.3.2 The material thickness

The developed PBM approach with SP offers multiple ways to control the thickness of the printed material. This distinguishes it from most PADs, where the material shape can mainly be manipulated in two planar dimensions. However, the third dimension – thickness – plays a critical role in determining the flow characteristics of the devices. First, it determines the amount of liquid flowing through a cross-section of the chip at a given moment, significantly influencing the analysis time. Second, the total liquid capacitance of the microfluidic device is proportional to the material thickness. This is especially relevant given that a 10% increase in thickness amounts to only 0.02 mm of change in the case of 0.2 mm thick material, while the sample volume must increase by 10% to achieve the same result. Finally, material thickness affects the spreading of reagents and liquids during both chip production and analysis. This can have a major impact on the repeatability of the devices. For instance, with thicker materials, the diameter of the applied sample spot is smaller, which in turn affects the spreading and separation of analyte spots in TLC. Similarly, the area of pipetted colorimetric reagent spots on the porous material can vary, influencing colour intensity and potentially affecting result interpretation. Therefore, good control over the porous material thickness is essential to better manipulate the flow of different liquids in the devices and ensure their overall accuracy and repeatability.

The different parameters for controlling the thickness of the printed material were investigated in publication II. The methods included changing the mixture composition (particle size and their ratio to the binding agent solution), screen mesh density and the number of printed layers. However, other aspects of the SP setup and process can also have a considerable influence, such as the pressure and speed of the squeegee during printing, the gap distance and ambient room conditions. Although many of these factors can be kept relatively constant, the

manual nature of the printing process and lack of humidity control still led to variation in material thickness throughout this work. For instance, in the case of the chips in publication IV, the thickness varied between 190 and 300 µm using the same printing protocol. This variance had a significant impact on the analysis results through the factors discussed in the previous paragraph, and the usable thickness range was limited to 220–270 µm. Although this still encompassed around 20% variance in material thickness, the relative standard deviation (RSD) of the analysis results remained under 10% due to the applied detection principles. Finally, this emphasised the need to include material thickness measurement as a chip quality control measure.

In addition to the average thickness variation between replicate chips, there were also changes in thickness across a single chip. Most often, the thickness was higher at the upper part of the chip and gradually decreased along its length. This can be explained by the shear-thinning properties of the printing mixture, i.e. the viscosity of the paste slightly decreases during printing, leading to a change in thickness. This could possibly be reduced through further optimisation of the mixture composition. Moreover, since this thickness gradient was especially prominent when multiple layers were printed on top of each other, limiting the number of layers or altering the printing direction could help diminish the effect. An alternative approach would be to include a post-treatment step that scrapes off a thin layer from the top of the printed material at a constant height. Finally, if the entire printing procedure was performed in a fully controlled environment and automated (i.e. by using an SP machine), higher repeatability in material thickness would likely be achieved. Some preliminary investigations with an SP machine and similar pastes have already been conducted by our collaborating partners in Denmark. Based on their experiments, the variability in thickness appears to have been limited to an RSD of 5%.

5.3.3 Control over porosity and functionality of the printed material

The possibility to print particles with different sizes and the influence of this parameter on the resulting material characteristics were investigated in publication II. It was shown that different silica particles ranging from 5 to 142 µm in diameter could be used to produce printed materials with the desired shape using SP. This demonstrates that the porosity and wetting rate of the material can be controlled over a wide range. The wetting times for the same distance increased from 30 to 270 seconds depending on the particle size. It must be noted that for larger particles, a screen with bigger mesh openings had to be used to ensure that all of the paste passes through the screen mesh. However, this limits the achievable resolution of the chips, therefore less intricate designs can be made when using larger particles.

During the thesis work, several experiments with functionalised silica and other particle types were conducted. For functionalised silica, commercially available particles with both weak and strong cation- and anion-exchange sur-

faces were printed. The functional surface groups included 3-carboxypropyl (PCA), 3-sulfopropyl (PSA), quaternary ammonium and primary amine (aminopropyl). In addition to obtaining material with the desired shape, the surface functionality was confirmed by capturing either cations or anions onto the functionalised surface. This is discussed in more detail in Section 5.4.3. Furthermore, silica particles with C18 surface groups were also successfully printed. In this case, achieving a homogeneous mixture with the XG solution required more time, and initial prints were not completely uniform, containing several holes. However, the material adhered to the substrate and displayed hydrophobic properties, showing the potential for integrating this type of particle within the chips. Demonstrations of printed materials with different particles are presented in **Figure 13**.

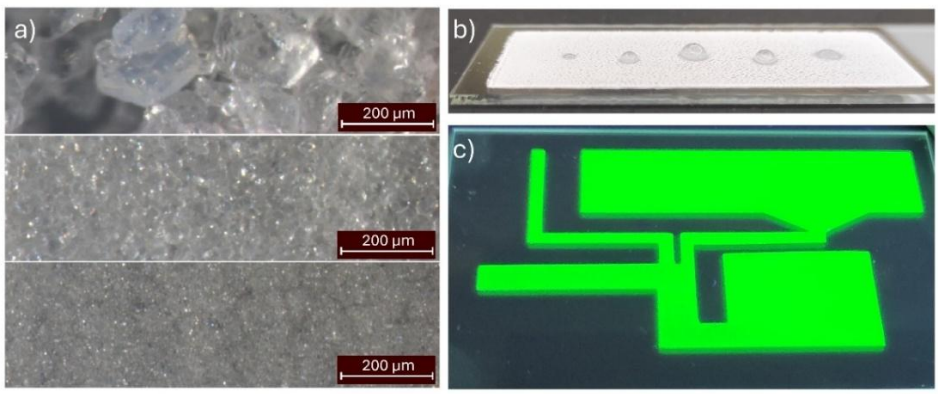

Figure 13. Printed materials with different particles. **a)** Optical microscope images of materials with varying of particle size (63-142 µm, 15-25 µm, 5 µm from top to bottom). **b)** Water droplets on a material with C18 functionalised silica particles. **c)** Material containing fluorescent particles under UV light.

Although the combination of silica gel particles with XG was found to be particularly favourable due to the strong adhesion, the possibility of printing other types of particles using XG as the binding agent was also successfully tested. These included cellulose powder and various polymeric ion-exchange resins (e.g. Chelex 100 and AmberChrom). However, in the case of the latter, it was necessary to mix the polymeric particles with regular silica gel (e.g. in a 50:50 mass ratio) to prevent the material from cracking and flaking off the substrate after drying. Moreover, optimising the drying temperature and time became more critical, since some of these particles did not tolerate excessive heat. Incorporating silica particles also improved the handling of the paste during printing (by reducing excessive shear-thickening behaviour) and enhanced the wetting rate of the resulting material.

In general, the possibility to combine different particles to create a material with tailored properties can be considered one of the key advantages of the developed

approach. For instance, it enables fine-tuning of the ion-exchange capacity or the incorporation of multiple resins within the same material. Furthermore, the addition of other particulate components to impart further functionalities is also feasible. In this work, two such modifications were tested: first, by adding a small amount of fluorescent indicator into the mixture to make the material fluorescent (analogous to TLC plates containing fluorescent indicators for visualisation); and second, by including calcium carbonate in the paste to give the material acid-neutralising ability (see Section 5.4.4 for further details).

While SP enables the formation of material from various available particle types, particles with the desired surface chemistry may not always be available, or the method might still prove unsuitable (e.g. due to the drying step after printing). In such cases, the surface chemistry of the particles can also be modified. For silica particles, different silane-group-containing reagents can be used relatively easily. This was briefly investigated in this thesis, by functionalising the printed silica surface with a silane polyethylene glycol (PEG) compound bearing an N-hydroxysuccinimide (NHS) group for further reactions. The NHS group was subsequently reacted with a primary amine-containing fluorescent dye (5-aminofluorescein) for visualisation. A comparison between a control (without any reactions) and a modified chip is shown in **Figure 14**. The chips were prepared in two parts: first, the narrow rectangular regions were printed and subjected to the surface reactions; then, the larger surrounding areas were printed to allow the elution of excess reagents. In the case of the modified surface, part of the fluorescent dye remained in place, whereas for the unmodified control region, it was fully eluted. Verification measurements with infrared spectroscopy showed the presence of C=O bonds (at around 1715 cm^{-1}) for the particles with surface modification.

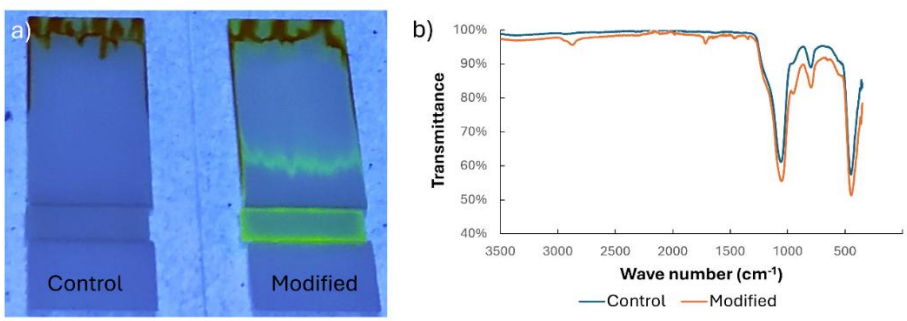

Figure 14. Surface modification of the printed material. **a)** Images of the chips under UV light. The left chip is the control: after elution with water, the fluorescent dye has been washed away. On the right chip, a significant portion of the fluorescent compound remains at the modified region. **b)** Infrared spectra of particles from regions with and without surface modification. The peaks indicate the presence of PEG (increased C-H bonds) and carbonyl groups (at 1715 cm^{-1}) with the modified particles.

5.4 Multi-step analysis

One of the primary goals of this work was to improve the analytical performance – particularly selectivity and sensitivity – of currently used on-site analysis tests. Sensitive and highly specific colorimetric reagents are rare. For instance, in the case of metal cations, there are several good reagents that are very sensitive (e.g. DTZ and PAN), but they form complexes with numerous metal ions. On the other hand, preconcentration of analytes is often needed to reach the necessary sensitivities for many real-world samples. To achieve high selectivity and sensitivity simultaneously, various common sample preparation steps used in laboratory analysis were integrated into the developed test. Each of publications II–IV focused on a specific application example. In publication II, a chip for the detection of five heavy metal cations was developed (HM chip); in publication III, a test for measuring biotin was demonstrated; and in publication IV, a test for monitoring iron and copper ions (FeCu test) was developed. In addition, the first patent application (publication V) covered several aspects of the general SP process (with XG as the binder) and the combination of multiple analysis steps as demonstrated in publications II and III. However, due to this overlap, it is not separately referenced in the following sections of the thesis.

5.4.1 Integrating TLC with the tests

Although incorporating chromatography into capillary flow-based on-site analysis tests presents several difficulties, it was still considered the most promising and universal approach for achieving selectivity in various applications. Moreover, since silica gel is the main component of the printed material, the extensive research base involving silica-based TLC could be readily utilised in this work. In addition, different types of chromatography – based either on general surface interactions or specific affinity/complexation to the analytes – were investigated. In publications II and III, the focus was primarily on realising selectivity through chromatographic separation. Both setups are shown in **Figure 15**.

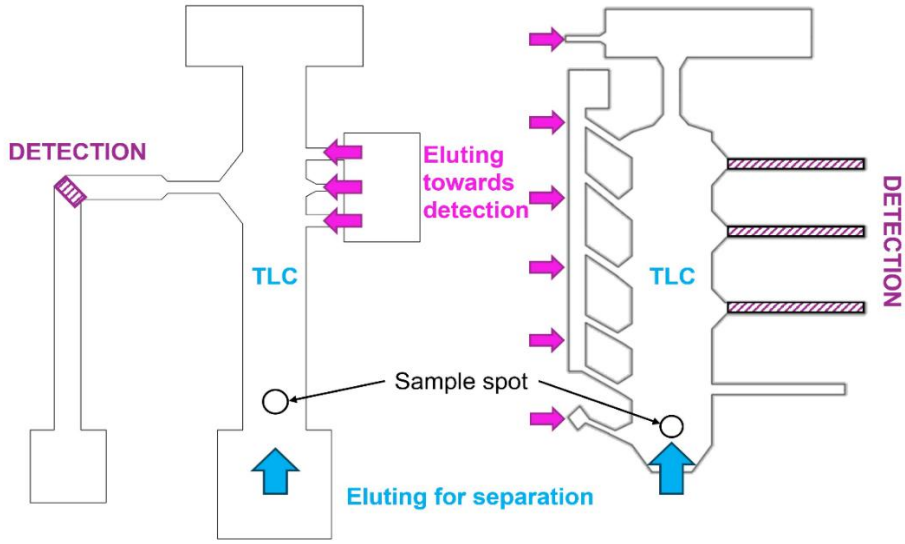

Figure 15. Schemes of the integrated TLC systems in the developed biotin and HM chips (publications III and II). The designs are not to scale.

In publication II, five metal cations (iron(III), lead(II), copper(II), cadmium(II), nickel(II)) were separated on the silica gel surface using a 0.15 M aqueous sodium nitrate solution as the eluent. A 1.5 µl sample was pipetted near one end of the TLC strip, and the elution was performed in an open TLC chamber. This separation principle can be regarded as a combination of hydrophilic interaction chromatography (HILIC) and ion chromatography, since both phases are strongly hydrophilic and the influx of ions moves the analyte ions. All metal ions except for Fe^{3+} moved with the eluent flow, and their separation on a plain printed TLC plate is shown in **Figure 16a**. Due to significant tailing of the analyte spots, several distinct design ideas were tested to improve the separation.

Initially, different arch-shaped TLC strips (**Figure 16c**) with 90-degree turns were employed to lengthen the separation path while maintaining the 50 × 75 mm substrate size. Although improved separation was observed, increased tailing occurred, and the analyte eluting closest to the front (Ni^{2+}) tended to get stuck at the strip edges. Moreover, integrating the detection step into such arch-shaped designs proved difficult. Therefore, the final design (**Figure 16b**) employed a more straightforward TLC strip with minor modifications. The effective separation length was increased through side channels and wider top section of the TLC strip, which also slowed down the flow rate. This helped reduce tailing by minimising the impact of mass transfer effects on analyte elution. While further optimisation could have improved the final separation, the demonstrated results already showed that the developed SP approach allows for enhancement of TLC performance through tailored chip geometries.

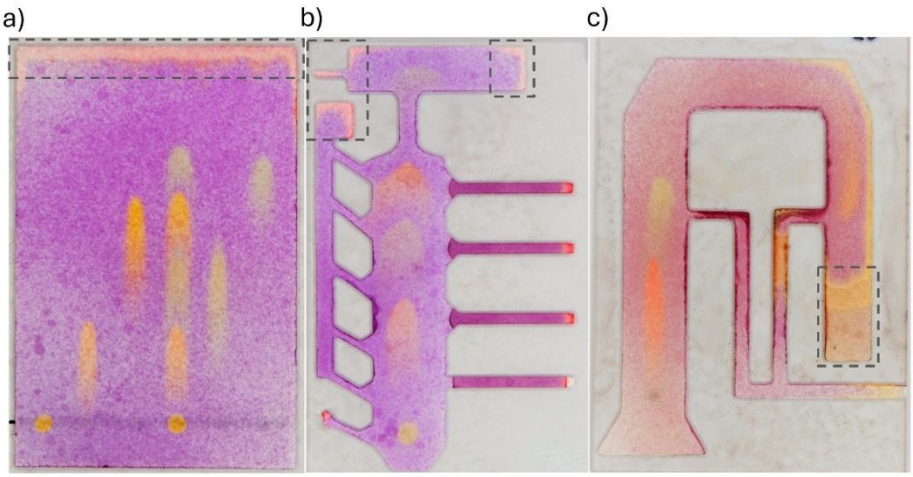

Figure 16. Separation of metal cations on printed chips. **a)** Separation on a plain TLC plate. The components in the mixture in column 4 are in order from most to least retained: Fe^{3+}, Pb^{2+}, Cu^{2+}, Cd^{2+}, Ni^{2+}. The movement of the individual analytes can be seen adjacent to the mixture. **b)** Improved separation of the mixture using the final HM chip. **c)** Example of separation using an arch-shaped TLC strip. The analyte spots on all chips were visualised by spraying a DTZ solution in acetone onto the plates. Areas with interfering signals from contaminants in the paste are marked with dashed lines.

One additional problem observed during the development of this test was the presence of interfering compounds in the material, which influenced analyte movement and contributed to colour development with DTZ. This interference originated from the silica particles and remnant glycerol, which was initially included to prevent the paste from drying during printing. The influence of glycerol can be seen in **Figure 16c** as an orange-yellow front at the end of the TLC arch. This was eliminated in the final chip version by omitting glycerol from the paste. The colour originating from the silica gel was most likely due to metal ions present in the particles that formed complexes with DTZ.

Different silica particles were tested to address this issue, and the influence of silica can be seen by comparing **Figure 16a** and **b** with **16c**, where the background exhibits a clearly different colour from the pure violet of dry DTZ. However, an entirely contamination-free silica source could not be found. Therefore, after printing, the chips were first eluted through with a dilute eluent (0.1 M aqueous $NaNO_3$), followed by deionised water, which moved the interferents to the edges of the design. This can be seen in **Figure 16a** as a bright red front (surrounded by a dashed rectangle) and in **Figure 16b** at several corners of the design. It must be noted that such interference was also observed in other developed chips and represents a significant issue that must be addressed during test development.

An alternative approach to integrating TLC into the tests was demonstrated in publication III, for the detection of biotin (vitamin B_7 or H). Normal-phase

chromatography was used to separate biotin from its metabolites (shown in **Figure 17**), after which it was bound by avidin and detected. The printed silica surface acted as the stationary phase, and a mixture of chloroform, acetone, methanol and acetic acid (in a 5 : 2.5 : 1 : 0.05 volumetric ratio, based on a previous report[110]) served as the eluent. In this example, the shape of the printed material had less impact on the separation of compounds, although widening of the TLC strip in the middle (i.e. due to side channels) still helped suppress longitudinal spreading of the biotin spot. A significantly greater issue, however, was the highly volatile eluent mixture, which required a well-saturated TLC chamber to achieve repeatable results. Since vapours from the organic solvents negatively impacted the subsequent analysis steps (e.g. avidin functionality), and use of a saturated TLC chamber would be impractical in real-world settings, an alternative method for eluent introduction was implemented. For this, liquid reservoirs containing the necessary eluents, along with a plastic cover to limit evaporation, were incorporated into the test to perform the TLC step. The fabrication of the reservoirs and the complete device assembly is discussed in more detail in Section 5.5.

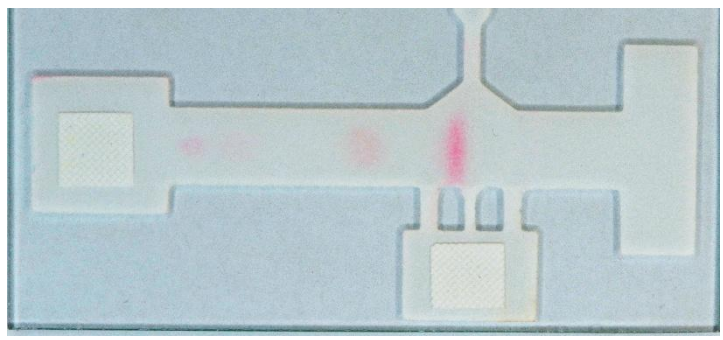

Figure 17. Separation of biotin and its metabolites on the printed microfluidic chip. Biotin appears as the rightmost ellipsoidal spot. The chip was visualised by spraying it with a solution of p-dimethylaminocinnamaldehyde (p-DACA) in ethanol and sulphuric acid.

In both examples, TLC was successfully applied for separation purposes, and sufficient selectivity was achieved. Different types of separation principles were demonstrated, showing the general applicability of TLC for enhancing the analytical performance of capillary-driven microfluidics. In the case of the biotin test, the separation step was also fully integrated into the device by incorporating the eluent into a blister reservoir and controlling its evaporation during the analysis. The required time for the separation step was reasonable for both cases – approximately 13 minutes for the HM chip and around 8 minutes for the biotin test. However, in terms of the total analysis time, the need for drying and performing subsequent elution steps prior to detection must also be considered.

5.4.2 Combining TLC with detection

Unless the analytes themselves absorb light in the visible spectrum, a subsequent development step must follow the separation to make the analytes visible for colorimetric detection. The most common TLC development technique involves spraying the eluted TLC plate with visualisation reagents. However, this approach is unsuitable for on-site tests, as it is poorly repeatable (especially for quantitative analysis) even under laboratory conditions, and it requires handling of potentially hazardous chemicals. Therefore, an alternative method of introducing the analyte to a colorimetric reagent of known concentration had to be employed. Two different versions of this were implemented with the HM chip.

For Fe^{3+} detection, the colorimetric reagent (potassium ferrocyanide) was eluted over the sample addition area, where Fe^{3+} had been retained during elution. As a result, an immobile coloured complex formed (blue spot in **Figure 18a**). Fe^{3+} concentration could be estimated based on the colour intensity. While this detection approach is simple and applicable to other systems, it is limited by the specific elution behaviour of the system components. Both the analyte and the formed complex must remain immobile, while the preferably colourless reagent is eluted across the analyte spot. Moreover, for the specific case of the HM chip, performing detection at the sample application site carries a relatively high risk of interference from other sample components.

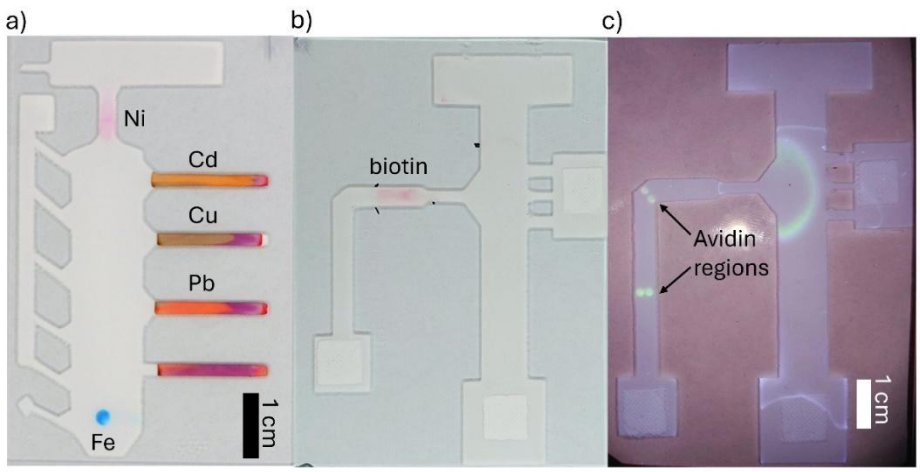

Figure 18. Combination of TLC and detection. **a)** HM chip after the detection step with 5 mM analyte concentration. **b)** Biotin chip after the second elution step, showing that biotin has been guided to the detection strip. Biotin is visualised by spraying it with p-DACA solution. **c)** Biotin chip after the full analysis and under UV light; bound biotin-F can be seen at the avidin regions (test and contol areas).

The second approach, applied for the detection of Cd^{2+}, Cu^{2+}, Pb^{2+} and Ni^{2+}, could be considered more versatile, as it requires only the movement of analytes. Ni^{2+}

was bound and detected during the TLC separation, which is discussed in more detail in Section 5.4.3. For Cd^{2+}, Cu^{2+} and Pb^{2+}, however, an additional step was required. After separation, these metals were eluted perpendicularly into detection channels that contained the water-insoluble colorimetric reagent DTZ adsorbed onto the silica surface. A 0.2 M aqueous sodium acetate buffer (pH = 5) was used for this step. Upon contact with the reagent, immobile metal-DTZ complexes formed, and the summed colorimetric signal intensity from the complex was used for quantitative analysis. The principle of this step is similar to distance-based PADs and is also an example of complexation chromatography, making the entire analysis a demonstration of two-dimensional chromatography.

The same principle, in the form of affinity chromatography, was applied with the biotin test (**Figure 18b** and **c**). The separated biotin was eluted with deionised water over a region containing dried avidin, which captured the analyte from the eluent flow. However, for detection, a third elution step was necessary. This involved eluting fluorescently labelled biotin (from the opposite side) over the same avidin region and applying competitive assay principles to determine the biotin concentration in the sample.

Although combining TLC and detection through separate elution steps was successful in both instances, it led to increased complexity and reduced robustness of the system. The main issue in both cases was the precise placement of analyte spots after TLC separation. Even if the components were successfully separated, their exact position on the chip or, in other words, their retention factor could still vary due to parameters such as material thickness and eluent evaporation. However, to ensure repeatable results, variations in analyte placement needed to be minimal. The chip designs accounted for small deviations by (1) incorporating a funnel shape at the start of the detection channels; and (2) positioning the small eluent channels for the second eluent so that they surrounded the analyte spot, preventing it from being eluted in the wrong direction.

In the case of the HM chip, an additional advantage was provided by DTZ. The colours of the metal-DTZ complexes differ significantly between metals (see **Figure 18a**), and the colours of adjacently separated analytes were highly contrasting (e.g. the green copper complex appeared between the orange-yellow cadmium and red lead complexes). Therefore, even if two complexes formed within the same detection channel (because part of one analyte was eluted to the wrong channel), they could still be clearly distinguished and quantified using the image processing algorithm.

Another complication in combining two orthogonal elution steps is the need to dry the material between these steps. Without drying, the second elution step would be difficult, since the material would already be saturated with liquid. In addition, the eluents used in different steps may be incompatible with each other or with the reagents deposited in subsequent regions (e.g. the organic solvents used in the TLC step of the biotin test can adversely affect the avidin used later in the analysis). Therefore, intermediate drying is essential in some cases. However, if incompatibility is not an issue and a viable flow path for the liquid exists

(e.g. as in the third elution step of the biotin chip), the drying step can be omitted. The main benefit of this is a reduced total analysis time.

For the HM chip, drying was accelerated by placing the chip in an oven at approximately 90 °C for five minutes before the second elution step. This enabled the entire analysis to be completed in 30 minutes. By contrast, with a fully integrated system (e.g. with a cover over the chip), it would have taken at least twice as long. The biotin test offers a more representative estimate of drying time and total analysis duration, since the chip was covered and all elution steps were performed without intermediate disassembly. In that case, the three elution steps were completed in approximately 50 minutes, but because a final drying step was required for signal detection, the total analysis time still reached up to 1.5 hours. A more detailed discussion on evaporation control, especially regarding the biotin test, is provided in Section 5.5.2.

5.4.3 Improving the sensitivity with SPE

During the development of the HM chip, it became evident that a significant increase in sensitivity was required for real-world samples. To some extent, this could be achieved by increasing the sample volume. Only 1.5 µl of sample was applied to the test, but even a several hundred-fold increase would still remain within a reasonable range compared to similar capillary-driven microfluidic tests. To maintain simplicity and avoid multiple off-chip steps, an integrated SPE region was identified as the most practical and universal solution for enhancing the sensitivity. The sample could be either eluted through or directly loaded onto the SPE region, after which the subsequent analysis steps could be carried out using pre-concentrated analytes. Although numerous experiments were conducted to integrate SPE regions with the developed approach, only a small part of this work was covered in publication IV.

As mentioned in Section 5.3.3, different particles were tested for preparing the SPE region. To preconcentrate heavier metal cations, these included silica particles functionalised with PCA or PSA groups and polymeric particles containing iminodiacetate groups (Chelex 100). The printed SPE materials were evaluated by loading a larger volume (e.g. 50 µl) of a dilute metal solution onto the chip and subsequently spraying it with a colorimetric reagent to determine the size of the resulting analyte spot. Moreover, an increased ionic background or a follow-up elution step with a salt solution (e.g. 0.1 M aqueous $NaNO_3$) was typically used to assess the strength of analyte retention by the SPE region.

It was found that although PCA functionalised silica retained metal ions from dilute solution, the retention was significantly reduced in the presence of background ions. Better results were achieved with PSA groups and with a silica gel mixture containing Chelex 100 (see **Figure 19**). The retained metals were subsequently successfully eluted from the SPE region using either acidic solutions or strong chelating agents (e.g. EDTA, citrate ions). Finally, SPE-based sensitivity enhancement was briefly tested for biotin by printing silica gel modified with quaternary amine groups. Successful capture and retention of biotin in

aqueous solvent was achieved, and the analyte could later be eluted using a dilute acidic solution (see **Figure 19d** and **e**).

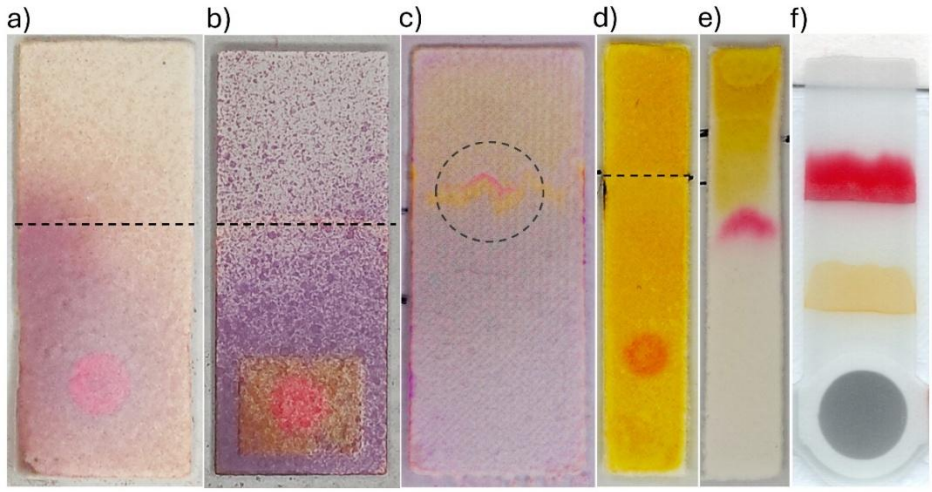

Figure 19. Examples of tested SPE systems on printed materials. **a)** Capture of Zn^{2+} ions on PSA silica particles. 40 µl of 0.1 mM Zn^{2+} in aqueous 0.1 M $NaNO_3$ was pipetted onto the plate. The sample front is indicated with a dashed line, and retained Zn appears as a pink disk after spraying with DTZ solution. **b)** Capture of Zn^{2+} ions on a mixture of Chelex and silica gel (40:60). The SPE region is printed in the middle of regular silica gel, and 50 µl of test solution was added. **c)** Elution of Zn^{2+} ions on the SPE material (encircled narrow pink strip). 0.5 M HCl was used to move Zn^{2+} ions on the SPE material with 40% Chelex. **d)** Biotin spotted on a quaternary amine functionalised silica and subsequently eluted with water. Biotin is visualised with p-DACA, and the water front is marked with a dashed line. **e)** Biotin eluted on the SPE material using 3% HCl solution. **f)** Capture of iron and copper ions (2 ppm) with the FeCu test. The grey disk indicates the sample addition area; yellow area corresponds to the copper-BC complex, and the red to the iron-BP complex.

Although the use of functionalised particles was considered the most universal approach for implementing SPE on the tests, more selective alternatives were also explored. For example, the use of insoluble colorimetric reagents capable of selectively binding analytes during their elution was demonstrated. This mechanism was applied in the HM chip for the detection of Ni^{2+} using dimethylglyoxime (DMG), which was deposited on a narrow, bottleneck-shaped silica gel region and captured nickel ions during the TLC step. However, in that case, DMG was not fully retained on the surface and gradually eluted, making it unsuitable for concentrating analyte ions from larger sample volumes under the applied conditions.

A better implementation of this approach was achieved in publication IV with the FeCu test, where 400 µl of sample was eluted through the entire chip, enabling significant preconcentration. A region with dried bathophenanthroline (BP) was

used for Fe^{2+}, and bathocuproine (BC) for Cu^{+} preconcentration and detection (**Figure 19f**). Compared to DMG, these reagents are more hydrophobic and therefore better retained on the material's surface. Moreover, even after forming positively charged complexes with the metals, they remained strongly retained due to the slightly negatively charged silica gel surface. In the case of PADs, auxiliary reagents are often required to enable BP-based detection in this manner. Overall, the preconcentration of analytes using an SPE region that was fully integrated into the test was successfully demonstrated in publication IV. However, due to the high selectivity of the photometric reagents towards the analytes, this implementation was relatively analyte-specific and may be challenging to adapt to other targets.

5.4.4 Combining SPE with chromatography and detection

In the vision of this work, the combination of SPE, chromatography and colorimetric detection would result in a universal multi-step analytical platform that could be adjusted for many different applications. All the steps individually, and some combinations, were successfully implemented and previously discussed. In addition, preliminary experiments were conducted to demonstrate the combination of a separate SPE region with complexation chromatography-based detection. As a result, it was possible to increase the sample volume by over 1000-fold, to several millilitres, when compared to the HM chip. Although this approach was similar to the FeCu test, as the same analytes and detection principles were used, only a small volume of liquid was eluted through the detection regions. This allowed for the incorporation of an additional analyte into the system and improved the sensitivity while potentially reducing the total required analysis time. The operating principles of the device are briefly discussed in this section, and some illustrative schemes, and preliminary results are shown in **Figures 20** and **21**.

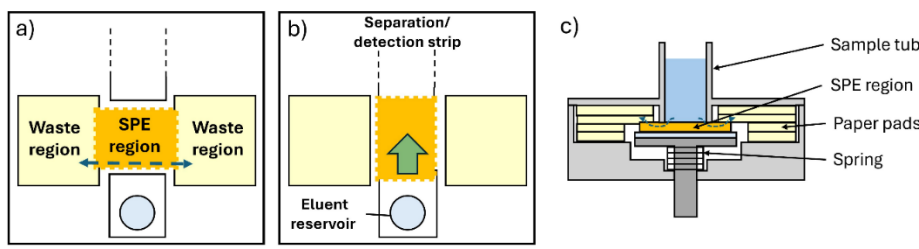

Figure 20. Operating principles of the system with a fully integrated SPE step. **a)** Scheme of the sample loading and preconcentration step. **b)** Elution of analytes from the SPE region to the separation and detection strip. **c)** Cross-section of the system during the sample loading step, after sample addition.

The sample was loaded into the sample tube above the rectangular SPE region (consisting of PSA-functionalised silica particles), which was located on a separate manually rotatable piece. Waste regions were placed adjacent to the SPE piece (left and right), consisting of multiple layers of thick paper pads. In the initial position, the SPE region was connected to the waste regions, and the contact was ensured by a spring underneath the SPE piece (**Figure 20a** and **c**). The SPE region was also pressed into contact with the sample addition tube to ensure that the entire sample passed through the SPE material, rather than flooding the surface and running over it. After the sample had passed through the SPE material, the piece was manually pulled down and rotated by 90 degrees to connect the further regions (top and bottom on **Figure 20a** and **b**) with the SPE region. The top region was a printed silica gel strip (with the glass substrate facing upwards), where different colorimetric reagents had been dried (BC, DTZ, BP). The bottom region consisted of a piece of filter paper onto which 30 µl of 0.2 M aqueous sodium citrate had been dried (at the edge near the SPE piece). Finally, 0.1 M aqueous sodium ascorbate solution was applied to the paper, dissolving the sodium citrate, which subsequently eluted the analytes off the SPE and over the detection strip. A picture of the device and some results are shown in **Figure 21**.

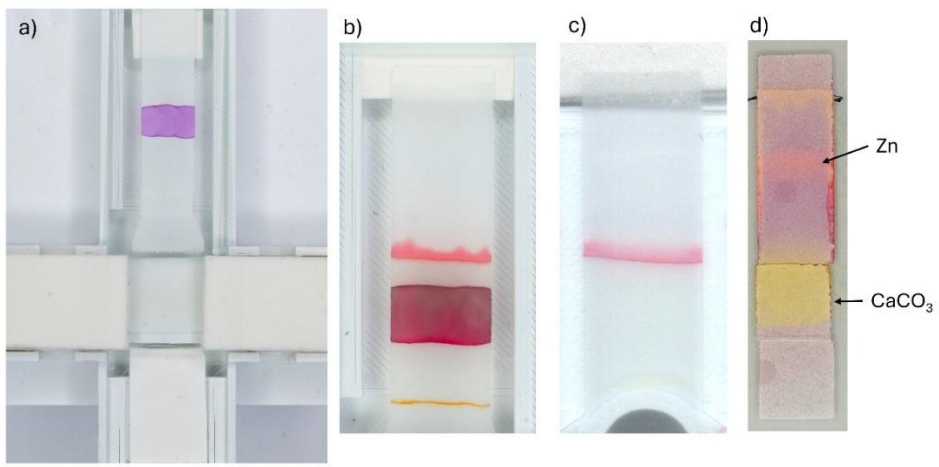

Figure 21. Preliminary results for integrating a separate SPE step with subsequent separation and detection steps. **a)** Picture of the assembled device after the sample has passed through. The SPE region is connected to the waste areas. The cover and sample addition tube have been removed to allow the SPE region to dry. **b)** Detection results for a 50 ppb mixture of Fe^{2+}, Zn^{2+} and Cu^{2+} ions. The Zn-DTZ complex appears in the central detection region as a brighter pink-violet area against the dimmer, darker DTZ background. **c)** Comparative results with the FeCu test. The analyte concentration is 50 ppb (both Fe and Cu), and the Cu signal is barely visible as a pale yellow line. **d)** Implementation of a $CaCO_3$ region for acid neutralisation. Zn^{2+} ions were eluted over a $CaCO_3$ area (yellow square) using a mixture of HCl and NaCl. Acid neutralisation is indicated by the absence of Zn at the eluent front and a colour change in only a narrow strip of the $CaCO_3$ region. DTZ solution was sprayed over the plate for visualisation.

In the example shown in **Figure 21b**, 2 ml of sample containing a mixture of Cu^{2+}, Zn^{2+} and Fe^{2+} ions (each at 50 ppb concentration) was loaded onto the SPE region, and it took approximately 20 minutes for the liquid to pass through. As an additional step, the cover structure was briefly removed to allow the SPE region to dry at room temperature for 10 minutes. This was primarily done to improve the detection results with DTZ. The total analysis time was approximately 40 minutes, which was faster than that of the developed FeCu chip (around 55 minutes) despite a fivefold increase in sample volume. Moreover, at 50 ppb, both Fe and Cu showed strong signals and remained clearly detectable down to 10 ppb, demonstrating significant improvement in sensitivity. Similarly, detection of Zn^{2+} at relevant concentrations was also achieved, increasing the device's applicability, particularly for micronutrient-related analyses.

Finally, a similar setup could be used to integrate a conventional TLC step with the SPE region (e.g. as a potential improvement to the HM chip). To achieve the separation, a stationary phase with stronger retention of metal cations could be employed (e.g. a weak cation-exchange material), which would compete with the citrate complexes. Alternatively, a strongly acidic solution could be used to elute the analytes from the SPE region. To prevent the acid from affecting the subsequent TLC step, calcium carbonate can be mixed and printed with the silica gel particles. When the acidic solution flows through this region, the acid is neutralised. Meanwhile, analyte ions can still pass through, and if the acidic eluent also provides sufficient ionic background, they can subsequently be separated and detected in the same way as with the HM chip. The use of $CaCO_3$ in this manner was briefly investigated, and initial results are shown in **Figure 21d**.

5.5 Complete analysis devices/tests

While the printed microfluidic chip constitutes the main functional component of the test, additional elements are required to make it usable outside the laboratory. These include a protective cover to shield the chip and provide control over evaporation, reservoirs for storing liquid reagents on the chip, and other functional components to automate and facilitate the analysis. Exploded views of the developed biotin and FeCu tests are shown in **Figure 22**. Furthermore, the means for on-site sample addition and accessibility for signal readout must be considered during the final test assembly.

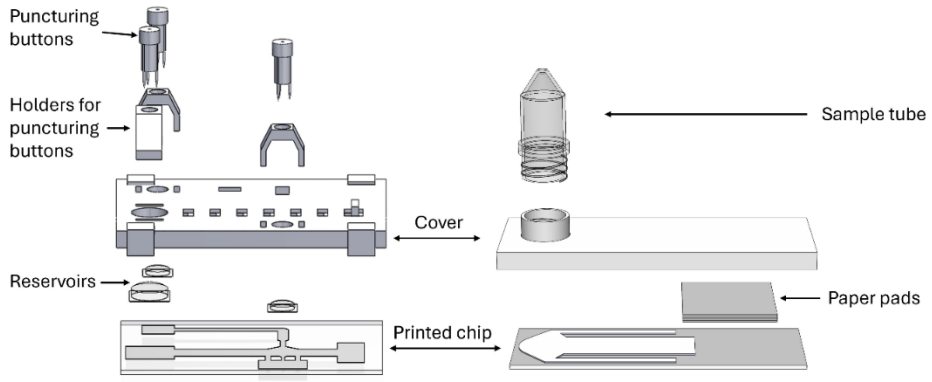

Figure 22. Exploded view of the biotin test (left) and FeCu test (right). Main components are labelled and indicated with arrows.

5.5.1 Reagent deposition and storage

For most of this work, dry reagents were included on specific chip areas using a simple solution-based deposition method: reagents were pipetted onto the chips and dried. This approach was applied to various colorimetric reagents as well as proteins (e.g. avidin). It was confirmed in publication III that avidin retained its functionality even after drying on the printed material. For reagents dissolved in more volatile solvents (e.g. ethanol, chloroform), the atmosphere above the chip was saturated with solvent vapours prior to reagent application, and the chips were then quickly dried in an oven. This procedure helped ensure uniform coverage and avoided inconsistencies in reagent concentration (e.g. due to the coffee ring effect). Alternatively, some reagents could be mixed directly into the printing paste before printing (see Section 5.3.3), enabling the entire chip production to be completed through the SP process alone.

Although solution-based reagent deposition is often the simplest and preferred method for porous materials, it can sometimes be unsuitable. For example, in publication IV, the entire sample had to be pre-conditioned before it was eluted through the test. However, since the conditioning reagents (e.g. ascorbic acid, potassium alum) are highly soluble in water, they would have been quickly eluted away with the first portion of the sample. Therefore, the preconditioning was performed in microcentrifuge tubes by adding the sample to solid salts and allowing them to dissolve before applying the sample to the test. This helped ensure that the reduction of analyte ions, as well as their replacement in potential complexes with strong chelating agents, occurred uniformly throughout the entire sample.

Many simple PADs rely on the sample itself as the liquid that carries analytes through the test. However, in more complex tests, where multiple elution steps are required or the exact composition of eluents is critical (e.g. the eluent in TLC), additional solutions are necessary. While this can be done manually by the user,

who pipettes a buffer onto a specific area on the test after adding the sample, it greatly increases the complexity and likelihood of user error, especially for non-experts outside the laboratory. A preferred solution would involve storing eluents directly in the device and releasing them in a controlled manner. This was addressed in publication III, where all necessary solvents were stored in medicine blisters (**Figure 23a**) and directly integrated into the final device. Although such blister reservoirs are available commercially, they are very expensive for storing different liquids. This is especially the case for rapid prototyping and testing, when the optimal compositions and volumes are not yet established. Moreover, for highly volatile organic mixtures (such as the TLC mixture used in the biotin test), suitable commercial reservoirs were, at the time of writing this thesis, apparently unavailable on the market. Therefore, custom reservoirs were prepared using either already empty or manually emptied medicine blisters. The detailed protocol can be found in the Supplementary information of publication III.

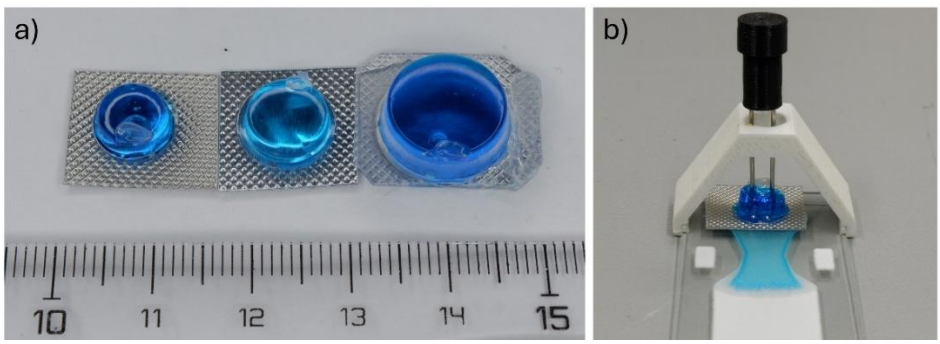

Figure 23. Fabricated reservoirs and the eluent release from them. **a)** Liquid reservoirs of varying sizes used for the biotin test. The reservoirs are filled with a food colouring solution. **b)** Depiction of eluent release from the reservoir onto a printed chip.

In addition to their availability and suitable size range, medicine blisters were chosen as the liquid containers due to the ease with which eluents can be released from them. The aluminium foil at the base of the blisters can be easily pierced, allowing the liquid to flow out. In publication III, this was achieved by puncturing buttons with syringe needles that were inserted through the top of the blisters (see **Figure 23b**). Alternatively, a sharp puncturing element can be positioned underneath the blister, so that when pressure is applied from above, the foil tears and releases the liquid. However, it is essential that good contact is formed between the liquid in the reservoir and the porous material beneath it. This ensures continuous and repeatable eluent release. Moreover, this contact prevents the liquid from spreading beyond the intended region – a particular concern when working with organic solvents such as acetone or chloroform, which are prone to flooding the substrate if containment is insufficient.

5.5.2 Chip protection and evaporation control

Although the printed material is generally stable and adheres well to the substrate, it is also vulnerable to physical damage and abrasions. Moreover, due to the excellent adsorption properties of silica gel, the printed chip is prone to adsorbing contaminants from the surrounding environment. In addition, any deposited reagents may be susceptible to these or other environmental factors (e.g. light). Therefore, a protective cover was required to preserve the integrity of the analysis chip and to ensure the repeatability of the tests. At the same time, the cover served as the structural component that integrates all the necessary elements of the test (the chip, sample inlet port and reservoirs). Both the biotin and FeCu tests included a 3D-printed PLA cover that was secured to the chip with auxiliary clamps (**Figure 24**).

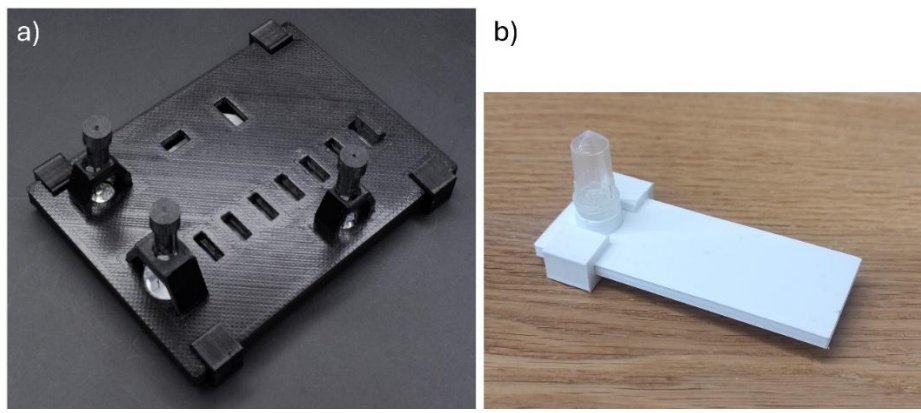

Figure 24. Pictures of the fully assembled tests developed in this work. **a)** Biotin test; **b)** FeCu test with the sample addition tube attached to the test.

In addition to preservation, protection and accommodation of auxiliary elements, the cover also plays an important role during the analysis. In publication IV, it prevented the chip from drying during the analysis and after the sample had passed through the test. This improved the repeatability of the test's performance and reduced the need for precise timing of the signal readout. Otherwise, the transparency of the silica gel, and consequently the colour intensity, would change until the chips had completely dried. This was even more critical in publication III, where the cover was used to actively control evaporation during analysis. During the first elution step, the chip had to be enclosed to prevent the highly volatile eluent from evaporating and thereby altering the separation and movement of biotin. Rapid evaporation afterwards was equally important, as the remaining eluent would have interfered with the subsequent analysis steps. To enable this, shutters were incorporated into the cover, which could be manually closed or opened to either limit or promote eluent evaporation. While essential

for the first elution step, they also helped accelerate the later elution and drying steps.

5.5.3 Ease of use of the devices

As discussed in Section 2.4.4 and defined as one of the goals of this work, the developed devices should be simple to operate to be suitable for real-world commercial applications. While the specifics of ease of use can be subjective, in the context of this work it is assumed that minimal actions – such as pressing one or more buttons (e.g. eluent release in the biotin test) or performing other straightforward tasks that are unambiguous to an untrained user – are acceptable. However, even in an ideal scenario, the user is still required to introduce the sample to the test and must interpret the results within a reasonable amount of time. Moreover, for quantitative results, the applied sample volume must be precise, and digital registration and analysis of the formed signal are almost always necessary.

The introduction of an exact sample volume to the test on-site can be challenging. This becomes especially important when working with volumes in the range of a few microlitres, where even a small variation (e.g. due to droplets remaining behind during the transfer) can significantly affect the results. In the current work, a range of sample volumes (from 1.5 µl to 2 ml) was used across different tests. The use of small volumes was unavoidable for the tests in publications II and III, since TLC was the first analysis step and the diameter of the sample spot had to be kept minimal. At the same time, the small volume was beneficial in limiting the influence of sample pH or ionic strength. However, in both cases, the achieved sensitivity was not sufficient for most real-world samples, and the issue with droplets occurred even in laboratory settings when using automatic pipettes. Therefore, in publication IV a considerably larger sample volume (400 µl) was used. This amount could be transferred more reliably using commercially available disposable exact-volume pipettes, which could be easily included with the test. Alternatively, precisely tuning the size of the paper adsorption pads was considered as a means to limit the volume that passes through the test. However, as noted previously in Section 2.3.4, the slow expansion of the cellulose network during wetting made it difficult to set a consistent final volume and time. This could potentially be better achieved with a thick, multi-layer screen-printed silica gel, since only the small amount of XG would gradually absorb additional water over time.

For the quantitative readout of the colorimetric signal, multiple options for on-site tests exist, as discussed in Section 2.4.2. To better understand the advantages and disadvantages of different approaches, a distinct detection strategy was applied to each of the tests developed in publications II–IV. A digital camera with a controlled height and lighting setup was used for the HM chip; a smartphone with a custom-made lighting box was used for the biotin test; and multiple flatbed scanners were investigated for the FeCu test. Although these detection approaches were somewhat interchangeable, the setup for the biotin test was more demanding due to the fluorescent signal, which required a specialised UV light source.

The camera and the smartphone required the use of auxiliary equipment, which had to be precisely set up and aligned with the test, making the entire process susceptible to errors. Nevertheless, with multiple control areas and advanced image processing algorithms that can automatically adjust for variations in imaging conditions, smartphones represent the most promising option for widespread on-site testing due to their wide availability. Moreover, it should be noted that the use of a transparent glass substrate greatly benefited the use of flatbed scanners, but it could limit certain device designs, as the scanner bed must be in close contact with the detection region. In the current work, flatbed scanners proved to be the most convenient option for signal readout. The test could simply be placed in one corner of the scanner bed and covered with a box (to eliminate external lighting), allowing an image with well-defined lighting conditions and signal placement to be captured. Finally, as briefly investigated in publication IV, images from different scanners can be relatively easily adjusted to provide consistent results for the same test. In the case of smartphones, such adjustment may be more complicated due to the wider variety of models and software used.

5.5.4 Automation of steps

To achieve ease of use with more complex multi-step tests (e.g. the biotin test), further automation is needed to reduce the test's hands-on time and to minimise user errors. For this reason, an automated system for the timed release of eluents from reservoirs or for changing the state of valves was developed. This system is based on a spring-loaded actuator that remains in one state while the triggering paper is dry, and switches to the other state as the paper wets and loses structural integrity, no longer resisting the spring's force. Although this approach is compatible with the particle-based microfluidics developed in this work, it is even more suitable for fully paper-based chips, since some versions require the porous material to be pierced or bent to function. Two main modifications of the mechanism are presented in **Figure 25**, followed by a detailed explanation of their working principles.

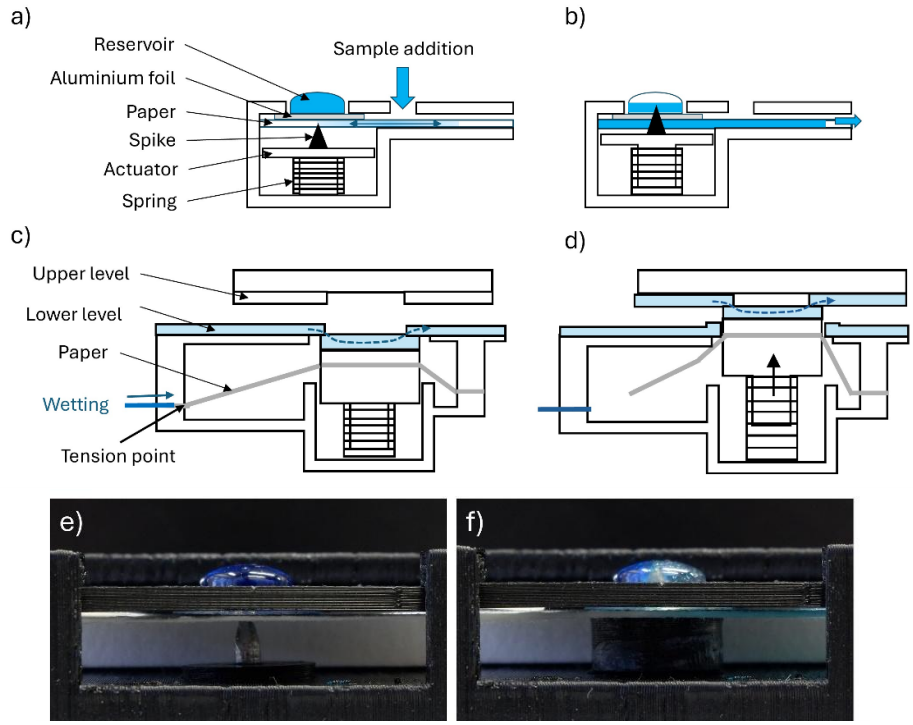

Figure 25. Developed spring-loaded automation mechanisms. **a)** Scheme of the automatic reservoir puncturing system in standby state. **b)** Automatic eluent release from the reservoir after the paper has wetted. **c)** Alternative version for valved connections without the spike. The liquid flow can pass through the system only on the lower level. The retaining paper strip begins to wet from the left side. **d)** The valved connection in triggered state, after the retaining paper has torn. Eluent flow can pass through the system only on the upper level. **e)** Photo of the system shown in (a). **f)** Photo of the system shown in (b); sample was added to the paper from the left side and the blue solution from the reservoir starts to elute to the right side.

For releasing the eluents from the reservoir (**Figure 25a** and **b**), a sharp spike was placed beneath the reservoir, separated from the aluminium foil by a strip of paper. The paper strip was fixed at the ends and, when dry, it held the spike in place against the spring's pressure (**Figure 25a**). However, when the sample is introduced to the test, the paper strip begins to wet and loses its strength. Once the liquid front reaches the spike, the spring forces it through the weakened paper, puncturing the aluminium foil at the bottom of the reservoir (**Figure 25b**). Moreover, depending on the force of the spring and the spike's shape, the aluminium foil may tear easily, and some paper is pushed into the reservoir. This is important, as it ensures complete discharge of the liquid from the reservoir via capillary action.

The alternative modification of the mechanism shown in **Figure 25c** and **d** functions without the spike and may be more suitable for valved connections. In

this case, the spring still applies pressure on the paper, but the potential breaking point (the area under most stress and wetted first) is located further from the actuator. This means an automated movement can be triggered at a point further away in the test from the triggering eluent. The paper will also tear completely upon breaking and will not be in direct contact with the part of the flow system (e.g. valve) that is moved. This can prevent cross-contamination and the mixing of unwanted liquids within the test.

Overall, this automation approach can be considered relatively simple and was demonstrated to be reliable. Essentially, no external power is required to activate the mechanism, and based on the experiments, the initial state of the system remains completely stable until a liquid is introduced to the paper. Multiple such elements could also be combined in a single test to perform complex analyses, where one element activates the next in sequence. One potential drawback, however, is the increase in required components for the test, as well as a more complicated assembly process, which leads to higher costs. Moreover, the final test dimensions will increase slightly, and if a scanner is used for signal detection, the placement of the liquid handling system must be carefully considered. This entire automation system was filed as a patent application (publication VI).

5.6 Comparison of developed on-site tests

During this work, three application examples targeting different analytes were developed, each with a varying degree of completeness in terms of real-world applicability. The analytical parameters of these tests, along with their general strengths and weaknesses, are compared and discussed in this section. The key parameters for each test are presented in **Table 3**. Finally, a comparison between the FeCu test developed in this work and relevant previously published PADs is provided in **Table 4**.

5.6.1 Comparison of developed prototypes in this work

Regarding analytical performance, all developed tests exhibited relatively good selectivity. This was achieved through the use of selective reagents, the TLC step employed in the HM and biotin tests, and the sequential placement of reagents in the FeCu test. The HM chip can be considered the least selective of the three, as tailing and variations in analyte separation could lead to interfering signals. Moreover, in the case of spiked samples, the sample matrix had a greater influence on the results than in the other two tests.

Considerably larger issues were observed with the sensitivity and working range of the tests. Only the FeCu test demonstrated sufficiently high sensitivity and a reasonably wide working range (spanning two orders of magnitude) to be suitable for real-world applications. This outcome was expected, given that the sample volume for the FeCu test was over 250 times greater than in the other tests. Nevertheless, the sensitivities of the other tests may still be adequate for

specific applications. For instance, the biotin test could be used alongside the Roche Cobas analysis test for anti-doping monitoring, where extremely high biotin concentrations can otherwise lead to false-negative results.[111]

In terms of usability, the total analysis and hands-on time, need for auxiliary equipment as well as the general ease of use (i.e. the required steps from the user) are compared. Although the analysis time with the HM test was the shortest, it required heating the chip to accelerate drying steps. Additionally, the overall hands-on time and user effort were higher than for the other tests. For the biotin test, the hands-on time was relatively short, and the steps were simple (e.g. pressing the eluent release button); however, the timing of the different steps had to be relatively precise. The total analysis time was also the longest, even when the chip was disassembled and dried in an oven. Finally, the FeCu test required minimal hands-on time, with the main additional user-dependent action being the attachment of the sample tube to the test after 15 minutes of preconditioning. Importantly, none of the steps in this test were time-sensitive (i.e. the timing for conditioning and signal readout had a greater tolerance). Regarding the signal readout, the need for UV light sources and their reliable positioning relative to the detection regions and imaging device made the biotin test more complex.

Two more subjective parameters for comparing the tests are their integrity (i.e. whether the test can be used without the need for external laboratory equipment) and robustness (i.e. the ability of the test to remain unaffected by small variations between different tests, user handling, and general environmental factors). The HM test consisted only of the printed analysis chip with colorimetric reagents. This meant that eluents had to be provided externally, and the user had to perform multiple manual steps throughout the analysis. The biotin test was considerably more self-contained, including even the volatile organic solvents in integrated eluent reservoirs. Its main drawback in terms of integrity was the need for disassembly to accelerate the final drying step and improve signal readout. The latter was necessary due to the size and placement of the detection windows in the cover, which caused interfering shadows during signal readout, when the fully assembled device was placed in the reader box.

Regarding robustness, both the biotin and HM tests exhibited considerable variation in the separation and accurate placement of analytes (i.e. retention factor) during the TLC step. In addition, the reliable containment and release of the TLC eluent in the biotin test was inconsistent, largely due to the manual assembly of the reservoirs and the overall test device. Furthermore, the use of highly volatile eluents that pose health risks to users (i.e. chloroform, methanol) should ideally be avoided. In contrast, the FeCu test could be considered completely self-contained, aside from the scanner required for signal readout. Due to its simple working principle and straightforward assembly, it was also relatively robust, with the main variation in performance originating from differences in the thickness of the printed chips. These characteristics of the FeCu test were further demonstrated by the successful completion of several analyses entirely on-site for publication IV.

Table 3. Comparison of the tests developed in this work

Publication	**II**	**III**	**IV**
Analytes	Fe^{3+}, Pb^{2+}, Cu^{2+}, Cd^{2+}, Ni^{2+}	Biotin (vitamin H)	Total dissolved iron and copper
Combination of methods	TLC + (complexation chromatography +) colorimetric detection	TLC + affinity chromatography + competitive assay + fluorescence detection	SPE/complexation chromatography + colorimetric detection
Detection limit (LOD)	Ni^{2+}: 0.14 mM others: 0.1 mM	0.37 µM	Fe: 0.18 µM Cu: 0.6 µM
Quantification limit	Ni^{2+}: 0.3 mM others: 0.2 mM	Not determined	Fe: 0.9 µM Cu: 0.79 µM
Dynamic range	Ni^{2+}: 0.14–1.4 mM others: 0.1–1.4 mM	0.37–0.98 µM	Fe: 0.18–90 µM Cu: 0.6–79 µM
Selectivity	Moderately selective	Highly selective	Highly selective
Analysis time	0.5–1 h (depending on drying steps)	1.5–3 h (depending on final drying step)	~1 h
Detection	Digital camera + controlled lighting setup	Smartphone + 3D-printed reader with UV LEDs	Flatbed scanner
Ease of use	Medium; requires separate eluents, containers and heating	Medium; multiple time-sensitive steps; disassembly for drying and detection	Easy; only requires attachment of sample tube after preconditioning
Problems with robustness	Tailing of analyte spots during TLC and inaccurate placement	Biotin placement after TLC; TLC eluent storage, release and evaporation	Small droplets remaining in sample tube after analysis
Limitations in test integrity	External laboratory equipment and chemicals required	Requires disassembly and heating for final drying	No significant limitations
Applicability in real-world analysis	Low, requires high analyte concentrations, sensitive to sample matrix (e.g. Fe^{3+}, Ni^{2+})	Medium, suitable for specific applications (e.g. anti-doping monitoring)	High, suitable for monitoring drinking water and nutrient solution analysis

In conclusion, each test had distinct strengths and introduced a different form of novelty. The biotin test was the most complex and innovative in terms of multi-step on-site analysis, combining three sequential elution steps in a device that incorporated all necessary reagents, which could be released using a simple push-button system. However, from a practical standpoint, the FeCu test proved to be the most reliable and robust, with suitability for analysing a range of real-world samples. Consequently, the FeCu test was selected for comparison with previously reported PADs in the following section.

5.6.2 Comparison of the FeCu test to previously published PADs

Over the past decade, numerous examples of PADs have been reported for the on-site measurement of iron and copper ions in aqueous samples. A selection of these tests and their characteristics is presented in **Table 4**, for comparison with the FeCu test developed in this work. In addition to analytical parameters, the apparent usability of the tests and their potential for real-world applications have also been assessed. The examples include both single-analyte devices and multiplexed systems capable of simultaneously determining up to six different analytes.

Before the discussion, however, two important aspects regarding iron determination must be considered. The first is the presence of iron in paper or other base materials used (e.g. silica gel). In cases of low detection limits, this can produce an interfering background signal or simply cause inconsistencies in colour formation. Such background signals can be observed in several publications listed in **Table 4**, yet they are often completely overlooked in the discussion. In the FeCu test developed in this work, an extensive washing protocol was applied to the particles used, which minimised the background signal and improved both the LOD and repeatability of the tests.

The second important aspect concerns the oxidation state of iron during device development and in the analysis of real-world samples. Many studies focus solely on the determination of Fe^{3+} using phenanthroline-based reagents, as this is the dominant form of iron in surface waters. However, since the colorimetric reagent forms a coloured complex only with Fe^{2+}, a reducing agent is required for the analysis. If calibrations are performed only with Fe^{3+} solutions and the efficiency or required duration of the reduction step is not properly considered, the tests may incorrectly estimate the actual iron concentration in real samples. For this reason, a sample pretreatment in separate tubes was included in the FeCu test: the sample was added onto a pre-loaded mixture of ascorbic acid and sodium ascorbate, which then dissolved and reduced Fe^{3+} to Fe^{2+} over 15 minutes. This separate step was important to ensure more accurate results for various real samples.

Table 4. Comparison of the FeCu test with previously reported PADs for iron and copper detection from aqueous samples

Analyte	Reagent	LOD (ppm)	Test range (ppm)	Readout device	Analysis time	Sample volume	Comments	Year, ref
$Fe^{2+,3+}$ Cu^{2+}	BP DTO	20 100	20–1300 100–1300	Visual, distance-based	40 min	50 µl	Well-defined analysis endpoint, digested solid sample	2015, [55]
Fe^{3+}	phen	40	40–350	Scanner	ND	25 µl	Hot spring water was used as sample, with iron content over 100 ppm	2016, [113]
$Fe^{2+,3+}$ Cu^{2+}	BP Zincon	0.1 0.1 (0.001)	0.1–20 0.1–20	Visual, radial-distance based	3 min / 9min	100 µl / 1 L	Single analyte tests; separate SPE system is used, selectivity is not thoroughly discussed	2018, [83]
Cu^{2+}	PAN	0.022	0.064–0.44	Scanner	3 min	1 ml	Auxiliary equipment and reagents needed for SPE step, multiple user steps, likely under-estimated analysis time	2019, [81]
Cu^{2+} Fe^{2+}	TPTZ DPC	0.1	0.1–1 0.1–0.5	Scanner (+ visual estimation)	ND	100 µl/ 500ul	Analytical parameters apply only to single analyte tests. Combined test results appeared semiquantitative	2019, [114]
Fe^{3+} Cu^{2+}	phen BC	0.2 0.03	0.3–18 0.05–24	Smartphone + controlled lighting	ca 17 min	130 µl	6-analyte test, only spiked real-world samples with relatively high concentration (8 or 11 ppm for Cu)	2019, [65]
Cu^{2+}	BC	0.32	0.32–63.55	Scanner	120 min	300 µl	5-analyte test, mainly spiked real-world samples	2021, [54]
Fe^{3+} Cu^{2+}	BP BC	1.1 0.3	0.5–15 0.1–5	Smartphone + lightbox	ca 22 min	400 µl	Additional equipment free sample application	2023, [63]
$Fe^{2+,3+}$	D-3,4-HPO	0.07	0.25–2	Scanner	10 min	25 µl	Magnesium is a strong interferent	2023, [115]

Analyte	Reagent	LOD (ppm)	Test range (ppm)	Readout device	Analysis time	Sample volume	Comments	Year, ref
Cu^{2+}	Mod-RHOB	0.01	0.05–0.5	Scanner	7 min	20 µl	Potentially poor long-term stability, salt content affects performance	2024, [116]
Fe^{3+}	BP	0.002	0.005–0.08	Smartphone + controlled lighting	ca 20 min	250 ml (150 ml)	6-analyte test, big sample volume, requires separate sample tank, sample volume can be controlled	2024, [117]
Cu^{2+}	BC	0.007	0.013–0.2					
$Fe^{2+,3+}$	BP	0.01	0.05–5	Scanner	55 min	400 µl	**This work**, suitable for nutrient solutions and other samples with chelating agents	2025, IV
Cu^{2+}	BC	0.038	0.05–5					

Reagents: Bathophenanthroline (BP), bathocuproine (BC), Dithiooxamide (DTO), 1,10-phenanthroline (phen), 1-(2-pyridylazo)-2-naphthol (PAN); 2,4,6-Tris(2-pyridyl)-s-triazine (TPTZ), 1,5-diphenylcarbazide (DPC), Naphthalene-3-hydroxy-4-pyridinone (D-3,4-HPO); rhodamine-based chelator (Mod-RHOB)

When comparing the analytical performance of the tests, device selectivity, sensitivity and working range, and their suitability for real-world sample analysis must be considered. With some exceptions, the primary target sample in most of these tests was drinking water. According to WHO guidelines, the iron content in drinking water should not exceed 0.3 ppm, and copper should not exceed 2 ppm.[112] However, in many real-world samples, iron concentration can reach several ppm, while copper concentrations are typically below 1 ppm, or often even below 0.1 ppm. Therefore, the optimal working range for widely applicable analysis tests should encompass 0.1–5 ppm for both analytes. In **Table 4**, besides the FeCu test developed in this work, only three other tests for copper and one for iron fully cover this range. Regarding detection limits, only a few tests have been demonstrated to measure the analytes below 0.1 ppm, most of which require a separate SPE system or auxiliary components. Selectivity was typically achieved through the use of highly selective reagents (e.g. BP, BC), although some issues were still reported (e.g. interference from magnesium). Moreover, based on the test developed in this work, an interfering signal in iron detection from Cu^{+} ions was identified as a significant risk when reducing agents and BP were combined. To mitigate this, copper ions were captured and detected before the sample reached the iron detection region containing BP, thereby eliminating the risk of interference.

In terms of device-specific characteristics, the analysis time, applied sample volume and analyte capture efficiency are compared. The analysis times in **Table 4** vary significantly, ranging from 3 minutes to 2 hours. However, it must be noted that in at least one case, the reported analysis time (3 minutes) does not appear sufficient for an ordinary user to complete the entire analysis (which includes a separate SPE step, two liquid introductions to the test, and multiple scanning steps). On average, 10–20 minutes appear to be the typical analysis time, although even 2 hours can be considered acceptable for quantitative on-site results. One of the main factors influencing the analysis time is the sample volume. Lower volumes generally allow for faster analysis. The applied sample volumes mostly fall between 20–500 µl, except in the case of specialised preconcentration systems, where volumes between 1 ml and 1 L were used. Unsurprisingly, the highest sensitivities were achieved with these large-volume systems. In the case of the FeCu test, higher sensitivity was prioritised over potentially shorter analysis time, and therefore the total analysis time for the test developed in this work was longer than in many other examples.

To estimate the "analyte capture efficiency" of the tests, the applied sample volume was compared to the detection limit of each device. As noted above, larger sample volumes should result in higher sensitivity (i.e. lower limits of detection), although this relationship is not necessarily linear and strongly depends on the elution times. The comparison was made by estimating the sample volume required for the test to detect an analyte concentration of 0.1 ppm. Moreover, if the sample was divided among multiple detection channels, the available sample volume was divided by the number of channels. For iron, only one test[115] demonstrated better capture efficiency than the FeCu test developed in this work,

while several others – particularly those using the same reagent (BP) – were over 20 times less efficient. For copper, the results were closer: three tests[65,114,116] showed better analyte capture capabilities than the FeCu test. Among them, one also employed BC as the reagent and appeared to achieve approximately 20 times greater analyte capture efficiency.[65] However, in that case, only spiked real-world samples were tested in the verification experiments, and the added copper concentration was extremely high (over 200 times the reported LOD). Overall, it can be concluded that when using the same reagents, PBM instead of paper substrates can result in more efficient reagent use.

In terms of ease of use, most of the tests described in the literature were relatively simple and only required the user to add the sample, perform the detection of the signal and read the results. This also applies to the FeCu test developed in this work, as the sample preconditioning step in a separate tube involved only minor actions. In contrast, tests employing a preconcentration system were more complex and required extra components to carry out the analysis. Moreover, if the analytes needed to be separately eluted from the SPE material, the user had to handle various external reagents. It is worth noting that the precise method for introducing the sample to the test was typically not described in the articles (with the only exceptions[63,117] noted in the Comments column of **Table 4**). As a result, for an ordinary end-user without access to an automatic pipette, the actual use of the test can be more complicated and may lead to inaccurate results. In some cases, however, the disposable exact-volume pipettes used for the FeCu test could offer a practical solution. Finally, regarding fully quantitative signal readout, the applied methods were almost evenly split between scanners and smartphones with additional lighting control. Therefore, neither approach can be considered entirely free of auxiliary equipment or universally portable (e.g. relying solely on a smartphone regardless of model).

In conclusion, the FeCu test developed in this work performed on par with the best PADs across most categories and can therefore be considered, among the strongest overall examples. At the same time, the use of particle-based technology eliminated the need for multiple auxiliary reagents, thereby simplifying the test's production. In several other PADs, numerous reagents with multiple addition steps per analyte were required to achieve the desired selectivity, sensitivity and overall functionality. In contrast, the FeCu test was significantly streamlined, with only the colorimetric reagents deposited on the chip. Moreover, the broader applicability of the FeCu test was demonstrated using samples containing strong chelating agents (e.g. EDTA, DTPA), and the test's performance was verified with actual nutrient solution samples. Such complex real-world samples were not addressed by any of the PADs listed in **Table 4**, and the presence of the chelating agent would likely have strongly interfered with the performance of most of those tests.

6. SUMMARY

Performing on-site analysis with simple, low-cost devices is of vital importance in various industries as well as for the general well-being of people around the world. Although paper-based microfluidic devices have been seen as an exceptionally promising direction to solve this problem, their analytical performance and real-world implementation have remained limited. In this study, alternatives to paper were investigated that retain the simplicity of capillary-driven tests while offering better control over material characteristics. Moreover, the focus was set on developing devices that solve real-world problems and are suitable for non-professional users.

Three distinct approaches to produce a capillary flow-based microfluidic chip similar to PADs were developed during this work, thereby proving hypothesis 1. Among these, the most promising approach relied on using silica microparticles with xanthan gum binder in combination with screen printing to form analysis chips with the desired designs. Particles with different sizes and modifications were combined this way to control the properties of the resulting material (porosity, thickness and surface functionality), which proved the first part of hypothesis 2. This is also critical for achieving better flow control and analytical performance in capillary-driven tests. At the same time, screen printing allowed fast and inexpensive prototyping while being easily scalable for later mass production proving the second and third parts of hypothesis 2.

To further improve the tests' selectivity and sensitivity, incorporating TLC and SPE steps was demonstrated in multiple application examples. These included a test for five metal cations in water samples, a biotin monitoring test for urine samples and a total dissolved copper and iron ions test for different water samples that could even contain strong chelating agents (e.g. EDTA in nutrient solutions for agriculture). Such fully integrated TLC-based capillary flow on-site tests are the first of their kind. Similarly, a completely integrated SPE system was demonstrated that allowed up to 1000-fold preconcentration of analytes. Finally, the analytical characteristics of the developed iron and copper test are at least on par with, and in many instances better than some of the best previously demonstrated paper-based devices. Based on all this, it can be claimed that hypothesis 3 was proven, at least to a certain extent.

In conclusion, several novel aspects were investigated and demonstrated that could significantly improve and advance currently developed paper-based analytical devices. In addition to the four published scientific research articles, two patent applications were filed during the course of this thesis. One of them (publication V) covers the general aspects of screen-printed particle-based microfluidics and the combination of multiple analysis steps on a single chip. In the other (publication VI), an automation system for stored eluent release and the formation of valved connections was developed. Both of these could significantly contribute to producing inexpensive multi-step analysis devices that require only limited user involvement.

7. REFERENCES

(1) Whitesides, G. M. The Origins and the Future of Microfluidics. *Nature* **2006**, *442* (7101), 368–373. https://doi.org/10.1038/nature05058.

(2) Narayanamurthy, V.; Jeroish, Z. E.; Bhuvaneshwari, K. S.; Bayat, P.; Premkumar, R.; Samsuri, F.; Yusoff, M. M. Advances in Passively Driven Microfluidics and Lab-on-Chip Devices: A Comprehensive Literature Review and Patent Analysis. *RSC Adv.* **2020**, *10* (20), 11652–11680. https://doi.org/10.1039/D0RA00263A.

(3) Mark, D.; Haeberle, S.; Roth, G.; Stetten, F. von; Zengerle, R. Microfluidic Lab-on-a-Chip Platforms: Requirements, Characteristics and Applications. *Chem. Soc. Rev.* **2010**, *39* (3), 1153–1182. https://doi.org/10.1039/B820557B.

(4) Streets, A. M.; Huang, Y. Microfluidics for Biological Measurements with Single-Molecule Resolution. *Current Opinion in Biotechnology* **2014**, *25*, 69–77. https://doi.org/10.1016/j.copbio.2013.08.013.

(5) *Advances in Microfluidic Technologies for Energy and Environmental Applications*; Ren, Y., Ed.; InTechOpen, 2020. https://doi.org/10.5772/intechopen.81935.

(6) Rivet, C.; Lee, H.; Hirsch, A.; Hamilton, S.; Lu, H. Microfluidics for Medical Diagnostics and Biosensors. *Chemical Engineering Science* **2011**, *66* (7), 1490–1507. https://doi.org/10.1016/j.ces.2010.08.015.

(7) Mancera-Andrade, E. I.; Parsaeimehr, A.; Arevalo-Gallegos, A.; Ascencio-Favela, G.; Parra-Saldivar, R. Microfluidics Technology for Drug Delivery: A Review. *FBE* **2018**, *10* (1), 74–91. https://doi.org/10.2741/E809.

(8) Fernández-la-Villa, A.; Pozo-Ayuso, D. F.; Castaño-Álvarez, M. Microfluidics and Electrochemistry: An Emerging Tandem for next-Generation Analytical Microsystems. *Current Opinion in Electrochemistry* **2019**, *15*, 175–185. https://doi.org/10.1016/j.coelec.2019.05.014.

(9) Culbertson, C. T.; Mickleburgh, T. G.; Stewart-James, S. A.; Sellens, K. A.; Pressnall, M. Micro Total Analysis Systems: Fundamental Advances and Biological Applications. *Analytical Chemistry* **2014**, *86* (1), 95–118. https://doi.org/10.1021/ac403688g.

(10) *Lab-on-a-Chip Devices and Micro-Total Analysis Systems: A Practical Guide*, 2015th edition.; Castillo-León, J., Svendsen, W. E., Eds.; Springer: New York, 2014.

(11) Mohammed, M. I.; Haswell, S.; Gibson, I. Lab-on-a-Chip or Chip-in-a-Lab: Challenges of Commercialization Lost in Translation. *Procedia Technology* **2015**, *20*, 54–59. https://doi.org/10.1016/j.protcy.2015.07.010.

(12) Chin, C. D.; Linder, V.; Sia, S. K. Commercialization of Microfluidic Point-of-Care Diagnostic Devices. *Lab on a Chip* **2012**, *12* (12), 2118. https://doi.org/10.1039/c2lc21204h.

(13) Mabey, D.; Peeling, R. W.; Ustianowski, A.; Perkins, M. D. Diagnostics for the Developing World. *Nat Rev Microbiol* **2004**, *2* (3), 231–240. https://doi.org/10.1038/nrmicro841.

(14) Land, K. J.; Boeras, D. I.; Chen, X.-S.; Ramsay, A. R.; Peeling, R. W. REASSURED Diagnostics to Inform Disease Control Strategies, Strengthen Health Systems and Improve Patient Outcomes. *Nat Microbiol* **2019**, *4* (1), 46–54. https://doi.org/10.1038/s41564-018-0295-3.

(15) Nishat, S.; Jafry, A. T.; Martinez, A. W.; Awan, F. R. Paper-Based Microfluidics: Simplified Fabrication and Assay Methods. *Sensors and Actuators B: Chemical* **2021**, *336*, 129681. https://doi.org/10.1016/j.snb.2021.129681.

(16) Noviana, E.; Ozer, T.; Carrell, C. S.; Link, J. S.; McMahon, C.; Jang, I.; Henry, C. S. Microfluidic Paper-Based Analytical Devices: From Design to Applications. *Chem. Rev.* **2021**, *121* (19), 11835–11885. https://doi.org/10.1021/acs.chemrev.0c01335.
(17) Cate, D. M.; Adkins, J. A.; Mettakoonpitak, J.; Henry, C. S. Recent Developments in Paper-Based Microfluidic Devices. *Analytical Chemistry* **2015**, *87* (1), 19–41. https://doi.org/10.1021/ac503968p.
(18) Gubala, V.; Harris, L. F.; Ricco, A. J.; Tan, M. X.; Williams, D. E. Point of Care Diagnostics: Status and Future. *Analytical Chemistry* **2012**, *84* (2), 487–515. https://doi.org/10.1021/ac2030199.
(19) FDA. *Recommendations for Clinical Laboratory Improvement Amendments of 1988 (CLIA) Waiver Applications for Manufacturers of In Vitro Diagnostic Devices*. https://www.fda.gov/regulatory-information/search-fda-guidance-documents/recommendations-clinical-laboratory-improvement-amendments-1988-clia-waiver-applications (accessed 2025-01-21).
(20) Tirandazi, P.; Hidrovo, C. H. An Integrated Gas-Liquid Droplet Microfluidic Platform for Digital Sampling and Detection of Airborne Targets. *Sensors and Actuators B: Chemical* **2018**, *267*, 279–293. https://doi.org/10.1016/j.snb.2018.03.057.
(21) Mentele, M. M.; Cunningham, J.; Koehler, K.; Volckens, J.; Henry, C. S. Microfluidic Paper-Based Analytical Device for Particulate Metals. *Anal. Chem.* **2012**, *84* (10), 4474–4480. https://doi.org/10.1021/ac300309c.
(22) Chowdhury, S.; Mazumder, M. A. J.; Al-Attas, O.; Husain, T. Heavy Metals in Drinking Water: Occurrences, Implications, and Future Needs in Developing Countries. *Science of The Total Environment* **2016**, *569–570*, 476–488. https://doi.org/10.1016/j.scitotenv.2016.06.166.
(23) *Marschner's Mineral Nutrition of Higher Plants*, 3rd edition.; Marschner, P., Ed.; Elsevier/Academic Press, 2011.
(24) Ferreira, F. T. S. M.; Catalão, K. A.; Mesquita, R. B. R.; Rangel, A. O. S. S. New Microfluidic Paper-Based Analytical Device for Iron Determination in Urine Samples. *Anal Bioanal Chem* **2021**, *413* (30), 7463–7472. https://doi.org/10.1007/s00216-021-03706-9.
(25) Pérez-Rodríguez, M.; Cañizares-Macías, M. del P. A Prototype Microfluidic Paper-Based Chromatic Device for Simultaneous Determination of Copper(II) and Zinc(II) in Urine. *Talanta Open* **2023**, *7*, 100178. https://doi.org/10.1016/j.talo.2022.100178.
(26) Amine, A.; Palleschi, G. Phosphate, Nitrate, and Sulfate Biosensors. *Analytical Letters* **2004**, *37* (1), 1–19. https://doi.org/10.1081/AL-120027770.
(27) Gautam, N.; Verma, R.; Ram, R.; Singh, J.; Sarkar, A. Development of a Biodegradable Microfluidic Paper-Based Device for Blood-Plasma Separation Integrated with Non-Enzymatic Electrochemical Detection of Ascorbic Acid. *Talanta* **2024**, *266*, 125019. https://doi.org/10.1016/j.talanta.2023.125019.
(28) Lee, S.; O'Dell, D.; Hohenstein, J.; Colt, S.; Mehta, S.; Erickson, D. NutriPhone: A Mobile Platform for Low-Cost Point-of-Care Quantification of Vitamin B12 Concentrations. *Sci Rep* **2016**, *6* (1), 28237. https://doi.org/10.1038/srep28237.
(29) Safavieh, R.; Juncker, D. Capillarics: Pre-Programmed, Self-Powered Microfluidic Circuits Built from Capillary Elements. *Lab Chip* **2013**, *13* (21), 4180–4189. https://doi.org/10.1039/C3LC50691F.
(30) Olanrewaju, A.; Beaugrand, M.; Yafia, M.; Juncker, D. Capillary Microfluidics in Microchannels: From Microfluidic Networks to Capillaric Circuits. *Lab on a Chip* **2018**, *18* (16), 2323–2347. https://doi.org/10.1039/C8LC00458G.

(31) Kolliopoulos, P.; Kumar, S. Capillary Flow of Liquids in Open Microchannels: Overview and Recent Advances. *npj Microgravity* **2021**, *7* (1), 1–6. https://doi.org/10.1038/s41526-021-00180-6.
(32) Ahmed, S.; Bui, M.-P. N.; Abbas, A. Paper-Based Chemical and Biological Sensors: Engineering Aspects. *Biosensors and Bioelectronics* **2016**, *77*, 249–263. https://doi.org/10.1016/j.bios.2015.09.038.
(33) Brody, J. P.; Yager, P.; Goldstein, R. E.; Austin, R. H. Biotechnology at Low Reynolds Numbers. *Biophysical Journal* **1996**, *71* (6), 3430–3441. https://doi.org/10.1016/S0006-3495(96)79538-3.
(34) Washburn, E. W. The Dynamics of Capillary Flow. *Phys. Rev.* **1921**, *17* (3), 273–283. https://doi.org/10.1103/PhysRev.17.273.
(35) Osborn, J. L.; Lutz, B.; Fu, E.; Kauffman, P.; Stevens, D. Y.; Yager, P. Microfluidics without Pumps: Reinventing the T-Sensor and H-Filter in Paper Networks. *Lab on a Chip* **2010**, *10* (20), 2659. https://doi.org/10.1039/c004821f.
(36) Fang, L.; Jiang, J.; Wang, J.; Deng, C. Non-Uniform Capillary Model for Unidirectional Fiber Bundles Considering Pore Size Distribution. *Journal of Reinforced Plastics and Composites* **2014**, *33* (15), 1430–1440. https://doi.org/10.1177/0731684414533739.
(37) Hassan, S.; Tariq, A.; Noreen, Z.; Donia, A.; Zaidi, S. Z. J.; Bokhari, H.; Zhang, X. Capillary-Driven Flow Microfluidics Combined with Smartphone Detection: An Emerging Tool for Point-of-Care Diagnostics. *Diagnostics* **2020**, *10* (8), 509. https://doi.org/10.3390/diagnostics10080509.
(38) Niculescu, A.; Chircov, C.; Alexandra Catalina, B.; Grumezescu, A. Fabrication and Applications of Microfluidic Devices: A Review. *International Journal of Molecular Sciences* **2021**, *22*, 2011. https://doi.org/10.3390/ijms22042011.
(39) Chen, L.; Guo, X.; Sun, X.; Zhang, S.; Wu, J.; Yu, H.; Zhang, T.; Cheng, W.; Shi, Y.; Pan, L. Porous Structural Microfluidic Device for Biomedical Diagnosis: A Review. *Micromachines* **2023**, *14* (3), 547. https://doi.org/10.3390/mi14030547.
(40) Kaur, N.; Toley, B. J. Paper-Based Nucleic Acid Amplification Tests for Point-of-Care Diagnostics. *Analyst* **2018**, *143* (10), 2213–2234. https://doi.org/10.1039/C7AN01943B.
(41) Hu, J.; Wang, S.; Wang, L.; Li, F.; Pingguan-Murphy, B.; Lu, T. J.; Xu, F. Advances in Paper-Based Point-of-Care Diagnostics. *Biosensors and Bioelectronics* **2014**, *54*, 585–597. https://doi.org/10.1016/j.bios.2013.10.075.
(42) Schilling, K. M.; Lepore, A. L.; Kurian, J. A.; Martinez, A. W. Fully Enclosed Microfluidic Paper-Based Analytical Devices. *Anal. Chem.* **2012**, *84* (3), 1579–1585. https://doi.org/10.1021/ac202837s.
(43) *ONE+STEP DUS 10 Urinalysis Reagent Test Strips | Tub of 100*. Premier Healthcare & Hygiene Ltd. https://www.premierhh.co.uk/products/dus10-urinalysis-reagent-test-strips-100 (accessed 2025-04-28).
(44) Martinez, A. W.; Phillips, S. T.; Whitesides, G. M.; Carrilho, E. Diagnostics for the Developing World: Microfluidic Paper-Based Analytical Devices. *Anal. Chem.* **2010**, *82* (1), 3–10. https://doi.org/10.1021/ac9013989.
(45) Yagoda, H. Applications of Confined Spot Tests in Analytical Chemistry: Preliminary Paper. *Ind. Eng. Chem. Anal. Ed.* **1937**, *9* (2), 79–82. https://doi.org/10.1021/ac50106a012.
(46) Müller, R. H.; Clegg, D. L. Automatic Paper Chromatography. *Anal. Chem.* **1949**, *21* (9), 1123–1125. https://doi.org/10.1021/ac60033a032.

(47) Martinez, A. W.; Phillips, S. T.; Butte, M. J.; Whitesides, G. M. Patterned Paper as a Platform for Inexpensive, Low-Volume, Portable Bioassays. *Angewandte Chemie International Edition* **2007**, *46* (8), 1318–1320. https://doi.org/10.1002/anie.200603817.
(48) Boodaghi, M.; Shamloo, A. A Comparison of Different Geometrical Elements to Model Fluid Wicking in Paper-Based Microfluidic Devices. *AIChE Journal* **2020**, *66* (1), e16756. https://doi.org/10.1002/aic.16756.
(49) Walji, N.; MacDonald, B. D. Influence of Geometry and Surrounding Conditions on Fluid Flow in Paper-Based Devices. *Micromachines* **2016**, *7* (5), 73. https://doi.org/10.3390/mi7050073.
(50) Böhm, A.; Carstens, F.; Trieb, C.; Schabel, S.; Biesalski, M. Engineering Microfluidic Papers: Effect of Fiber Source and Paper Sheet Properties on Capillary-Driven Fluid Flow. *Microfluid Nanofluid* **2014**, *16* (5), 789–799. https://doi.org/10.1007/s10404-013-1324-4.
(51) Lin, Y.; Gritsenko, D.; Feng, S.; Teh, Y. C.; Lu, X.; Xu, J. Detection of Heavy Metal by Paper-Based Microfluidics. *Biosensors and Bioelectronics* **2016**, *83*, 256–266. https://doi.org/10.1016/j.bios.2016.04.061.
(52) Hitzbleck, M.; Delamarche, E. Reagents in Microfluidics: An 'in' and 'out' Challenge. *Chemical Society Reviews* **2013**, *42* (21), 8494. https://doi.org/10.1039/c3cs60118h.
(53) Komuro, N.; Takaki, S.; Suzuki, K.; Citterio, D. Inkjet Printed (Bio)Chemical Sensing Devices. *Anal Bioanal Chem* **2013**, *405* (17), 5785–5805. https://doi.org/10.1007/s00216-013-7013-z.
(54) Kamnoet, P.; Aeungmaitrepirom, W.; Menger, R. F.; Henry, C. S. Highly Selective Simultaneous Determination of Cu(II), Co(II), Ni(II), Hg(II), and Mn(II) in Water Samples Using Microfluidic Paper-Based Analytical Devices. *Analyst* **2021**, *146* (7), 2229–2239. https://doi.org/10.1039/D0AN02200D.
(55) Cate, D. M.; Noblitt, S. D.; Volckens, J.; Henry, C. S. Multiplexed Paper Analytical Device for Quantification of Metals Using Distance-Based Detection. *Lab Chip* **2015**, *15* (13), 2808–2818. https://doi.org/10.1039/C5LC00364D.
(56) Microfluidic ChipShop. Lab-on-a-Chip Catalogue, 2023.
(57) Czurratis, D.; Beyl, Y.; Grimm, A.; Brettschneider, T.; Zinober, S.; Lärmer, F.; Zengerle, R. Liquids On-Chip: Direct Storage and Release Employing Micro-Perforated Vapor Barrier Films. *Lab Chip* **2015**, *15* (13), 2887–2895. https://doi.org/10.1039/C5LC00510H.
(58) Smith, S.; Sewart, R.; Becker, H.; Roux, P.; Land, K. Blister Pouches for Effective Reagent Storage on Microfluidic Chips for Blood Cell Counting. *Microfluid Nanofluid* **2016**, *20* (12), 163. https://doi.org/10.1007/s10404-016-1830-2.
(59) Niedl, R. R.; Beta, C. Hydrogel-Driven Paper-Based Microfluidics. *Lab on a Chip* **2015**, *15* (11), 2452–2459. https://doi.org/10.1039/C5LC00276A.
(60) Mitchell, H. T.; Schultz, S. A.; Costanzo, P. J.; Martinez, A. W. Poly(N-Isopropylacrylamide) Hydrogels for Storage and Delivery of Reagents to Paper-Based Analytical Devices. *Chromatography* **2015**, *2* (3), 436–451. https://doi.org/10.3390/chromatography2030436.
(61) Tang, R.; Yang, H.; Choi, J. R.; Gong, Y.; Hu, J.; Wen, T.; Li, X.; Xu, B.; Mei, Q.; Xu, F. Paper-Based Device with on-Chip Reagent Storage for Rapid Extraction of DNA from Biological Samples. *Microchim Acta* **2017**, *184* (7), 2141–2150. https://doi.org/10.1007/s00604-017-2225-0.

(62) Tang, R.; Yang, H.; Gong, Y.; You, M.; Liu, Z.; Choi, J. R.; Wen, T.; Qu, Z.; Mei, Q.; Xu, F. A Fully Disposable and Integrated Paper-Based Device for Nucleic Acid Extraction, Amplification and Detection. *Lab Chip* **2017**, *17* (7), 1270–1279. https://doi.org/10.1039/C6LC01586G.
(63) Aryal, P.; Brack, E.; Alexander, T.; Henry, C. S. Capillary Flow-Driven Microfluidics Combined with a Paper Device for Fast User-Friendly Detection of Heavy Metals in Water. *Anal. Chem.* **2023**, *95* (13), 5820–5827. https://doi.org/10.1021/acs.analchem.3c00378.
(64) Evans, E.; Gabriel, E. F. M.; Benavidez, T. E.; Coltro, W. K. T.; Garcia, C. D. Modification of Microfluidic Paper-Based Devices with Silica Nanoparticles. *Analyst* **2014**, *139* (21), 5560–5567. https://doi.org/10.1039/C4AN01147C.
(65) Li, F.; Hu, Y.; Li, Z.; Liu, J.; Guo, L.; He, J. Three-Dimensional Microfluidic Paper-Based Device for Multiplexed Colorimetric Detection of Six Metal Ions Combined with Use of a Smartphone. *Anal Bioanal Chem* **2019**, *411* (24), 6497–6508. https://doi.org/10.1007/s00216-019-02032-5.
(66) Zhang, Y.; Fan, J.; Nie, J.; Le, S.; Zhu, W.; Gao, D.; Yang, J.; Zhang, S.; Li, J. Timing Readout in Paper Device for Quantitative Point-of-Use Hemin/G-Quadruplex DNAzyme-Based Bioassays. *Biosensors and Bioelectronics* **2015**, *73*, 13–18. https://doi.org/10.1016/j.bios.2015.04.081.
(67) Abbas, A.; Brimer, A.; Slocik, J. M.; Tian, L.; Naik, R. R.; Singamaneni, S. Multifunctional Analytical Platform on a Paper Strip: Separation, Preconcentration, and Subattomolar Detection. *Analytical Chemistry* **2013**, *85* (8), 3977–3983. https://doi.org/10.1021/ac303567g.
(68) Cassano, C. L.; Fan, Z. H. Laminated Paper-Based Analytical Devices (LPAD): Fabrication, Characterization, and Assays. *Microfluidics and Nanofluidics* **2013**, *15* (2), 173–181. https://doi.org/10.1007/s10404-013-1140-x.
(69) Martinez, A. W.; Phillips, S. T.; Whitesides, G. M. Three-Dimensional Microfluidic Devices Fabricated in Layered Paper and Tape. *Proceedings of the National Academy of Sciences* **2008**, *105* (50), 19606–19611. https://doi.org/10.1073/pnas.0810903105.
(70) Liu, H.; Crooks, R. M. Three-Dimensional Paper Microfluidic Devices Assembled Using the Principles of Origami. *J. Am. Chem. Soc.* **2011**, *133* (44), 17564–17566. https://doi.org/10.1021/ja2071779.
(71) Toley, B. J.; Wang, J. A.; Gupta, M.; Buser, J. R.; Lafleur, L. K.; Lutz, B. R.; Fu, E.; Yager, P. A Versatile Valving Toolkit for Automating Fluidic Operations in Paper Microfluidic Devices. *Lab Chip* **2015**, *15* (6), 1432–1444. https://doi.org/10.1039/C4LC01155D.
(72) Fratzl, M.; Chang, B. S.; Oyola-Reynoso, S.; Blaire, G.; Delshadi, S.; Devillers, T.; Ward, T.; Dempsey, N. M.; Bloch, J.-F.; Thuo, M. M. Magnetic Two-Way Valves for Paper-Based Capillary-Driven Microfluidic Devices. *ACS Omega* **2018**, *3* (2), 2049–2057. https://doi.org/10.1021/acsomega.7b01839.
(73) Chen, H.; Cogswell, J.; Anagnostopoulos, C.; Faghri, M. A Fluidic Diode, Valves, and a Sequential-Loading Circuit Fabricated on Layered Paper. *Lab on a Chip* **2012**, *12* (16), 2909. https://doi.org/10.1039/c2lc20970e.
(74) Houghtaling, J.; Liang, T.; Thiessen, G.; Fu, E. Dissolvable Bridges for Manipulating Fluid Volumes in Paper Networks. *Analytical Chemistry* **2013**, *85* (23), 11201–11204. https://doi.org/10.1021/ac4022677.
(75) Lutz, B.; Liang, T.; Fu, E.; Ramachandran, S.; Kauffman, P.; Yager, P. Dissolvable Fluidic Time Delays for Programming Multi-Step Assays in Instrument-Free Paper Diagnostics. *Lab Chip* **2013**, *13* (14), 2840–2847.

https://doi.org/10.1039/C3LC50178G.
(76) Lenk, G.; Stemme, G.; Roxhed, N. Dry Reagent Storage in Dissolvable Films and Liquid Triggered Release for Programmed Multi-Step Lab-on-Chip Diagnostics. In *Micro Electro Mechanical Systems (MEMS), 2015 28th IEEE International Conference on*; IEEE, 2015; pp 451–454.
(77) Milani, A.; Statham, P. J.; Mowlem, M. C.; Connelly, D. P. Development and Application of a Microfluidic In-Situ Analyzer for Dissolved Fe and Mn in Natural Waters. *Talanta* **2015**, *136*, 15–22. https://doi.org/10.1016/j.talanta.2014.12.045.
(78) Songjaroen, T.; Dungchai, W.; Chailapakul, O.; Henry, C. S.; Laiwattanapaisal, W. Blood Separation on Microfluidic Paper-Based Analytical Devices. *Lab Chip* **2012**, *12* (18), 3392–3398. https://doi.org/10.1039/C2LC21299D.
(79) Moghadam, B. Y.; Connelly, K. T.; Posner, J. D. Isotachophoretic Preconcenetration on Paper-Based Microfluidic Devices. *Analytical Chemistry* **2014**, *86* (12), 5829–5837. https://doi.org/10.1021/ac500780w.
(80) Bagheri, N.; Cinti, S.; Nobile, E.; Moscone, D.; Arduini, F. Multi-Array Wax Paper-Based Platform for the Pre-Concentration and Determination of Silver Ions in Drinking Water. *Talanta* **2021**, *232*, 122474. https://doi.org/10.1016/j.talanta.2021.122474.
(81) Wu, Q.; He, J.; Meng, H.; Wang, Y.; Zhang, Y.; Li, H.; Feng, L. A Paper-Based Microfluidic Analytical Device Combined with Home-Made SPE Column for the Colorimetric Determination of Copper(II) Ion. *Talanta* **2019**, *204*, 518–524. https://doi.org/10.1016/j.talanta.2019.06.006.
(82) Satarpai, T.; Shiowatana, J.; Siripinyanond, A. Paper-Based Analytical Device for Sampling, on-Site Preconcentration and Detection of Ppb Lead in Water. *Talanta* **2016**, *154*, 504–510. https://doi.org/10.1016/j.talanta.2016.04.017.
(83) Hofstetter, J. C.; Wydallis, J. B.; Neymark, G.; Iii, T. H. R.; Harrington, J.; Henry, C. S. Quantitative Colorimetric Paper Analytical Devices Based on Radial Distance Measurements for Aqueous Metal Determination. *Analyst* **2018**, *143* (13), 3085–3090. https://doi.org/10.1039/C8AN00632F.
(84) Bao, B.; Wang, Z.; Thushara, D.; Liyanage, A.; Gunawardena, S.; Yang, Z.; Zhao, S. Recent Advances in Microfluidics-Based Chromatography—A Mini Review. *Separations* **2021**, *8* (1), 3. https://doi.org/10.3390/separations8010003.
(85) Murphy, A.; Gorey, B.; Guzman, K. de; Kelly, N.; Nesterenko, E. P.; Morrin, A. Microfluidic Paper Analytical Device for the Chromatographic Separation of Ascorbic Acid and Dopamine. *RSC Adv.* **2015**, *5* (113), 93162–93169. https://doi.org/10.1039/C5RA16272F.
(86) Marczenko, Z.; Freiser, H. Spectrophotometric Determination of Trace Elements. *C R C Critical Reviews in Analytical Chemistry* **1981**, *11* (3), 195–260. https://doi.org/10.1080/10408348108542732.
(87) Dawan, P.; Satarpai, T.; Tuchinda, P.; Shiowatana, J.; Siripinyanond, A. A Simple Analytical Platform Based on Thin-Layer Chromatography Coupled with Paper-Based Analytical Device for Determination of Total Capsaicinoids in Chilli Samples. *Talanta* **2017**, *162*, 460–465. https://doi.org/10.1016/j.talanta.2016.10.077.
(88) Shiroma, L. Y.; Santhiago, M.; Gobbi, A. L.; Kubota, L. T. Separation and Electrochemical Detection of Paracetamol and 4-Aminophenol in a Paper-Based Microfluidic Device. *Analytica Chimica Acta* **2012**, *725*, 44–50. https://doi.org/10.1016/j.aca.2012.03.011.
(89) Cid-Hernández, M.; López Dellamary-Toral, F. A.; González-Ortiz, L. J.; Sánchez-Peña, M. J.; Pacheco-Moisés, F. P. Two-Dimensional Thin Layer Chromatography-Bioautography Designed to Separate and Locate Metabolites with Antioxidant

Activity Contained on Spirulina Platensis. *Int J Anal Chem* **2018**, *2018*, 4605373. https://doi.org/10.1155/2018/4605373.
(90) Kraffczyk, F.; Helger, R.; Lang, H. Two-Dimensional Thin-Layer Chromatography on Two-Layer Plates of Amino Acids. *Clinical Chemistry* **1970**, *16* (8), 662–666. https://doi.org/10.1093/clinchem/16.8.662.
(91) Alsaeed, B.; Mansour, F. R. Distance-Based Paper Microfluidics; Principle, Technical Aspects and Applications. *Microchemical Journal* **2020**, *155*, 104664. https://doi.org/10.1016/j.microc.2020.104664.
(92) Sackmann, E. K.; Fulton, A. L.; Beebe, D. J. The Present and Future Role of Microfluidics in Biomedical Research. *Nature* **2014**, *507* (7491), 181–189. https://doi.org/10.1038/nature13118.
(93) Fu, L.-M.; Wang, Y.-N. Detection Methods and Applications of Microfluidic Paper-Based Analytical Devices. *TrAC Trends in Analytical Chemistry* **2018**, *107*, 196–211. https://doi.org/10.1016/j.trac.2018.08.018.
(94) Schaumburg, F.; Vidocevich, J. P.; Gerlero, G. S.; Pujato, N.; Macagno, J.; Kler, P. A.; Berli, C. L. A. A Free Customizable Tool for Easy Integration of Microfluidics and Smartphones. *Sci Rep* **2022**, *12* (1), 8969. https://doi.org/10.1038/s41598-022-13099-z.
(95) Dong, M.; Wu, J.; Ma, Z.; Peretz-Soroka, H.; Zhang, M.; Komenda, P.; Tangri, N.; Liu, Y.; Rigatto, C.; Lin, F. Rapid and Low-Cost CRP Measurement by Integrating a Paper-Based Microfluidic Immunoassay with Smartphone (CRP-Chip). *Sensors* **2017**, *17* (4), 684. https://doi.org/10.3390/s17040684.
(96) Mudanyali, O.; Dimitrov, S.; Sikora, U.; Padmanabhan, S.; Navruz, I.; Ozcan, A. Integrated Rapid-Diagnostic-Test Reader Platform on a Cellphone. *Lab Chip* **2012**, *12* (15), 2678–2686. https://doi.org/10.1039/C2LC40235A.
(97) Beni, V.; Nilsson, D.; Arven, P.; Norberg, P.; Gustafsson, G.; Turner, A. P. Printed Electrochemical Instruments for Biosensors. *ECS Journal of Solid State Science and Technology* **2015**, *4* (10), S3001–S3005.
(98) Teengam, P.; Siangproh, W.; Tontisirin, S.; Jiraseree-amornkun, A.; Chuaypen, N.; Tangkijvanich, P.; Henry, C. S.; Ngamrojanavanich, N.; Chailapakul, O. NFC-Enabling Smartphone-Based Portable Amperometric Immunosensor for Hepatitis B Virus Detection. *Sensors and Actuators B: Chemical* **2021**, *326*, 128825. https://doi.org/10.1016/j.snb.2020.128825.
(99) Wang, H.; Li, Y.; Wei, J.; Xu, J.; Wang, Y.; Zheng, G. Paper-Based Three-Dimensional Microfluidic Device for Monitoring of Heavy Metals with a Camera Cell Phone. *Anal Bioanal Chem* **2014**, *406* (12), 2799–2807. https://doi.org/10.1007/s00216-014-7715-x.
(100) Lutz, B. R.; Trinh, P.; Ball, C.; Fu, E.; Yager, P. Two-Dimensional Paper Networks: Programmable Fluidic Disconnects for Multi-Step Processes in Shaped Paper. *Lab on a Chip* **2011**, *11* (24), 4274. https://doi.org/10.1039/c1lc20758j.
(101) Fu, E.; Lutz, B.; Kauffman, P.; Yager, P. Controlled Reagent Transport in Disposable 2D Paper Networks. *Lab Chip* **2010**, *10* (7), 918–920. https://doi.org/10.1039/B919614E.
(102) Apilux, A.; Ukita, Y.; Chikae, M.; Chailapakul, O.; Takamura, Y. Development of Automated Paper-Based Devices for Sequential Multistep Sandwich Enzyme-Linked Immunosorbent Assays Using Inkjet Printing. *Lab Chip* **2013**, *13* (1), 126–135. https://doi.org/10.1039/C2LC40690J.
(103) Connelly, J. T.; Rolland, J. P.; Whitesides, G. M. "Paper Machine" for Molecular Diagnostics. *Anal. Chem.* **2015**, *87* (15), 7595–7601.

https://doi.org/10.1021/acs.analchem.5b00411.
(104) Verma, M. S.; Tsaloglou, M.-N.; Sisley, T.; Christodouleas, D.; Chen, A.; Milette, J.; Whitesides, G. M. Sliding-Strip Microfluidic Device Enables ELISA on Paper. *Biosens Bioelectron* **2018**, *99*, 77–84. https://doi.org/10.1016/j.bios.2017.07.034.
(105) Gao, B.; Liu, H.; Gu, Z. Patterned Photonic Nitrocellulose for Pseudo-Paper Microfluidics. *Analytical Chemistry* **2016**, *88* (10), 5424–5429. https://doi.org/10.1021/acs.analchem.6b00802.
(106) Kong, X.; Chong, X.; Squire, K.; Wang, A. X. Microfluidic Diatomite Analytical Devices for Illicit Drug Sensing with Ppb-Level Sensitivity. *Sensors and Actuators B: Chemical* **2018**, *259*, 587–595. https://doi.org/10.1016/j.snb.2017.12.038.
(107) Zhang, Z.; Lang, S.; Pearson, K.; Farhan, Y.; Tao, Y.; Xiao, G. Printed Capillary Microfluidic Devices and Their Application in Biosensing. *Micromachines* **2023**, *14* (11), 2059. https://doi.org/10.3390/mi14112059.
(108) Bilanovic, D.; Starosvetsky, J.; Armon, R. H. Cross-Linking Xanthan and Other Compounds with Glycerol. *Food Hydrocolloids* **2015**, *44*, 129–135. https://doi.org/10.1016/j.foodhyd.2014.09.024.
(109) Patel, J.; Maji, B.; Moorthy, N. S. H. N.; Maiti, S. Xanthan Gum Derivatives: Review of Synthesis, Properties and Diverse Applications. *RSC Adv.* **2020**, *10* (45), 27103–27136. https://doi.org/10.1039/D0RA04366D.
(110) Teo, P.; Liu, D.; Dai, M. High Performance Thin Layer Chromatography Method for Determination of Biotin in Edible Bird's Nest. *Asian Journal of Chemistry* **2012**, *24*, 5573–5575.
(111) Sobolevsky, T.; Ahrens, B. Biotin as a Masking Agent in Chorionic Gonadotropin Assays Utilizing Biotinylated Antibodies. *Drug Testing and Analysis* **2021**, *13* (11–12), 1929–1935. https://doi.org/10.1002/dta.3141.
(112) *Guidelines for Drinking-Water Quality: Fourth Edition Incorporating the First Addendum*; WHO Guidelines Approved by the Guidelines Review Committee; World Health Organization: Geneva, 2017.
(113) Ogawa, K.; Kaneta, T. Determination of Iron Ion in the Water of a Natural Hot Spring Using Microfluidic Paper-Based Analytical Devices. *ANAL. SCI.* **2016**, *32* (1), 31–34. https://doi.org/10.2116/analsci.32.31.
(114) Huangfu, C.; Zhang, Y.; Jang, M.; Feng, L. A μPAD for Simultaneous Monitoring of Cu2+, Fe2+ and Free Chlorine in Drinking Water. *Sensors and Actuators B: Chemical* **2019**, *293*, 350–356. https://doi.org/10.1016/j.snb.2019.02.092.
(115) Aguiar, J. I. S.; Ribeiro, S. O.; Leite, A.; Rangel, M.; Rangel, A. O. S. S.; Mesquita, R. B. R. Iron Determination in Natural Waters Using a Synthesised 3-Hydroxy-4-Pyridione Ligand in a Newly Developed Microfluidic Paper-Based Device. *Chemosensors* **2023**, *11* (2), 101. https://doi.org/10.3390/chemosensors11020101.
(116) Aguiar, J. I. S.; Ribeiro, S. O.; Leite, A.; Rangel, M.; Rangel, A. O. S. S.; Mesquita, R. B. R. Use of a Rhodamine-Based Chelator in a Microfluidic Paper-Based Analytical Device for the *in-Situ* Copper Quantification in Natural Waters. *Talanta* **2024**, *271*, 125683. https://doi.org/10.1016/j.talanta.2024.125683.
(117) Aryal, P.; Boes, J.; Brack, E.; Alexander, T.; Henry, C. S. Fill, Fold, Photo: Preconcentration and Multiplex Detection of Trace Level Heavy Metals in Water. *ACS Sens.* **2024**. https://doi.org/10.1021/acssensors.4c01708.

8. SUMMARY IN ESTONIAN

Uudsete keemilise analüüsi kiirtestide arendus – alternatiivsetest materjalidest ja tehnoloogiatest kuni toimivate prototüüpideni

Võimalus teostada keemilisi analüüse kohapeal lihtsate, kompaktsete ja odavate (kiir)testidega on oluline paljudes valdkondades, mõjutades inimeste heaolu terves maailmas. Paberipõhised mikrofluiidika seadmed on perspektiivne tehnoloogiline lahendus selle ülesande täitmiseks. Küll aga pole siiani nende testide võimekus olnud piisav, et jõuda masstootmisesse ja tarbimisse. Seetõttu oli antud töö eesmärgiks uurida alternatiive paberile, mis säilitaks kapillaarjõududel toimivate testide lihtsuse, pakkudes samas paremat kontrolli testi baasmaterjali omaduste üle. Samuti olid selle töö fookuses erinevad pärismaailma probleemid ning nende lahendamiseks prototüüp-testide arendamine, mis oleks seejuures sobilikud tavakasutajatele.

Käesolevas töös arendati välja kolm erinevat võimalust paberisarnase, kapillaarjõududel toimiva mikrofluiidika kiibi valmistamiseks, mis olid tõestuseks esimesele püstitatud hüpoteesile (alternatiivseid materjale paberile on võimalik arendada). Neist kõige paremaks osutus silikageeli mikroosakeste ja ksantaankummi lahuse kombinatsioonil baseeruv segu, mis võimaldas siiditrükki kasutades soovitud kujuga materjali (*i.e.* mikrofluiidika või analüüsi kiipi) trükkida. See meetod võimaldas ka erineva suuruse ja pinnakeemiaga osakeste kombineerimist, et paremini kontrollida materjali omadusi (poorsust, paksust ja pinnakeemiat), tõestades sellega teise hüpoteesi esimest alapunkti (erinevaid materjale saab kombineerida ühele kiibile). Läbi selle on võimalik paremini kontrollida kiibile kantavaid vedelikke ning tõsta testi analüütilist võimekust. Lisaks saab siiditrükki kasutada kiireks ja odavaks prototüüpimiseks ning see sobib hilisemaks masstootmiseks, mis tõestab teise hüpoteesi ülejäänud alapunkte.

Parema analüütilise võimekuse (selektiivsuse ja tundlikkuse) saavutamiseks kasutati kiipidel planaarkromatograafiat (TLC) ja tahke faasi ekstraktsiooni (SPE). Nende analüüsisammude toimimist näidati töö käigus publitseeritud artiklites, kus rakenduste hulka kuulus viie metallikatiooni lahutamine ja määramine veeproovidest, biotiini lahutamine metaboliitidest ning määramine tehisuriiniproovist ning vase ja raua ioonide määramine erinevatest joogi ja taimede toitevee proovidest. Selliseid täielikult integreeritud TLC sammuga teste võib pidada täiesti uudseteks. Samuti demonstreeriti antud töös integreeritud SPE süsteemi, mis võimaldas kuni tuhandekordset analüütide kontsentreerimist. Lõpetuseks võib antud töö jooksul arendatud vase ja rauaioonide testi pidada vähemalt võrdseks ning mitmeti paremaks teistest sarnasetest paberipõhistest testidest. Neile asjaoludele tuginedes võib väita, et töös püstitatud hüpotees kolm sai suuresti tõestatud (uudsete meetoditega tehtud kiibi pakuvad paremat analüütilist võimekust).

Kokkuvõttes uuriti ja demonstreeriti käesolevas töös mitmeid uudseid lahendusi, mis võivad oluliselt parandada ja edasi arendada hetkel eksisteerivaid paberi-

põhiseid analüütilisi seadmeid. Käesoleva doktoritöö raames anti lisaks neljale avaldatud teadusartiklile sisse kaks patenditaotlust. Neist esimene käsitles üldisi aspekte osakestepõhiste mikrofluiidika kiipide valmistamise kohta ning nendes mitme analüüsisammu kombineerimist. Teises patenditaotluses demonstreeriti automatiseerimise süsteemi, et vabastada eelsalvestatud reservuaaridest vedelikke ning katkestada ja luua uusi ühendusi kiibi erinevate osade vahel, et juhtida sellel vedelike ja ainete liikumist. Mõlemad lahendused võivad märkimisväärselt kaasa aidata odavate, mitmesammuliste analüüsiseadmete tootmistele, mis vajavad minimaalset kasutajapoolset sekkumist.

ACKNOWLEDGEMENTS

First and foremost, I am extremely grateful to my supervisors. Dr. Hanno Evard has been a constant source of guidance, encouragement, and support. From countless discussions and brainstorming sessions to planning and problem-solving, his insight and commitment were central to this work. Professor Ivo Leito has guided me throughout my entire academic path, and his mentorship over the years has shaped how I think and approach research. I'm deeply grateful for his steady support and belief in my potential at every stage.

I would also like to thank all the current and former members of our research group, whose thoughts and ideas have shaped this work in numerous ways. Collaborating with you – whether on publications and patents or in discussions about the direction and purpose of our research – has been both intellectually rewarding and personally enriching. And of course, the fun times we shared, from exciting group activities and board game nights to casual conversations, made the journey unforgettable.

Finally, to my family and friends: thank you for being the steady ground beneath my feet. Your support, patience, and encouragement kept me balanced through the highs and lows and reminded me that life exists well beyond the boundaries of research.

This work was supported by the Estonian Research Council grants PSG431 and EAG295.

PUBLICATIONS

CURRICULUM VITAE

Name: Indrek Saar
Date of birth: May 15, 1995
Citizenship: Estonian
E-mail: indrek95@hotmail.com

Education:

2020–…	University of Tartu, chemistry, Ph.D.
2018–2020	University of Tartu, materials science, MSc, *cum laude*
2014–2017	University of Tartu, materials science, BSc, *cum laude*

Professional employment:

2023–…	Silklytics OÜ, cofounder, main engineer
2024	University of Tartu, Institute of Chemistry, Analytical chemistry specialist

Scientific publications:

1. **Saar, I**.; Evard, H. "Real-World Implementation of Particle-Based Microfluidics: On-Spot Test for Iron and Copper Ions in Water" ACS Omega 2025, 10 (1), 1800–1808.
2. Laaneväli, A.; **Saar, I**.; Nasirova, N.; Evard, H. "Multi-Step Particle-Based Microfluidic Test for Biotin Measurement" Microfluidics and Nanofluidics 2024, 28 (10), 71.
3. **Saar, I**.; Evard, H. "Screen Printed Particle-Based Microfluidics: Optimization and Exemplary Application for Heavy Metals Analysis" Micromachines 2023, 14 (7), 1369.
4. Evard, H.; Priks, H.; **Saar, I**.; Aavola, H.; Tamm, T.; Leito, I. "A New Direction in Microfluidics: Printed Porous Materials" Micromachines 2021, 12 (6), ARTN 671.
5. Yrjana, V.; **Saar, I**.; Ilisson, M.; Kadam, S.; Leito, I.; Bobacka, J. "Potentiometric Carboxylate Sensors Based on Carbazole-Derived Acyclic and Macrocyclic Ionophores" Chemosensors 2021, 9 (1), 4.
6. Rüütel, A.; Yrjana, V.; Kadam, S.; **Saar, I**.; Ilisson, M.; Darnell, A.; Haav, K.; Haljasorg, T.; Toom, L., Bobacka, J.; Leito, I. "Design, synthesis and application of carbazole macrocycles in anion sensors" Beilstein Journal of Organic Chemistry 2020, 16, 1901−1914.

Patent applications:

1. **Saar, I.**; Evard. H.; Zapata, E. "Method of producing an analysis device, analysis device, analysis arrangement and analysis method" PCT/IB2025/052999 Priority date: 03.2024
2. Evard, H.; **Saar, I.**; Laaneväli, A. "Analytic device, liquid handling system and chemical analysis method" WO2024126727A1, 2024 Priority date: 12.2022

ELULOOKIRJELDUS

Nimi: Indrek Saar
Sünniaeg: 15. mai 1995
Kodakondsus: Eesti
E-post: indrek95@hotmail.com

Haridus:

2020–…	Tartu Ülikool, keemia, Ph.D.
2018–2020	Tartu Ülikool, materjaliteadus, MSc, *cum laude*
2014–2017	Tartu Ülikool, materjaliteadus, BSc, *cum laude*

Teenistuskäik:

2023–…	Silklytics OÜ, kaasasutaja, peainsener
2024	Tartu Ülikool, keemia instituut, analüütilise keemia spetsialist

Publikatsioonide loetelu:

1. **Saar, I**.; Evard, H. "Real-World Implementation of Particle-Based Microfluidics: On-Spot Test for Iron and Copper Ions in Water" ACS Omega 2025, 10 (1), 1800–1808.
2. Laaneväli, A.; **Saar, I**.; Nasirova, N.; Evard, H. "Multi-Step Particle-Based Microfluidic Test for Biotin Measurement" Microfluidics and Nanofluidics 2024, 28 (10), 71.
3. **Saar, I**.; Evard, H. "Screen Printed Particle-Based Microfluidics: Optimization and Exemplary Application for Heavy Metals Analysis" Micromachines 2023, 14 (7), 1369.
4. Evard, H.; Priks, H.; **Saar, I**.; Aavola, H.; Tamm, T.; Leito, I. "A New Direction in Microfluidics: Printed Porous Materials" Micromachines 2021, 12 (6), ARTN 671.
5. Yrjana, V.; **Saar, I**.; Ilisson, M.; Kadam, S.; Leito, I.; Bobacka, J. "Potentiometric Carboxylate Sensors Based on Carbazole-Derived Acyclic and Macrocyclic Ionophores" Chemosensors 2021, 9 (1), 4.
6. Rüütel, A.; Yrjana, V.; Kadam, S.; **Saar, I**.; Ilisson, M.; Darnell, A.; Haav, K.; Haljasorg, T.; Toom, L., Bobacka, J.; Leito, I. "Design, synthesis and application of carbazole macrocycles in anion sensors" Beilstein Journal of Organic Chemistry 2020, 16, 1901−1914.

Patenditaotlused:

1. **Saar, I.**; Evard. H.; Zapata, E. "Method of producing an analysis device, analysis device, analysis arrangement and analysis method" PCT/IB2025/052999, Sisse antud 03.2024
2. Evard, H.; **Saar, I.**; Laaneväli, A. "Analytic device, liquid handling system and chemical analysis method" WO2024126727A1, 2024, Sisse antud 12.2022

DISSERTATIONES CHIMICAE UNIVERSITATIS TARTUENSIS

1. **Toomas Tamm.** Quantum-chemical simulation of solvent effects. Tartu, 1993, 110 p.
2. **Peeter Burk.** Theoretical study of gas-phase acid-base equilibria. Tartu, 1994, 96 p.
3. **Victor Lobanov.** Quantitative structure-property relationships in large descriptor spaces. Tartu, 1995, 135 p.
4. **Vahur Mäemets.** The ^{17}O and ^{1}H nuclear magnetic resonance study of H_2O in individual solvents and its charged clusters in aqueous solutions of electrolytes. Tartu, 1997, 140 p.
5. **Andrus Metsala.** Microcanonical rate constant in nonequilibrium distribution of vibrational energy and in restricted intramolecular vibrational energy redistribution on the basis of slater's theory of unimolecular reactions. Tartu, 1997, 150 p.
6. **Uko Maran.** Quantum-mechanical study of potential energy surfaces in different environments. Tartu, 1997, 137 p.
7. **Alar Jänes.** Adsorption of organic compounds on antimony, bismuth and cadmium electrodes. Tartu, 1998, 219 p.
8. **Kaido Tammeveski.** Oxygen electroreduction on thin platinum films and the electrochemical detection of superoxide anion. Tartu, 1998, 139 p.
9. **Ivo Leito.** Studies of Brønsted acid-base equilibria in water and non-aqueous media. Tartu, 1998, 101 p.
10. **Jaan Leis.** Conformational dynamics and equilibria in amides. Tartu, 1998, 131 p.
11. **Toonika Rinken.** The modelling of amperometric biosensors based on oxidoreductases. Tartu, 2000, 108 p.
12. **Dmitri Panov.** Partially solvated Grignard reagents. Tartu, 2000, 64 p.
13. **Kaja Orupõld.** Treatment and analysis of phenolic wastewater with microorganisms. Tartu, 2000, 123 p.
14. **Jüri Ivask.** Ion Chromatographic determination of major anions and cations in polar ice core. Tartu, 2000, 85 p.
15. **Lauri Vares.** Stereoselective Synthesis of Tetrahydrofuran and Tetrahydropyran Derivatives by Use of Asymmetric Horner-Wadsworth-Emmons and Ring Closure Reactions. Tartu, 2000, 184 p.
16. **Martin Lepiku.** Kinetic aspects of dopamine D_2 receptor interactions with specific ligands. Tartu, 2000, 81 p.
17. **Katrin Sak.** Some aspects of ligand specificity of P2Y receptors. Tartu, 2000, 106 p.
18. **Vello Pällin.** The role of solvation in the formation of iotsitch complexes. Tartu, 2001, 95 p.
19. **Katrin Kollist.** Interactions between polycyclic aromatic compounds and humic substances. Tartu, 2001, 93 p.

20. **Ivar Koppel.** Quantum chemical study of acidity of strong and superstrong Brønsted acids. Tartu, 2001, 104 p.
21. **Viljar Pihl.** The study of the substituent and solvent effects on the acidity of OH and CH acids. Tartu, 2001, 132 p.
22. **Natalia Palm.** Specification of the minimum, sufficient and significant set of descriptors for general description of solvent effects. Tartu, 2001, 134 p.
23. **Sulev Sild.** QSPR/QSAR approaches for complex molecular systems. Tartu, 2001, 134 p.
24. **Ruslan Petrukhin.** Industrial applications of the quantitative structure-property relationships. Tartu, 2001, 162 p.
25. **Boris V. Rogovoy.** Synthesis of (benzotriazolyl)carboximidamides and their application in relations with *N*- and *S*-nucleophyles. Tartu, 2002, 84 p.
26. **Koit Herodes.** Solvent effects on UV-vis absorption spectra of some solvatochromic substances in binary solvent mixtures: the preferential solvation model. Tartu, 2002, 102 p.
27. **Anti Perkson.** Synthesis and characterisation of nanostructured carbon. Tartu, 2002, 152 p.
28. **Ivari Kaljurand.** Self-consistent acidity scales of neutral and cationic Brønsted acids in acetonitrile and tetrahydrofuran. Tartu, 2003, 108 p.
29. **Karmen Lust.** Adsorption of anions on bismuth single crystal electrodes. Tartu, 2003, 128 p.
30. **Mare Piirsalu.** Substituent, temperature and solvent effects on the alkaline hydrolysis of substituted phenyl and alkyl esters of benzoic acid. Tartu, 2003, 156 p.
31. **Meeri Sassian.** Reactions of partially solvated Grignard reagents. Tartu, 2003, 78 p.
32. **Tarmo Tamm.** Quantum chemical modelling of polypyrrole. Tartu, 2003. 100 p.
33. **Erik Teinemaa.** The environmental fate of the particulate matter and organic pollutants from an oil shale power plant. Tartu, 2003. 102 p.
34. **Jaana Tammiku-Taul.** Quantum chemical study of the properties of Grignard reagents. Tartu, 2003. 120 p.
35. **Andre Lomaka.** Biomedical applications of predictive computational chemistry. Tartu, 2003. 132 p.
36. **Kostyantyn Kirichenko.** Benzotriazole – Mediated Carbon–Carbon Bond Formation. Tartu, 2003. 132 p.
37. **Gunnar Nurk.** Adsorption kinetics of some organic compounds on bismuth single crystal electrodes. Tartu, 2003, 170 p.
38. **Mati Arulepp.** Electrochemical characteristics of porous carbon materials and electrical double layer capacitors. Tartu, 2003, 196 p.
39. **Dan Cornel Fara.** QSPR modeling of complexation and distribution of organic compounds. Tartu, 2004, 126 p.
40. **Riina Mahlapuu.** Signalling of galanin and amyloid precursor protein through adenylate cyclase. Tartu, 2004, 124 p.

41. **Mihkel Kerikmäe.** Some luminescent materials for dosimetric applications and physical research. Tartu, 2004, 143 p.
42. **Jaanus Kruusma.** Determination of some important trace metal ions in human blood. Tartu, 2004, 115 p.
43. **Urmas Johanson.** Investigations of the electrochemical properties of polypyrrole modified electrodes. Tartu, 2004, 91 p.
44. **Kaido Sillar.** Computational study of the acid sites in zeolite ZSM-5. Tartu, 2004, 80 p.
45. **Aldo Oras.** Kinetic aspects of dATPαS interaction with $P2Y_1$ receptor. Tartu, 2004, 75 p.
46. **Erik Mölder.** Measurement of the oxygen mass transfer through the air-water interface. Tartu, 2005, 73 p.
47. **Thomas Thomberg.** The kinetics of electroreduction of peroxodisulfate anion on cadmium (0001) single crystal electrode. Tartu, 2005, 95 p.
48. **Olavi Loog.** Aspects of condensations of carbonyl compounds and their imine analogues. Tartu, 2005, 83 p.
49. **Siim Salmar.** Effect of ultrasound on ester hydrolysis in aqueous ethanol. Tartu, 2006, 73 p.
50. **Ain Uustare.** Modulation of signal transduction of heptahelical receptors by other receptors and G proteins. Tartu, 2006, 121 p.
51. **Sergei Yurchenko.** Determination of some carcinogenic contaminants in food. Tartu, 2006, 143 p.
52. **Kaido Tämm.** QSPR modeling of some properties of organic compounds. Tartu, 2006, 67 p.
53. **Olga Tšubrik.** New methods in the synthesis of multisubstituted hydrazines. Tartu. 2006, 183 p.
54. **Lilli Sooväli.** Spectrophotometric measurements and their uncertainty in chemical analysis and dissociation constant measurements. Tartu, 2006, 125 p.
55. **Eve Koort.** Uncertainty estimation of potentiometrically measured ph and pK_a values. Tartu, 2006, 139 p.
56. **Sergei Kopanchuk.** Regulation of ligand binding to melanocortin receptor subtypes. Tartu, 2006, 119 p.
57. **Silvar Kallip.** Surface structure of some bismuth and antimony single crystal electrodes. Tartu, 2006, 107 p.
58. **Kristjan Saal.** Surface silanization and its application in biomolecule coupling. Tartu, 2006, 77 p.
59. **Tanel Tätte.** High viscosity $Sn(OBu)_4$ oligomeric concentrates and their applications in technology. Tartu, 2006, 91 p.
60. **Dimitar Atanasov Dobchev**. Robust QSAR methods for the prediction of properties from molecular structure. Tartu, 2006, 118 p.
61. **Hannes Hagu**. Impact of ultrasound on hydrophobic interactions in solutions. Tartu, 2007, 81 p.
62. **Rutha Jäger.** Electroreduction of peroxodisulfate anion on bismuth electrodes. Tartu, 2007, 142 p.

63. **Kaido Viht.** Immobilizable bisubstrate-analogue inhibitors of basophilic protein kinases: development and application in biosensors. Tartu, 2007, 88 p.
64. **Eva-Ingrid Rõõm.** Acid-base equilibria in nonpolar media. Tartu, 2007, 156 p.
65. **Sven Tamp.** DFT study of the cesium cation containing complexes relevant to the cesium cation binding by the humic acids. Tartu, 2007, 102 p.
66. **Jaak Nerut.** Electroreduction of hexacyanoferrate(III) anion on Cadmium (0001) single crystal electrode. Tartu, 2007, 180 p.
67. **Lauri Jalukse.** Measurement uncertainty estimation in amperometric dissolved oxygen concentration measurement. Tartu, 2007, 112 p.
68. **Aime Lust.** Charge state of dopants and ordered clusters formation in CaF_2:Mn and CaF_2:Eu luminophors. Tartu, 2007, 100 p.
69. **Iiris Kahn**. Quantitative Structure-Activity Relationships of environmentally relevant properties. Tartu, 2007, 98 p.
70. **Mari Reinik.** Nitrates, nitrites, N-nitrosamines and polycyclic aromatic hydrocarbons in food: analytical methods, occurrence and dietary intake. Tartu, 2007, 172 p.
71. **Heili Kasuk.** Thermodynamic parameters and adsorption kinetics of organic compounds forming the compact adsorption layer at Bi single crystal electrodes. Tartu, 2007, 212 p.
72. **Erki Enkvist.** Synthesis of adenosine-peptide conjugates for biological applications. Tartu, 2007, 114 p.
73. **Svetoslav Hristov Slavov**. Biomedical applications of the QSAR approach. Tartu, 2007, 146 p.
74. **Eneli Härk.** Electroreduction of complex cations on electrochemically polished Bi(*hkl*) single crystal electrodes. Tartu, 2008, 158 p.
75. **Priit Möller.** Electrochemical characteristics of some cathodes for medium temperature solid oxide fuel cells, synthesized by solid state reaction technique. Tartu, 2008, 90 p.
76. **Signe Viggor.** Impact of biochemical parameters of genetically different pseudomonads at the degradation of phenolic compounds. Tartu, 2008, 122 p.
77. **Ave Sarapuu.** Electrochemical reduction of oxygen on quinone-modified carbon electrodes and on thin films of platinum and gold. Tartu, 2008, 134 p.
78. **Agnes Kütt.** Studies of acid-base equilibria in non-aqueous media. Tartu, 2008, 198 p.
79. **Rouvim Kadis.** Evaluation of measurement uncertainty in analytical chemistry: related concepts and some points of misinterpretation. Tartu, 2008, 118 p.
80. **Valter Reedo.** Elaboration of IVB group metal oxide structures and their possible applications. Tartu, 2008, 98 p.
81. **Aleksei Kuznetsov.** Allosteric effects in reactions catalyzed by the cAMP-dependent protein kinase catalytic subunit. Tartu, 2009, 133 p.

82. **Aleksei Bredihhin.** Use of mono- and polyanions in the synthesis of multisubstituted hydrazine derivatives. Tartu, 2009, 105 p.
83. **Anu Ploom.** Quantitative structure-reactivity analysis in organosilicon chemistry. Tartu, 2009, 99 p.
84. **Argo Vonk.** Determination of adenosine A_{2A}- and dopamine D_1 receptor-specific modulation of adenylate cyclase activity in rat striatum. Tartu, 2009, 129 p.
85. **Indrek Kivi.** Synthesis and electrochemical characterization of porous cathode materials for intermediate temperature solid oxide fuel cells. Tartu, 2009, 177 p.
86. **Jaanus Eskusson.** Synthesis and characterisation of diamond-like carbon thin films prepared by pulsed laser deposition method. Tartu, 2009, 117 p.
87. **Marko Lätt.** Carbide derived microporous carbon and electrical double layer capacitors. Tartu, 2009, 107 p.
88. **Vladimir Stepanov.** Slow conformational changes in dopamine transporter interaction with its ligands. Tartu, 2009, 103 p.
89. **Aleksander Trummal.** Computational Study of Structural and Solvent Effects on Acidities of Some Brønsted Acids. Tartu, 2009, 103 p.
90. **Eerold Vellemäe.** Applications of mischmetal in organic synthesis. Tartu, 2009, 93 p.
91. **Sven Parkel.** Ligand binding to 5-HT_{1A} receptors and its regulation by Mg^{2+} and Mn^{2+}. Tartu, 2010, 99 p.
92. **Signe Vahur.** Expanding the possibilities of ATR-FT-IR spectroscopy in determination of inorganic pigments. Tartu, 2010, 184 p.
93. **Tavo Romann**. Preparation and surface modification of bismuth thin film, porous, and microelectrodes. Tartu, 2010, 155 p.
94. **Nadežda Aleksejeva.** Electrocatalytic reduction of oxygen on carbon nanotube-based nanocomposite materials. Tartu, 2010, 147 p.
95. **Marko Kullapere.** Electrochemical properties of glassy carbon, nickel and gold electrodes modified with aryl groups. Tartu, 2010, 233 p.
96. **Liis Siinor.** Adsorption kinetics of ions at Bi single crystal planes from aqueous electrolyte solutions and room-temperature ionic liquids. Tartu, 2010, 101 p.
97. **Angela Vaasa.** Development of fluorescence-based kinetic and binding assays for characterization of protein kinases and their inhibitors. Tartu 2010, 101 p.
98. **Indrek Tulp.** Multivariate analysis of chemical and biological properties. Tartu 2010, 105 p.
99. **Aare Selberg.** Evaluation of environmental quality in Northern Estonia by the analysis of leachate. Tartu 2010, 117 p.
100. **Darja Lavõgina.** Development of protein kinase inhibitors based on adenosine analogue-oligoarginine conjugates. Tartu 2010, 248 p.
101. **Laura Herm.** Biochemistry of dopamine D_2 receptors and its association with motivated behaviour. Tartu 2010, 156 p.

102. **Terje Raudsepp.** Influence of dopant anions on the electrochemical properties of polypyrrole films. Tartu 2010, 112 p.
103. **Margus Marandi.** Electroformation of Polypyrrole Films: *In-situ* AFM and STM Study. Tartu 2011, 116 p.
104. **Kairi Kivirand.** Diamine oxidase-based biosensors: construction and working principles. Tartu, 2011, 140 p.
105. **Anneli Kruve.** Matrix effects in liquid-chromatography electrospray mass-spectrometry. Tartu, 2011, 156 p.
106. **Gary Urb.** Assessment of environmental impact of oil shale fly ash from PF and CFB combustion. Tartu, 2011, 108 p.
107. **Nikita Oskolkov.** A novel strategy for peptide-mediated cellular delivery and induction of endosomal escape. Tartu, 2011, 106 p.
108. **Dana Martin.** The QSPR/QSAR approach for the prediction of properties of fullerene derivatives. Tartu, 2011, 98 p.
109. **Säde Viirlaid.** Novel glutathione analogues and their antioxidant activity. Tartu, 2011, 106 p.
110. **Ülis Sõukand.** Simultaneous adsorption of Cd^{2+}, Ni^{2+}, and Pb^{2+} on peat. Tartu, 2011, 124 p.
111. **Lauri Lipping.** The acidity of strong and superstrong Brønsted acids, an outreach for the "limits of growth": a quantum chemical study. Tartu, 2011, 124 p.
112. **Heisi Kurig.** Electrical double-layer capacitors based on ionic liquids as electrolytes. Tartu, 2011, 146 p.
113. **Marje Kasari.** Bisubstrate luminescent probes, optical sensors and affinity adsorbents for measurement of active protein kinases in biological samples. Tartu, 2012, 126 p.
114. **Kalev Takkis.** Virtual screening of chemical databases for bioactive molecules. Tartu, 2012, 122 p.
115. **Ksenija Kisseljova**. Synthesis of aza-β^3-amino acid containing peptides and kinetic study of their phosphorylation by protein kinase A. Tartu, 2012, 104 p.
116. **Riin Rebane.** Advanced method development strategy for derivatization LC/ESI/MS. Tartu, 2012, 184 p.
117. **Vladislav Ivaništšev.** Double layer structure and adsorption kinetics of ions at metal electrodes in room temperature ionic liquids. Tartu, 2012, 128 p.
118. **Irja Helm.** High accuracy gravimetric Winkler method for determination of dissolved oxygen. Tartu, 2012, 139 p.
119. **Karin Kipper.** Fluoroalcohols as Components of LC-ESI-MS Eluents: Usage and Applications. Tartu, 2012, 164 p.
120. **Arno Ratas.** Energy storage and transfer in dosimetric luminescent materials. Tartu, 2012, 163 p.
121. **Reet Reinart-Okugbeni**. Assay systems for characterisation of subtype-selective binding and functional activity of ligands on dopamine receptors. Tartu, 2012, 159 p.

122. **Lauri Sikk.** Computational study of the Sonogashira cross-coupling reaction. Tartu, 2012, 81 p.
123. **Karita Raudkivi.** Neurochemical studies on inter-individual differences in affect-related behaviour of the laboratory rat. Tartu, 2012, 161 p.
124. **Indrek Saar.** Design of GalR2 subtype specific ligands: their role in depression-like behavior and feeding regulation. Tartu, 2013, 126 p.
125. **Ann Laheäär.** Electrochemical characterization of alkali metal salt based non-aqueous electrolytes for supercapacitors. Tartu, 2013, 127 p.
126. **Kerli Tõnurist.** Influence of electrospun separator materials properties on electrochemical performance of electrical double-layer capacitors. Tartu, 2013, 147 p.
127. **Kaija Põhako-Esko.** Novel organic and inorganic ionogels: preparation and characterization. Tartu, 2013, 124 p.
128. **Ivar Kruusenberg.** Electroreduction of oxygen on carbon nanomaterial-based catalysts. Tartu, 2013, 191 p.
129. **Sander Piiskop.** Kinetic effects of ultrasound in aqueous acetonitrile solutions. Tartu, 2013, 95 p.
130. **Ilona Faustova**. Regulatory role of L-type pyruvate kinase N-terminal domain. Tartu, 2013, 109 p.
131. **Kadi Tamm.** Synthesis and characterization of the micro-mesoporous anode materials and testing of the medium temperature solid oxide fuel cell single cells. Tartu, 2013, 138 p.
132. **Iva Bozhidarova Stoyanova-Slavova.** Validation of QSAR/QSPR for regulatory purposes. Tartu, 2013, 109 p.
133. **Vitali Grozovski**. Adsorption of organic molecules at single crystal electrodes studied by *in situ* STM method. Tartu, 2014, 146 p.
134. **Santa Veikšina**. Development of assay systems for characterisation of ligand binding properties to melanocortin 4 receptors. Tartu, 2014, 151 p.
135. **Jüri Liiv.** PVDF (polyvinylidene difluoride) as material for active element of twisting-ball displays. Tartu, 2014, 111 p.
136. **Kersti Vaarmets.** Electrochemical and physical characterization of pristine and activated molybdenum carbide-derived carbon electrodes for the oxygen electroreduction reaction. Tartu, 2014, 131 p.
137. **Lauri Tõntson**. Regulation of G-protein subtypes by receptors, guanine nucleotides and Mn^{2+}. Tartu, 2014, 105 p.
138. **Aiko Adamson.** Properties of amine-boranes and phosphorus analogues in the gas phase. Tartu, 2014, 78 p.
139. **Elo Kibena**. Electrochemical grafting of glassy carbon, gold, highly oriented pyrolytic graphite and chemical vapour deposition-grown graphene electrodes by diazonium reduction method. Tartu, 2014, 184 p.
140. **Teemu Näykki.** Novel Tools for Water Quality Monitoring – From Field to Laboratory. Tartu, 2014, 202 p.
141. **Karl Kaupmees.** Acidity and basicity in non-aqueous media: importance of solvent properties and purity. Tartu, 2014, 128 p.

142. **Oleg Lebedev**. Hydrazine polyanions: different strategies in the synthesis of heterocycles. Tartu, 2015, 118 p.
143. **Geven Piir.** Environmental risk assessment of chemicals using QSAR methods. Tartu, 2015, 123 p.
144. **Olga Mazina.** Development and application of the biosensor assay for measurements of cyclic adenosine monophosphate in studies of G protein-coupled receptor signalinga. Tartu, 2015, 116 p.
145. **Sandip Ashokrao Kadam.** Anion receptors: synthesis and accurate binding measurements. Tartu, 2015, 116 p.
146. **Indrek Tallo.** Synthesis and characterization of new micro-mesoporous carbide derived carbon materials for high energy and power density electrical double layer capacitors. Tartu, 2015, 148 p.
147. **Heiki Erikson.** Electrochemical reduction of oxygen on nanostructured palladium and gold catalysts. Tartu, 2015, 204 p.
148. **Erik Anderson.** *In situ* Scanning Tunnelling Microscopy studies of the interfacial structure between Bi(111) electrode and a room temperature ionic liquid. Tartu, 2015, 118 p.
149. **Girinath G. Pillai.** Computational Modelling of Diverse Chemical, Biochemical and Biomedical Properties. Tartu, 2015, 140 p.
150. **Piret Pikma.** Interfacial structure and adsorption of organic compounds at Cd(0001) and Sb(111) electrodes from ionic liquid and aqueous electrolytes: an *in situ* STM study. Tartu, 2015, 126 p.
151. **Ganesh babu Manoharan.** Combining chemical and genetic approaches for photoluminescence assays of protein kinases. Tartu, 2016, 126 p.
152. **Carolin Siimenson**. Electrochemical characterization of halide ion adsorption from liquid mixtures at Bi(111) and pyrolytic graphite electrode surface. Tartu, 2016, 110 p.
153. **Asko Laaniste.** Comparison and optimisation of novel mass spectrometry ionisation sources. Tartu, 2016, 156 p.
154. **Hanno Evard.** Estimating limit of detection for mass spectrometric analysis methods. Tartu, 2016, 224 p.
155. **Kadri Ligi.** Characterization and application of protein kinase-responsive organic probes with triplet-singlet energy transfer. Tartu, 2016, 122 p.
156. **Margarita Kagan.** Biosensing penicillins' residues in milk flows. Tartu, 2016, 130 p.
157. **Marie Kriisa.** Development of protein kinase-responsive photoluminescent probes and cellular regulators of protein phosphorylation. Tartu, 2016, 106 p.
158. **Mihkel Vestli.** Ultrasonic spray pyrolysis deposited electrolyte layers for intermediate temperature solid oxide fuel cells. Tartu, 2016, 156 p.
159. **Silver Sepp**. Influence of porosity of the carbide-derived carbon on the properties of the composite electrocatalysts and characteristics of polymer electrolyte fuel cells. Tartu, 2016, 137 p.
160. **Kristjan Haav**. Quantitative relative equilibrium constant measurements in supramolecular chemistry. Tartu, 2017, 158 p.

161. **Anu Teearu**. Development of MALDI-FT-ICR-MS methodology for the analysis of resinous materials. Tartu, 2017, 205 p.
162. **Taavi Ivan**. Bifunctional inhibitors and photoluminescent probes for studies on protein complexes. Tartu, 2017, 140 p.
163. **Maarja-Liisa Oldekop**. Characterization of amino acid derivatization reagents for LC-MS analysis. Tartu, 2017, 147 p.
164. **Kristel Jukk**. Electrochemical reduction of oxygen on platinum- and palladium-based nanocatalysts. Tartu, 2017, 250 p.
165. **Siim Kukk**. Kinetic aspects of interaction between dopamine transporter and *N*-substituted nortropane derivatives. Tartu, 2017, 107 p.
166. **Birgit Viira**. Design and modelling in early drug development in targeting HIV-1 reverse transcriptase and Malaria. Tartu, 2017, 172 p.
167. **Rait Kivi**. Allostery in cAMP dependent protein kinase catalytic subunit. Tartu, 2017, 115 p.
168. **Agnes Heering**. Experimental realization and applications of the unified acidity scale. Tartu, 2017, 123 p.
169. **Delia Juronen**. Biosensing system for the rapid multiplex detection of mastitis-causing pathogens in milk. Tartu, 2018, 85 p.
170. **Hedi Rahnel.** ARC-inhibitors: from reliable biochemical assays to regulators of physiology of cells. Tartu, 2018, 176 p.
171. **Anton Ruzanov.** Computational investigation of the electrical double layer at metal–aqueous solution and metal–ionic liquid interfaces. Tartu, 2018, 129 p.
172. **Katrin Kestav.** Crystal Structure-Guided Development of Bisubstrate-Analogue Inhibitors of Mitotic Protein Kinase Haspin. Tartu, 2018, 166 p.
173. **Mihkel Ilisson.** Synthesis of novel heterocyclic hydrazine derivatives and their conjugates. Tartu, 2018, 101 p.
174. **Anni Allikalt.** Development of assay systems for studying ligand binding to dopamine receptors. Tartu, 2018, 160 p.
175. **Ove Oll.** Electrical double layer structure and energy storage characteristics of ionic liquid based capacitors. Tartu, 2018, 187 p.
176. **Rasmus Palm.** Carbon materials for energy storage applications. Tartu, 2018, 114 p.
177. **Jörgen Metsik.** Preparation and stability of poly(3,4-ethylenedioxythiophene) thin films for transparent electrode applications. Tartu, 2018, 111 p.
178. **Sofja Tšepelevitš.** Experimental studies and modeling of solute-solvent interactions. Tartu, 2018, 109 p.
179. **Märt Lõkov.** Basicity of some nitrogen, phosphorus and carbon bases in acetonitrile. Tartu, 2018, 104 p.
180. **Anton Mastitski**. Preparation of α-aza-amino acid precursors and related compounds by novel methods of reductive one-pot alkylation and direct alkylation. Tartu, 2018, 155 p.
181. **Jürgen Vahter**. Development of bisubstrate inhibitors for protein kinase CK2. Tartu, 2019, 186 p.

182. **Piia Liigand.** Expanding and improving methodology and applications of ionization efficiency measurements. Tartu, 2019, 189 p.
183. **Sigrid Selberg.** Synthesis and properties of lipophilic phosphazene-based indicator molecules. Tartu, 2019, 74 p.
184. **Jaanus Liigand.** Standard substance free quantification for LC/ESI/MS analysis based on the predicted ionization efficiencies. Tartu, 2019, 254 p.
185. **Marek Mooste.** Surface and electrochemical characterisation of aryl film and nanocomposite material modified carbon and metal-based electrodes. Tartu, 2019, 304 p.
186. **Mare Oja.** Experimental investigation and modelling of pH profiles for effective membrane permeability of drug substances. Tartu, 2019, 306 p.
187. **Sajid Hussain.** Electrochemical reduction of oxygen on supported Pt catalysts. Tartu, 2019, 220 p.
188. **Ronald Väli.** Glucose-derived hard carbon electrode materials for sodium-ion batteries. Tartu, 2019, 180 p.
189. **Ester Tee.** Analysis and development of selective synthesis methods of hierarchical micro- and mesoporous carbons. Tartu, 2019, 210 p.
190. **Martin Maide.** Influence of the microstructure and chemical composition of the fuel electrode on the electrochemical performance of reversible solid oxide fuel cell. Tartu, 2020, 144 p.
191. **Edith Viirlaid.** Biosensing Pesticides in Water Samples. Tartu, 2020, 102 p.
192. **Maike Käärik.** Nanoporous carbon: the controlled nanostructure, and structure-property relationships. Tartu, 2020, 162 p.
193. **Artur Gornischeff.** Study of ionization efficiencies for derivatized compounds in LC/ESI/MS and their application for targeted analysis. Tartu, 2020, 124 p.
194. **Reet Link.** Ligand binding, allosteric modulation and constitutive activity of melanocortin-4 receptors. Tartu, 2020, 108 p.
195. **Pilleriin Peets.** Development of instrumental methods for the analysis of textile fibres and dyes. Tartu, 2020, 150 p.
196. **Larisa Ivanova.** Design of active compounds against neurodegenerative diseases. Tartu, 2020, 152 p.
197. **Meelis Härmas.** Impact of activated carbon microstructure and porosity on electrochemical performance of electrical double-layer capacitors. Tartu, 2020, 122 p.
198. **Ruta Hecht.** Novel Eluent Additives for LC-MS Based Bioanalytical Methods. Tartu, 2020, 202 p.
199. **Max Hecht.** Advances in the Development of a Point-of-Care Mass Spectrometer Test. Tartu, 2020, 168 p.
200. **Ida Rahu.** Bromine formation in inorganic bromide/nitrate mixtures and its application for oxidative aromatic bromination. Tartu, 2020, 116 p.
201. **Sander Ratso**. Electrocatalysis of oxygen reduction on non-precious metal catalysts. Tartu, 2020, 371 p.
202. **Astrid Darnell.** Computational design of anion receptors and evaluation of host-guest binding. Tartu, 2021, 150 p.

203. **Ove Korjus.** The development of ceramic fuel electrode for solid oxide cells. Tartu, 2021, 150 p.
204. **Merit Oss.** Ionization efficiency in electrospray ionization source and its relations to compounds' physico-chemical properties. Tartu, 2021, 124 p.
205. **Madis Lüsi**. Electroreduction of oxygen on nanostructured palladium catalysts. Tartu, 2021, 180 p.
206. **Eliise Tammekivi.** Derivatization and quantitative gas-chromatographic analysis of oils. Tartu, 2021, 122 p.
207. **Simona Selberg.** Development of Small-Molecule Regulators of Epi-transcriptomic Processes. Tartu, 2021, 122 p.
208. **Olivier Etebe Nonga.** Inhibitors and photoluminescent probes for in vitro studies on protein kinases PKA and PIM. Tartu, 2021, 189 p.
209. **Riinu Härmas.** The structure and H2 diffusion in porous carbide-derived carbon particles. Tartu, 2022, 123 p.
210. **Maarja Paalo.** Synthesis and characterization of novel carbon electrodes for high power density electrochemical capacitors. Tartu, 2022, 144 p.
211. **Jinfeng Zhao.** Electrochemical characteristics of Bi(hkl) and micro-meso-porous carbon electrodes in ionic liquid based electrolytes. Tartu, 2022, 134 p.
212. **Alar Heinsaar.** Investigation of oxygen electrode materials for high-temperature solid oxide cells in natural conditions. Tartu, 2022, 120 p.
213. **Jaana Lilloja.** Transition metal and nitrogen doped nanocarbon cathode catalysts for anion exchange membrane fuel cells. Tartu, 2022, 202 p.
214. **Maris-Johanna Tahk.** Novel fluorescence-based methods for illuminating transmembrane signal transduction by G-protein coupled receptors. Tartu, 2022, 200 p.
215. **Eerik Jõgi.** Development and Applications of E. coli Immunosensor. Tartu, 2022, 103 p.
216. **Alo Rüütel.** Design principles of synthetic molecular receptors for anion-selective electrodes. Tartu, 2022, 109 p.
217. **Tanel Sõrmus.** Development of stimuli-responsive and covalent bisubstrate inhibitors of protein kinases. Tartu, 2022, 148 p.
218. **Oleg Artemchuk.** Autotrophic nitrogen removal processes for nutrient removal from sidestream and mainstream wastewater. Tartu, 2022, 115 p.
219. **Andre Leesment.** Quantitative studies of Brønsted acidity in biphasic systems and gas-phase. Tartu, 2023, 83 p.
220. **Meeli Arujõe-Sado.** Structural effects in aza-peptide bond formation reaction. Tartu, 2023, 83 p.
221. **Jonas Mart Linge.** Electrochemical reduction of oxygen on silver-based catalysts. Tartu, 2023, 269 p.
222. **Tõnis Laasfeld.** Integrating Image Analysis and Quantitative Modeling for a Holistic View of GPCR Ligand Binding Dynamics. Tartu, 2023, 226 p.
223. **Ernesto de Jesus Zapata Flores.** Derivatization Reagents used in negative mode electrospray LC-MS. Tartu, 2023, 107 p.

224. **Patrick Teppor.** Obtaining platinum-free oxygen reduction catalysts through biomass valorization: a case study of peat. Tartu, 2023, 161 p.
225. **Peeter Valk.** Methanol Oxidation on Platinum-Rare-Earth Metal Oxide Activated Catalysts. Tartu, 2023, 162 p.
226. **Shidong Chen.** Unravelling prehistoric plant exploitation in eastern Baltic: organic residue analysis of plant-based materials by multi-method approach. Tartu, 2023, 245 p.
227. **Yogesh Kumar.** M-N_4 macrocycle-based catalysts for electrocatalysis of oxygen reduction and oxygen evolution. Tartu, 2023, 224 p.
228. **Kerli Martin.** Recognition of carboxylates by synthetic receptors – from structure-affinity studies to solid-contact anion-selective electrode prototyping. Tartu, 2024, 130 p.
229. **Huy Quí Vinh Nguyen.** Development of Carbon Supported Pt–CeO_2 Catalysts for Proton Exchange Membrane Fuel Cells. Tartu, 2024, 198 p.
230. **Heigo Ers**. Adsorption and Structuring Processes at Single Crystal Electrode – Ionic Liquid Interface – Insights from Simulations and *in situ* Studies. Tartu, 2024, 137 p.
231. **Ritums Cepitis.** Modelling Structural and Geometrical Effects in Carbon Dioxide and Oxygen Electrocatalysis. Tartu, 2024, 99 p.
232. **Kaarel Kisand.** Resorcinol-derived carbon-based catalysts for polymer electrolyte fuel cell cathodes. Tartu, 2024, 205 p.
233. **Akmal Kosimov**. Template-assisted Mechanosynthesis (TAMS) for the production of bifunctional transition metal-based catalysts. Tartu, 2024, 123 p.
234. **Larissa Silva Macieli.** Derivatization-targeted LC-MS analysis of compounds containing amino group. Tartu, 2024, 157 p.
235. **Silvester Jürjo.** Separation of rare earth elements from Estonian phosphorite ore using liquid extraction followed by electrochemical reduction. Tartu, 2024, 99 p.
236. **Jan-Michael C. Cayme.** Organic-inorganic interactions in experimental and archaeological ceramics. Tartu, 2025, 156 p.
237. **Miriam Koppel.** The diffusion of H2 adsorbed in carbide-derived carbons: a quasi-elastic neutron scattering study. Tartu, 2025, 138 p.
238. **Kenneth Tuul.** Evaluating lithium-ion pouch cells and hydrogen storage materials under extreme conditions using advanced techniques. Tartu, 2025, 188 p.
239. **Marta-Lisette Pikma.** Exploring the basicity of phosphanes and related compounds. Tartu, 2025, 100 p.